Imaging Life

Your resource for molecular imaging innovation

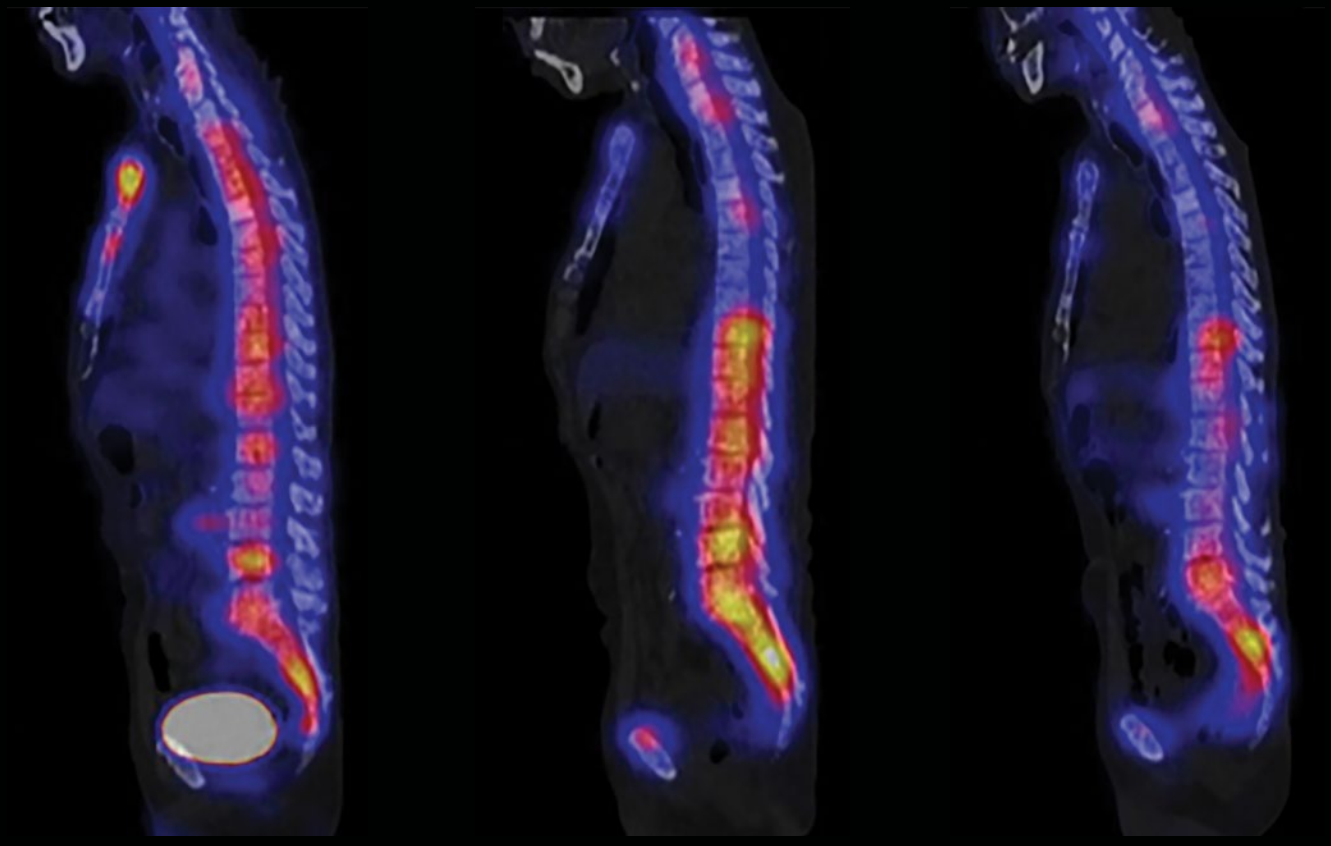

Empowering precision medicine



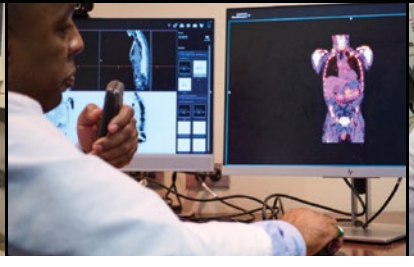
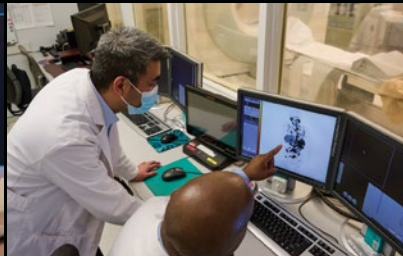

International Edition · Issue 19

SIEMENS Healthineers

"There's a clear advantage in [theranostic] possibilities to be used in prediction, for personalization in treatment, and to provide precision medicine for cancer patients."

Veera Ahtiainen, MD
The Comprehensive Cancer Center
Helsinki University Hospital
Helsinki, Finland

Read the full story on p. 16.

Cover images: Data courtesy on file.

Together, we are advancing the frontier on personalized care.

Welcome to another captivating issue of *Imaging Life*. We at Siemens Healthineers Molecular Imaging are excited to share these articles and case studies from our nuclear medicine community that focus on the forefront of personalized care.

Theranostics is a new concept for some and many are just beginning to understand this form of personalized care, but our molecular imaging modalities have been playing an important role in the field of theranostics for years—and we continue to strengthen and deepen our partnership with clinicians and researchers across the multiple continents in personalized oncology care.

We are honored to have partnered with Dr. Osborne and his patient John who generously shared their time, their personal insights, and even their home and office to share their theranostic journey with the goal of inspiring others. Their articles provide personal insight for those considering establishing a theranostics program at their medical facility and for patients seeking oncology treatment options. We hope this information will provide an image of the theranostics journey for patients and clinicians—and the possibilities it offers today and in the future.

For a more personal look into Dr. Osborne and John's theranostic patient care journey, I invite you to watch the patient video. Use the QR code on p. 21 to watch the video and explore our dedicated theranostics landing page.

Imaging Life does not stop there with theranostics coverage. Read how a cancer center in Helsinki, Finland, operates a cutting-edge theranostic program for their expanding number of patients seeking this type of treatment.

And we have yet another exciting story from Finland, this time from the Turku PET Centre, which recounts how Dr. Knuuti and his team use Biograph Vision Quadra™ to explore the possibilities of water perfusion research. Be sure to check out the breathtaking clinical images on p. 26.

We also interviewed two medical facilities in Latin America that tell us how Biograph Vision™ PET/CT is the perfect fit for their patient population and how true time of flight is leading to new advances in their patient care, allowing these facilities to expand treatment options.

These stories are just a sampling of the fascinating content covered in this issue of *Imaging Life*. I, along with our entire Molecular Imaging team, believe this issue will fuel your drive and commitment to provide the best options and outcomes for your patients.

Matt Shah,
Vice President, Global Sales & Marketing
Molecular Imaging Business Line
Siemens Healthineers

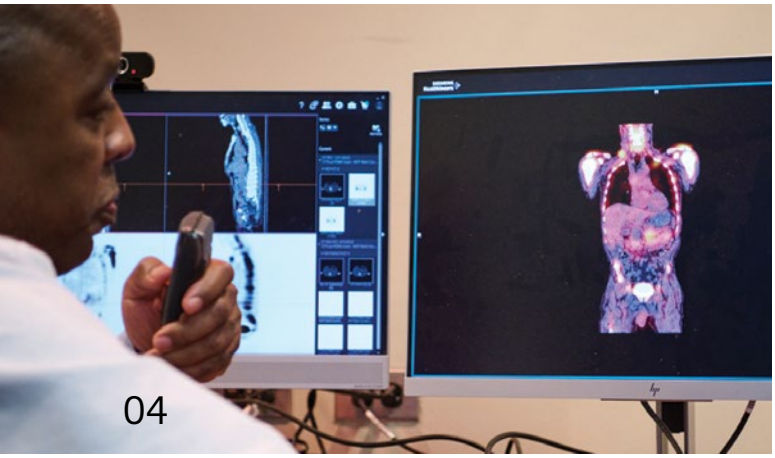

04

22

Spotlight

Expanding

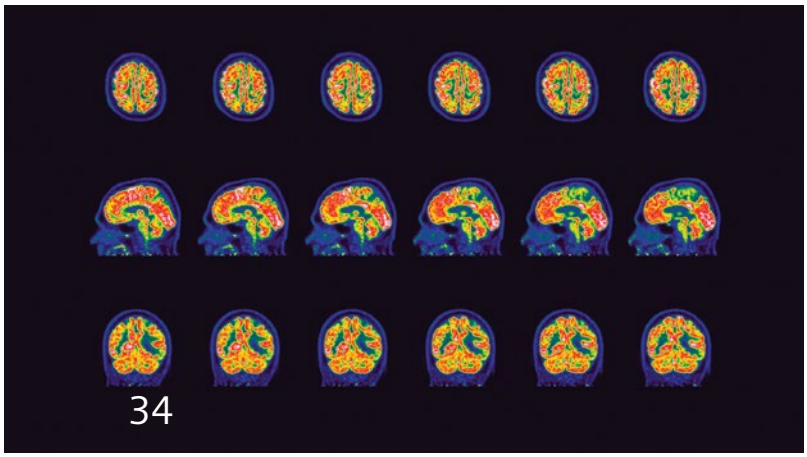

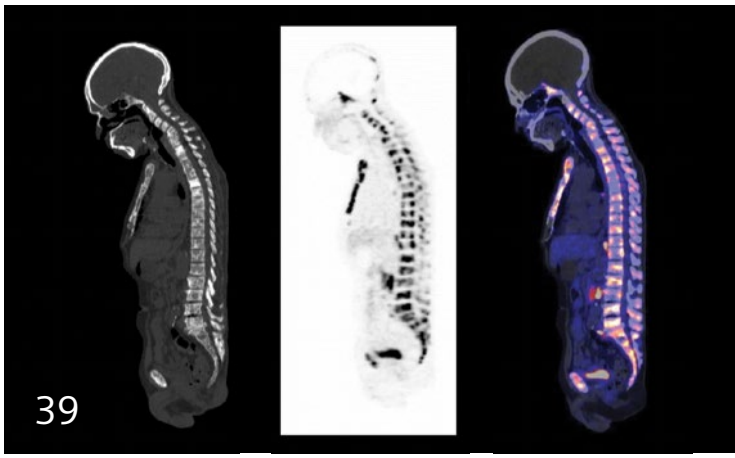

Advancing

Clinical results

A physician's experience: Theranostics offers personalized care for prostate cancer

Professor Joseph R. Osborne, MD, PhD, Chief of Molecular Imaging and Therapeutics and professor of radiology at a leading academic institution's hospital in New York City, NY, USA, discusses theranostics and its rapidly expanding role in prostate cancer care.

By Sameh Fahmy | Photography by James Farrell | Data courtesy on file

Osborne's colleague, a professor of urology, led the team that developed the first monoclonal antibodies to prostate-specific membrane antigen (PSMA) that effectively bind prostate cancer cells. The team later showed that after an antibody binds to PSMA, the antibody-PSMA complex is rapidly internalized into the cancer cell. In the early 2000s, they applied this knowledge to pioneer the application of PSMA-targeted agents to treat patients.

Advances like these laid the foundation for the March 2022 FDA clearance of a PSMA-targeted radioligand therapeutic agent for the treatment of advanced prostate cancer. This milestone allowed Osborne and his colleagues to transition from exploring the potential of PSMA targeting in a research setting to applying the theranostic approach in routine patient care.

"As soon as it became available clinically and was cleared, we jumped all over it," says Osborne, who is also chief of Molecular Imaging and Therapeutics at his institution. "The thing that we were working on became something that was of immediate impact to patients."

What is theranostics?

Theranostics is an innovative form of personalized therapy that focuses on both the accurate selection of patients and providing them with targeted radioligand therapy to improve their prognosis.[1] Theranostics refers to a process involving structurally similar diagnostic and therapeutic agents that share a molecular-specific target. Molecular targets are proteins on the surface of cancer cells and where the radioligand will bind. Throughout the theranostics process, molecular imaging techniques are used to identify, personalize, and monitor therapy response. Pharmaceuticals, such as radioligands, can be used to target and treat specific areas.[2] A radioligand is made up of a radioisotope that damages cancer cells and a target ligand that binds to specific markers on cancer cells.

Establishing a theranostics program

Osborne says patients are increasingly seeking treatment at his institution after learning it offers theranostic treatment, and he is open to sharing his experience establishing the program at his institution. He also wants to ensure all eligible patients—including those who have historically been underserved by the healthcare system—have access to such a promising development in prostate cancer care. "Of course, quality is really important. It's not like hanging a bag of saline or even administering chemotherapy. One has to go into this intentionally and with the right equipment, people, and instruments."

Besides diagnostic imaging that includes PET/CT and SPECT/CT, the theranostics care pathway also requires a clinical team trained to work safely with radiation. A floor plan that enables the sequestration of patients in rooms where they can access designated bathrooms without posing a risk to other patients is essential. Osborne notes that nurses, physicists, and technicians at his institution are well-versed in the treatment protocols, and newly recruited radiologists come in with the expectation that they will work closely with patients.

Theranostics for prostate cancer can involve medical oncologists, radiation therapists, and urologists. Osborne says. "It really is a team

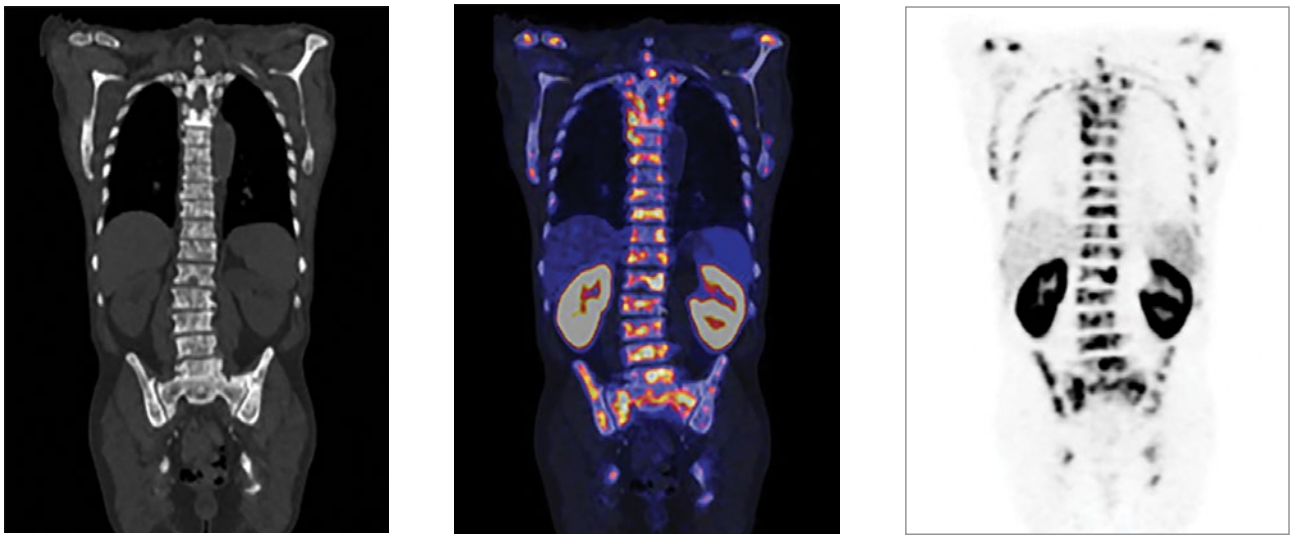

^{68}Ga-PSMA PET/CT coronal images of patient John. From left to right: coronal CT only, coronal fused PET/CT, and coronal PET only. Data courtesy on file.

Diagnosis and patient selection: John's PET/CT scans provided data showing he was a strong candidate for theranostics to treat his advanced-stage prostate cancer.

Personalized treatment: Osborne and his nuclear medicine team collaborated to provide personalized treatment for John.

approach, and it has to be a team approach if you're going to get the right patients into the program. No one single modality or one among us is going to do it."

Theranostics care pathway

The theranostics care pathway involves a series of steps and a range of laboratory diagnostic and imaging modalities. Beginning with patient selection, the additional steps include personalized treatment, therapy response monitoring, and follow-up and survivorship monitoring.

Diagnosis and patient selection

A patient is selected based on the review of multiple tests. In metastatic prostate cancer, treatment response is typically evaluated using CT or bone scans. In addition to detecting disease extent in patients with metastatic castration resistant prostate cancer, PSMA-ligand PET/CT is used to confirm eligibility for theranostic treatment, since documentation of PSMA expression in metastatic sites is required prior to initiation.

Osborne says that advances in PET/CT, such as the use of long axial field of view scanners equipped with time-of-flight technology, are accelerating patient care. "With the long axial field of view scanners, the scan times are getting into the range where they're almost as fast as CT, so the workflow depends on how fast the techs can get patients on and off the table," Osborne says. "If you're going to do a lot of patients, you have to be able to evaluate them in a reasonable way, which means quickly."

Osborne notes that although results from clinical trials have provided clearly defined PET/CT imaging

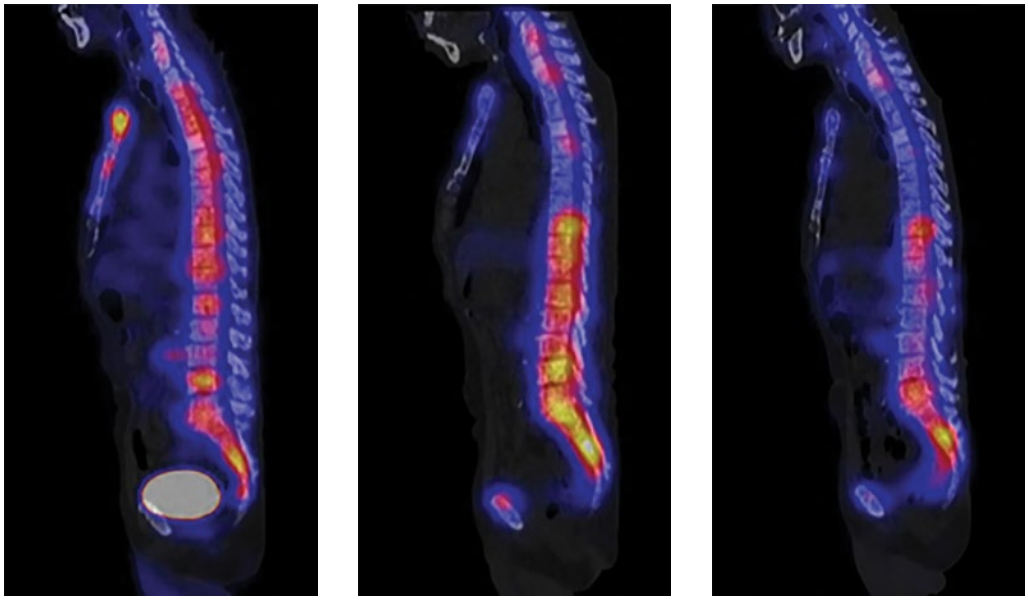

^{177}Lu-PSMA-fused SPECT/CT post-treatment images acquired throughout John's personalized treatment to assess therapy response. From left to right: sagittal fused SPECT/CT cycle 1, sagittal fused SPECT/CT cycle 3, and sagittal fused SPECT/CT cycle 6. Data courtesy on file.

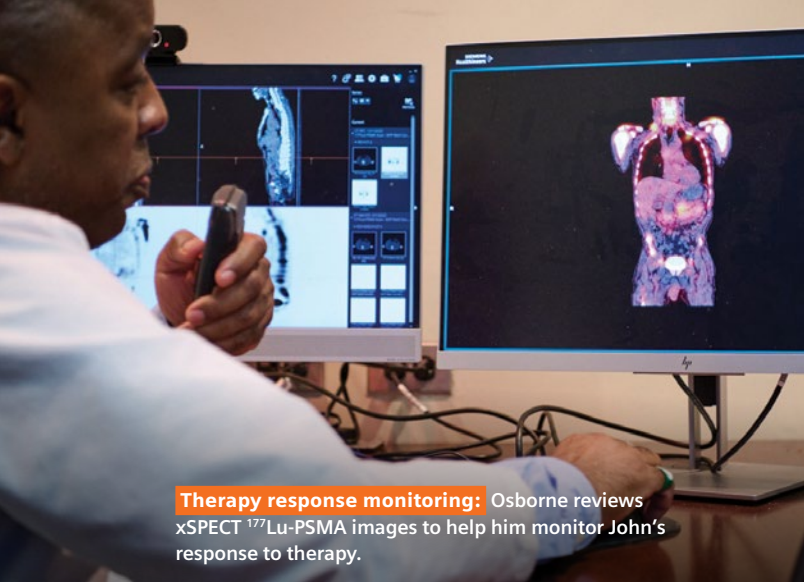

Therapy response monitoring: Osborne reviews xSPECT ^{177}Lu-PSMA images to help him monitor John's response to therapy.

Follow-up and survivorship monitoring: Osborne continues meeting regularly to monitor John's positive response and level of survivorship.

criteria for treatment eligibility, he and his colleagues are now working to translate those criteria into the routine care they deliver to the wider population of patients.

"We're trying to figure out who is going to benefit the most and where can we jump in and really find benefit," he says. "That is what all of us in the field, especially the subset of the field who have really tried to push things forward, are trying to figure out."

One of his early patients, a 78-year-old man named John with advanced prostate cancer, highlights the potential that the theranostic approach provides. Osborne emphasizes that patients such as John can gain not just longevity from applying theranostics, but also dramatically improved overall health. "It can bring back functional longevity, where someone gets back to doing the things they love for the people they love," he says. "And that's really what we're all in this for."

Personalized treatment

Another key step in the theranostic care pathway is personalized treatment. Because the theranostic approach uses the same ligand to monitor and treat patients, treatment is inherently personalized to the patient's specific disease state.

Osborne notes that total-body standard uptake value (SUV) mean is emerging as a key indicator of patient response to therapy. Using the xSPECT Quant™ tool in conjunction with Symbia™ SPECT/CT for SUV evaluation allows Osborne and his colleagues to assess response to treatment over time using a standardized, automated approach that produces accurate and reproducible quantitative values. *syngo*.via for Molecular Imaging facilitates the reading, interpretation, reporting, and sharing of results while enabling physicians to efficiently compare results over time to accurately track response to treatment.

"Reporting total-body SUV_{mean} is not what most physicians are used to doing, but it's something that is available to us if we just push a little bit harder with the output of imaging and the programs that we use," he says. "If we want to get towards doing total body SUV_{mean}, we'll be able to do that with *syngo*.via and xSPECT Quant."[3]

Therapy response monitoring

During the therapy response monitoring step in the theranostic care pathway, SPECT/CT is an essential tool used for visualizing PSMA-positive prostate lesions and metastases to help monitor the response to therapy. The PSMA-targeted radioligand therapeutic agent used for John is administered by injection into a vein over approximately five minutes, typically in six doses six weeks apart. The drug can cause severe and life-threatening myelosuppression, so physicians review complete blood counts before each infusion. Post-therapy quantitative SPECT/CT imaging examines the biodistribution of the radionuclide within the body so that physicians can guide further treatment.

"There are some instances where the SPECT/CT imaging that we do may say stop after two cycles because the patient is doing exceptionally well—or because it's not working," Osborne says. "Maybe if the patient is doing well, we stop and then maybe six months down the line we start again. The plasma markers, as well as the imaging, are going to tell us what to do."

Follow-up and survivorship monitoring

To follow up on a patient and monitor survivorship, Osborne and his colleagues rely on a combination of laboratory diagnostics and imaging modalities after treatment has concluded, including CTs, bone scans, and PSMA PET/CT. Depending on different theranostic programs, SPECT/CT can be utilized during this step.

Osborne discusses John's positive response with theranostics with John and his partner Mary.

He notes that the theranostic approach is evolving rapidly, and post-therapy follow-up and monitoring vary among practices. "Every place I talk to handles it differently," Osborne says, "and we're all trying to figure out the best way."

Ongoing development of theranostics therapies

Osborne noted that the results of clinical trials that are currently examining the use of theranostic treatment using different radioisotopes and in patients who have not undergone chemotherapy have the potential to dramatically expand the number of patients eligible for treatment. He and his colleagues provide theranostic PSMA therapy to between 5 to 10 patients each week, but he is already thinking about the increased need for infusion rooms and scanners that can handle an increase in patient volume.

"We have everything we need for the volume that we have right now, but I know we're going to need to do between 10 and 15 per week in a year, and then maybe 15 to 20 per week the year after, so I have to think about not letting what we have right now be our ceiling for growth, because I would like to grow as the indications grow."

Osborne believes advances in molecular imaging and the ongoing development of new theranostic therapies are creating a new era of personalized care. "We can't continue just throwing doses at patients," Osborne says. "The best theranostics is going to figure out which patients benefit, how, when, and with what kind of dose. And it's going to be different in different people."

He points out that the current guidelines for the use of PSMA theranostics specify that patients are

"For medical centers that are starting to put together a program, I would say 'the water is good, come on in.'"

Joseph Osborne, MD, chief of Molecular Imaging and Therapeutics, New York City, USA

eligible for treatment after unsuccessful treatment with chemotherapy, but several clinical trials are underway that could expand patient eligibility to include patients who have not received or are currently undergoing chemotherapy.

"If we find out that there are positive results in these trials, then all of a sudden we're looking at many more patients," Osborne says. "If they don't have to fail chemo, they're pre-chemo, they're less sick and more numerous, so I see the number of indications for the therapy potentially becoming more plentiful on a six-month basis. Every six months, we're going to learn something that's going to say, expand, or stay the same. And I haven't seen yet anything that says stay the same."

When asked about what he thinks about the future of theranostics, "The more places that do it, the better," Osborne says. "For medical centers that are starting to put together a program, I would say 'the water is good, come on in.'" ●

Sameh Fahmy, MS, is an award-winning freelance medical and technology journalist based in Athens, Georgia, USA.

For More Information

siemens-healthineers/theranostics

siemens-healthineers.com/prospecta

siemens-healthineers.com/petct

References

1 Yordanova A, Eppard E, Kürpig S, et al. Theranostics in nuclear medicine practice. *Onco Targets Ther*. 2017;10:4821-4828. Published 2017 Oct 3. doi:10.2147/OTT.S140671

2 Baum RP, Kulkarni HR, Schuchardt C, et al. 177Lu-Labeled Prostate-Specific Membrane Antigen Radioligand Therapy of Metastatic Castration-Resistant Prostate Cancer: Safety and Efficacy. *J Nucl Med*. 2016;57(7):1006-1013. doi:10.2967/jnumed.115.168443

3 DOI: 10.1200/JCO.2022.40.16_suppl.5002 *Journal of Clinical Oncology* 40, no. 16_suppl (June 01, 2022) 5002-5002. Published online June 02, 2022.

The statements by Siemens Healthineers customers described herein are based on results that were achieved in the customer's unique setting. Since there is no "typical" hospital and many variables exist (e.g., hospital size, case mix, level of IT adoption), there can be no guarantee that other customers will achieve the same results.

The statements by the patient and his partner in this article are their own specific experiences and opinions based on a clinical experience specific to the individual patient; they do not represent Siemens Healthineers views or opinions. Readers are cautioned that since there is no typical patient case and many variables exist, the outcome of other examinations, even identical or comparable with the present individual patient case, might not achieve similar results. This article is not intended to make any claims that Siemens Healthineers Molecular Imaging technologies can be used to diagnose, treat, cure, mitigate, or prevent patient's disease. Clinical claims in this article have not been clinically proven and evaluated by the FDA and/or other regulatory authorities. The patient and his partner portrayed in the article were reasonably compensated for their time and effort to share their story for this article.

The photography shooting took place under all necessary health and safety measures according to local COVID-19 regulations.

Data courtesy on file.

A patient's experience: Theranostics offers personalized care for prostate cancer

Enabled by molecular imaging technology, theranostics using a PSMA-targeted radioligand therapeutic agent has the potential to enhance and prolong life for prostate cancer patients such as John. "I was able to feel more of myself. It was remarkable," he says.

By Sameh Fahmy | Photography by James Farrell

John and Mary in their kitchen in New York City.

When John was first diagnosed with prostate cancer 15 years ago, his level of prostate-specific antigen (PSA) was 650. Within in a week, it jumped to 1,350, and his prognosis was bleak. "I was told that I would have from three months to three years, possibly, if I had decent treatment," the 78-year-old recalls.

After beginning chemotherapy, the treatments soon fell into a familiar and disturbing pattern: the benefits of each round of chemotherapy would ultimately be outweighed by the side effects he experienced. Over time, his options became limited, and eventually he was offered hospice care. Theranostics changed the trajectory of his disease and his life.

What is theranostics?

Theranostics is an innovative form of personalized therapy that focuses on both the accurate selection of patients and providing them with targeted radioligand therapy to improve their prognosis.[1] Theranostics refers to structurally similar diagnostic and therapeutic agents that share a molecular-specific target. Molecular targets are proteins on the surface of cancer cells and where the radioligand will bind. Throughout the theranostics process, molecular imaging techniques are used to identify, personalize, and monitor therapy response. Pharmaceuticals, such as radioligands, are used to target and treat specific areas.[2] A radioligand is made up of a radioisotope that damages cancer cells and a target ligand that binds to specific markers on cancer cells.

"The concept of theranostics has been around for decades, but it's really become actionable and exciting now because there are several prospective clinical trials showing a huge benefit," says Joseph R. Osborne, MD, PhD, chief of Molecular Imaging and Therapeutics and professor of radiology at a leading academic institution's hospital in New York City, USA.

A targeted, personalized approach

Radioisotopes of sodium iodide have long been used to diagnose and treat thyroid cancer, but Osborne notes that

Diagnosis and patient selection: John receives a PET/CT scan as part of the selection process.

Personalized treatment: Lab technician carefully prepares the radioligand therapy targeted specifically for John.

the recent development of theranostic agents that bind to prostate-specific membrane antigen (PSMA)—the antigen that is overexpressed in 90% of prostate malignancies[3]—has resulted in a significant expansion of the number of patients who can benefit from theranostics. Prostate cancer is the second most common cancer in men and the third leading cause of cancer death in men in the western hemisphere.[4]

With theranostics, patients are injected with radioactive isotopes linked to molecules that bind specifically to tumors. A PET/CT scan may be used to localize tumors within patients and also to assess how much of the radioisotope tumors take up. Once this targeting step is completed, the diagnostic isotope is replaced with a therapeutic agent that kills cancer cells by delivering radiation directly to tumors. This targeted, personalized approach has the potential to reduce side effects for patients and improve outcomes.

Patient's theranostics care pathway

The theranostics care pathway for the patient involves a series of steps and a range of laboratory diagnostic and imaging modalities. Beginning with patient selection, additional steps include personalized treatment, therapy response monitoring, and follow-up and survivorship monitoring. Read on to follow John along the theranostics care pathway.

Diagnosis and patient selection

John, a stage 4 prostate cancer patient, had been athletic for most of his life but by 2022 had deteriorated to the point where he could barely get out of bed. Of particular concern was that some of

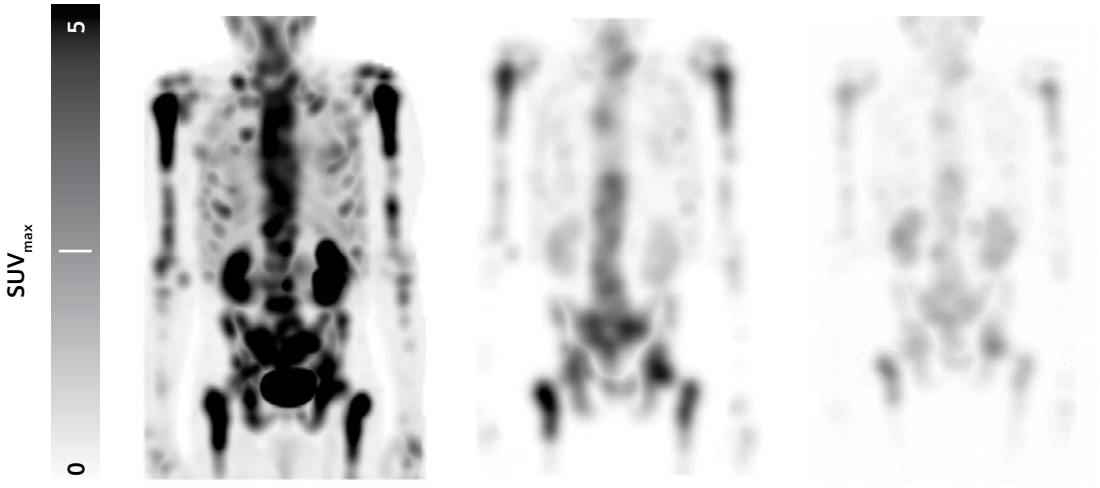

^{177}PSMA SPECT maximum intensity projection (MIP) images acquired throughout John's personalized treatment to assess therapy response. From left to right: coronal SPECT MIP cycle 1, coronal SPECT MIP cycle 3, and coronal SPECT MIP cycle 6. Data courtesy on file.

Therapy response monitoring: Osborne met regularly with John and Mary to discuss John's response throughout his six-week treatment cycle.

Follow-up and survivorship monitoring: Osborne and the nuclear medicine team review images from the PET/CT.

the side effects of his chemotherapy treatments, like numbness in his hands, could be permanent. He felt that the clinical trials he was eligible for were too physically demanding given his age and condition. Theranostic treatment offered new hope for John. He said it seemed like something he could tolerate, even in his severely weakened state.

Patients with metastatic castration-resistant prostate cancer (mCRPC) who have been treated with androgen receptor (AR) pathway inhibition and taxane-based chemotherapy qualify to undergo prostate cancer radioligand therapy.

In order to qualify for a prostate cancer radioligand therapy, patients must undergo a PSMA-ligand PET/CT to confirm PSMA expression in tumors. Based on the results of his PSMA PET/CT scan and his no-longer-successful hormone and chemotherapy treatments, John was eligible for theranostic treatment. After discussing it with his wife, Mary, and Osborne, he decided to undergo treatment.

"I was very weak when I came in to see Dr. Osborne, and we decided that this would be a good alternative," he says. "There were six treatments, six weeks apart, and that was appealing to me because I had time in between."

Personalized treatment

A patient receives pesonalized treatment based on molecular imaging with the diagnostic targeted radioligand to determine if the patient can benefit from a therapeutic radioligand. John began his treatment in April 2022. He experienced some nausea and vomiting after his first treatment, but those side effects quickly abated.

Mary was surprised to see him making breakfast the morning after

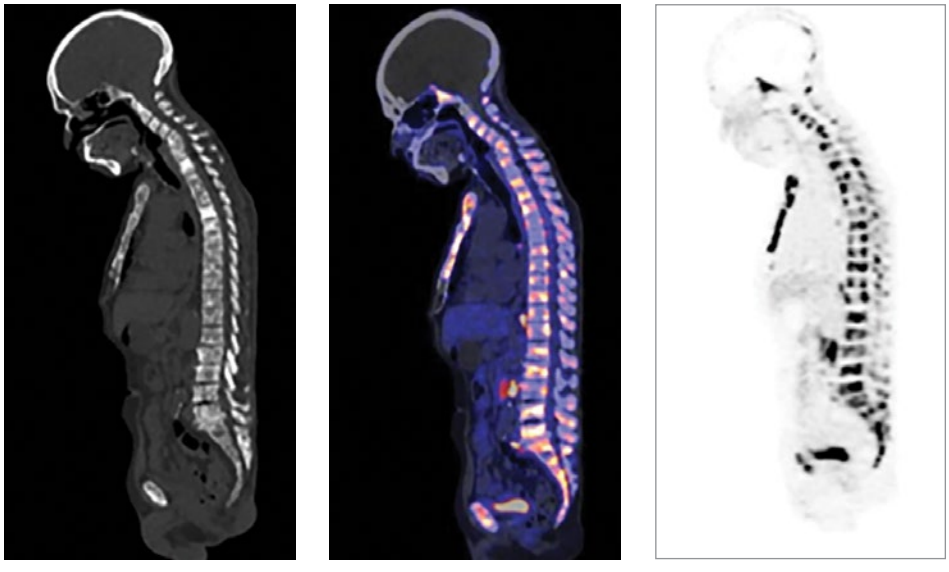

^{68}Ga-PSMA PET/CT images of John were utilized in the selection step to ensure he received the right treatment at the right time. From left to right: sagittal CT only, sagittal fused PET/CT, and sagittal PET only. Data courtesy on file.

John was able to prepare breakfast for Mary following his first theranostics treatment.

Osborne and John formed a close relationship during John's treatment and continues today.

his first treatment. "I couldn't believe it," she recalls. "He said, 'Mary, would you like some breakfast?' And I said, 'Well, of course!' He was very energetic, and we even have video of him dancing in August after his second treatment at our grandson's party. And I mean he is dancing," says Mary emphatically.

Therapy response monitoring

Monitoring response to therapy continues throughout the treatment regimen. John's physicians monitored his therapy response throughout his six treatments, which soon became an almost comfortable routine. He drove himself to the hospital, greeted staff, had his blood counts checked, and underwent infusion and then post-infusion quantitative SPECT/CT scanning.

John recalls that when his treatment first began, each visit to the hospital took between four and five hours. These visits combined scanning and infusions. As his treatment progressed, his physicians separated his treatment and post-imaging quantitative SPECT/CT over separate days to reduce the time he needed to be at the hospital in one sitting. Regardless of the protocol they used, he felt well enough to drive himself home.

"Dr. Osborne and the whole staff made me feel comfortable and genuinely cared about," he says. "I walked in for my third treatment and they said 'How do you feel, John?' and I did a little jig. They all laughed at that, and it was indicative of my improvement."

Follow-up and survivorship monitoring

Imaging and laboratory diagnostics play a vital role in post-therapy monitoring and follow-up. John says that in addition to increases in physical stamina—like his ability to climb stairs without becoming winded—he soon began to notice an improvement in his mental and emotional state. "It has a psychological effect on you to feel like you're unable to do anything, and your self-worthiness gets so low," he says.

He is now back to everyday tasks that he simply did not have the energy for

"I walked in for my third treatment and they said 'How do you feel, John?' and I did a little jig... It was indicative of my improvement."

John, prostate cancer patient, New York City, NY, USA

From left to right: Dr. Joe Osborne, Mary, and John

before, like paying the bills, and he has even been able to travel again. He continues to see his physicians for regular follow-up and monitoring, and he and his wife both emphasize how grateful they are.

John and Mary's experience

Theranostics has enabled John to return to a level of functioning that was almost inconceivable prior to his treatments. He and Mary urge families in similar situations to seek out the care they need.

"If I could give advice to anyone, I would say do your due dillegence," John says. "Also, the thinking starts to shift as you receive these treatments, and you begin to hold on to those positive affirmations and ways of thinking about yourself in a greater way. " When asked about her thoughts now that John is feeling stronger and has energy to do things again, Mary adds, "Being thankful and having gratitude is a very powerful thing." ●

Sameh Fahmy, MS, is an award-winning freelance medical and technology journalist based in Athens, Georgia, USA.

For More Information

siemens-healthineers/theranostics

siemens-healthineers.com/prospecta

siemens-healthineers.com/petct

References

1 Yordanova A, Eppard E, Kürpig S, et al. Theranostics in nuclear medicine practice. *Onco Targets Ther*. 2017;10:4821-4828. Published 2017 Oct 3. doi:10.2147/OTT.S140671

2 Baum RP, Kulkarni HR, Schuchardt C, et al. 177Lu-Labeled Prostate-Specific Membrane Antigen Radioligand Therapy of Metastatic Castration-Resistant Prostate Cancer: Safety and Efficacy. *J Nucl Med*. 2016;57(7):1006-1013. doi:10.2967/jnumed.115.168443

3 Silver DA, Pellicer I, Fair WR, Heston WD, Cordon-Cardo C. Prostate-specific membrane antigen expression in normal and malignant human tissues. *Clin Cancer Res*. 1997;3(1):81-85.

4 Gomes Marin, José Flávio et al. "Theranostics in Nuclear Medicine: Emerging and Re-emerging Integrated Imaging and Therapies in the Era of Precision Oncology." *Radiographics : a review publication of the Radiological Society of North America, Inc* 40 6 (2020): 1715-1740

The statements by Siemens Healthineers customers described herein are based on results that were achieved in the customer's unique setting. Since there is no "typical" hospital and many variables exist (e.g., hospital size, case mix, level of IT adoption), there can be no guarantee that other customers will achieve the same results.

The statements by the patient and his partner in this article are their own specific experiences and opinions based on a clinical experience specific to the individual patient; they do not represent Siemens Healthineers views or opinions. Readers are cautioned that since there is no typical patient case and many variables exist, the outcome of other examinations, even identical or comparable with the present individual patient case, might not achieve similar results. This article is not intended to make any claims that Siemens Healthineers Molecular Imaging technologies can be used to diagnose, treat, cure, mitigate, or prevent patient's disease. Clinical claims in this article have not been clinically proven and evaluated by the FDA and/or other regulatory authorities. The patient and his partner portrayed in the article were reasonably compensated for their time and effort to share their story for this article.

The photography shooting took place under all necessary health and safety measures according to local COVID-19 regulations.

Data courtesy on file.

The Comprehensive Cancer Center, Helsinki, Finland

Growing theranostics program is now everyday clinical practice in Finland

As a true pioneer in the frontier in cancer treatment, The Comprehensive Cancer Center in Helsinki offers precision therapy personalized to the needs of each individual patient.

By Claudette Lew | Photography by Matti Immonen

The new facilities at The Comprehensive Cancer Center were opened in early 2023, equipped with the latest molecular imaging equipment accessible to the multidisciplinary staff who provide theranostics to patients.

Most theranostics programs are housed within the Molecular Radiotherapy Unit at the center, and the unit has seen a significant increase in theranostics patients in recent years.

Cancer treatment has made tremendous progress in recent years, and the latest advancement in precision therapy is theranostics. Theranostics is the combination of therapy and diagnostics, pairing diagnostic biomarkers with therapeutic agents that share a specific target present in diseased cells or tissues. This new frontier in cancer treatment offers highly specific therapies that are revolutionizing how clinicians treat cancer.

"There's a lot of excitement around theranostics right now," said Veera Ahtiainen, MD, oncologist in the Molecular Radiotherapy Unit at The Comprehensive Cancer Center in Helsinki, Finland. Part of HUS Helsinki University Hospital, The Comprehensive Cancer Center is a world-renowned center for the treatment of cancer patients, using theranostics to treat many of them. "There's a clear advantage in its possibilities to be used in prediction, for personalization in treatment, and to provide precision medicine for cancer patients. We can diagnose and treat cancer, evaluate and measure the effectiveness of a given treatment, and carry out a treatment in a more targeted manner. We can better influence the care path of cancer patients and improve the patient's quality of life."

An established theranostics program

The unit is an integral part of The Comprehensive Cancer Center and uses a combination of molecular imaging and targeted radiotherapy to diagnose and treat cancer patients. As the country's largest and most versatile cancer center, it continues to be a critical resource for patients throughout Finland, reaching those living as far north as Lapland. The Comprehensive Cancer Center recently designed and built new state-of-the-art facilities to continue serving Finland's patient communities. The new center opened in early 2023, equipped with the latest molecular imaging equipment directly accessible to the multidisciplinary staff who provide theranostics and other cancer treatment to patients.

The team has seen the number of theranostics patients double in the last seven years, especially with the approval of prostate-specific membrane antigen (PSMA) labeled with lutetium 177 (^{177}Lu-PSMA) as a treatment for prostate cancer. At present, roughly 60 percent of their theranostics treatments are for prostate cancer, and 40 percent are

for treating neuroendocrine tumors, thyroid cancers, and other malignancies to a minor extent.

"Most theranostics programs are housed within The Comprehensive Cancer Center," explained Dr. Ahtiainen. "As an oncologist, I work directly with Vappu Reijonen, our physicist, on planning radiotherapies for all of our cancer patients."

Oncologist Veera Ahtiainen and medical physicist Vappu Reijonen collaborate closely to plan radiotherapies for all cancer patients, as the Molecular Radiotherapy Unit is a part of the radiotherapy department of The Comprehensive Cancer Center in Helsinki.

PET/CT for patient selection

The Molecular Radiotherapy Unit uses a combination of imaging techniques, including PET/CT, to determine the location and extent of the cancer in the patient's body. Patient selection is the first step in theranostics. "We use image-guided patient selection," explained Dr. Ahtiainen. "Usually, we need to see an uptake in the tumor volume in a patient's diagnostic PET/CT. Patient selection for theranostics treatment is then determined in multidisciplinary meetings with our clinicians." Utilizing the available diagnostic information, the team can design a personalized treatment plan that is tailored to the patient's individual needs.

SPECT/CT for imaging-enabled treatment evaluation

Another benefit of the theranostics approach is the potential, through quantitative SPECT/CT imaging, to measure treatment effectiveness. The team uses quantitative SPECT/CT, for example, to monitor the patient's response throughout the treatment and adjusts the treatment plan as necessary. The Molecular Radiotherapy Unit also performs SPECT/CT-based dosimetry to ensure the patient receives the most effective treatment possible while minimizing any potential side effects.

"Once patients begin treatment, we perform post-therapy imaging with our SPECT/CT. To individualize the treatment, molecular imaging is extremely valuable from a clinical perspective," explained Vappu Reijonen, medical physicist, "because molecular imaging not only allows us to determine patients who benefit from the treatment, but it also allows us to see exactly what we treat. I believe that all around the world, people are beginning to realize the importance of imaging and its role in making treatments like theranostics optimal."

At The Comprehensive Cancer Center, patients are evaluated with Siemens Healthineers Symbia Pro.specta™ SPECT/CT after each cycle of theranostics treatment. "Post-treatment scanning is a very important part of the process here," noted Dr. Ahtiainen. "From the post-treatment scans, we assess, together with laboratory results and the patient's clinical condition, the safety and tolerability of the

"There's a clear advantage in its possibilities to be used in prediction, for personalization in treatment, and to provide precision medicine for cancer patients."

Veera Ahtiainen, MD, oncologist in the Molecular Radiotherapy Unit at The Comprehensive Cancer Center in Helsinki University Hospital, Helsinki, Finland

treatment, and that we are seeing uptake in the tumor tissue, in comparison to normal tissue uptake. Cycle by cycle, we can observe the changes in the uptake in the tumor tissue and how the organs at risk are getting the accumulated dose. It's important for us to approach theranostics treatments from the perspective of using quantification and dosimetry for safety, as well as tracking effectiveness."

Facilitating the theranostics workflow

Considering the high volume of patients The Comprehensive Cancer Center sees for post-treatment scanning, the team routinely uses Symbia Pro.specta SPECT/CT system to facilitate their theranostics workflow. "We've designed our workflow to accommodate our patient volume so that it's feasible for us, but also for our patients. During scans, patients need to breathe freely and sometimes move. It's really important that the patient is comfortable during imaging, and with respiratory motion correction, we can minimize those artifacts," explained Reijonen.

The team relies on the system's intuitive interface and features that automate steps across the workflow to support them from patient setup through final imaging, resulting in consistent, reproducible studies. "The system is well-designed," noted Dr. Ahtiainen, "and has features that save time and are more practical, which can have a huge impact. Using the features on our Symbia Pro.specta, we can now implement treatment assessment and dosimetry more efficiently. We also utilize the system to perform diagnostic studies as well when needed."

Evolving theranostics into routine clinical practice

Although theranostics treatment is part of the everyday clinical practice at The Comprehensive Cancer Center, many more patients around the world can benefit from more precise and targeted cancer treatments, which can impact clinical outcomes. The Molecular Radiotherapy Unit at The Comprehensive Cancer Center is constantly evaluating the effectiveness of its treatments through ongoing research and clinical trials. This ensures that the unit's treatment protocols are based on the latest scientific evidence and are optimized for the best possible outcomes for patients.

"Theranostics has a long history, starting with radioactive iodine to treat thyroid cancer. Considering the imaging resources we have and the different software that has been developed for quantification and dosimetry, new treatments can quickly become part of the clinical routine," explained Dr. Ahtiainen. "But before we can apply theranostics treatments, it requires functioning facilities, expertise, and of course, the staff. It's important for us to spread awareness about using radiopharmaceuticals in cancer treatment. We have had a lot of visitors here in our new facility, and we're happy to share our best practices. We can show them how we implement treatments and what it requires from us or the patients."

"We've seen many successful, significant, and long-lasting positive treatment responses," added Reijonen. "It's nice to see that in heavily pre-treated patients, we have been able to deliver these treatments without difficulties with the tolerability, encouraging us to continue and develop further treatments."

The team is working on publishing data to support the effectiveness of theranostics treatments and highlighting some of their work.

The Symbia Pro.specta in Helsinki was installed in 2022 as the second in Europe for clinical use. "I think it was exciting for us all," said Reijonen.

"Our nuclear medicine technologists have given a lot of positive feedback about the everyday user-experience when imaging with Symbia Pro.specta," noted Reijonen.

"Molecular imaging not only allows us to determine patients who benefit from the treatment, but it also allows us to see exactly what we treat."

Vappu Reijonen, medical physicist, PhD, Molecular Radiotherapy Unit at The Comprehensive Cancer Center in Helsinki University Hospital, Helsinki, Finland

This research even includes optimizing existing treatments, such as radioactive iodine for thyroid cancer, and working on clinical trials with alpha-emitting nuclides.

Pioneers in theranostics

The team at The Comprehensive Cancer Center are true pioneers in a new frontier in cancer treatment, offering precision therapy that is personalized to the needs of each individual patient. Expanding the role of molecular imaging from detection to tissue characterization, treatment efficacy prediction, and treatment response measurement, clinicians can deliver highly targeted theranostics therapies that are more effective than traditional treatments. With the potential to revolutionize the way cancer is treated, theranostics is an exciting development that continues to hold great promise for the future of personalized medicine and precision healthcare. ●

Claudette Lew is a freelance medical writer and editor.

For More Information

siemens-healthineers/theranostics

siemens-healthineers.com/prospecta

siemens-healthineers.com/petct

Symbia Pro-specta SPECT/CT is not commercially available in all countries. Due to regulatory reasons, its future availability cannot be guaranteed.

The statements by Siemens Healthineers customers described herein are based on results that were achieved in the customer's unique setting. Since there is no "typical" hospital and many variables exist (e.g., hospital size, case mix, level of IT adoption), there can be no guarantee that other customers will achieve the same results.

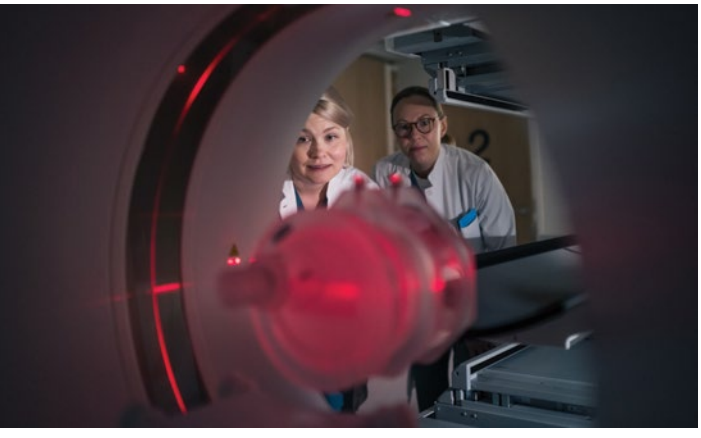

At the Molecular Radiotherapy Unit, Symbia Pro.specta is used for quantitative post-therapy imaging as well as for diagnostic nuclear imaging. "It is, of course, important to take good care of the regular quality assurance," says Reijonen.

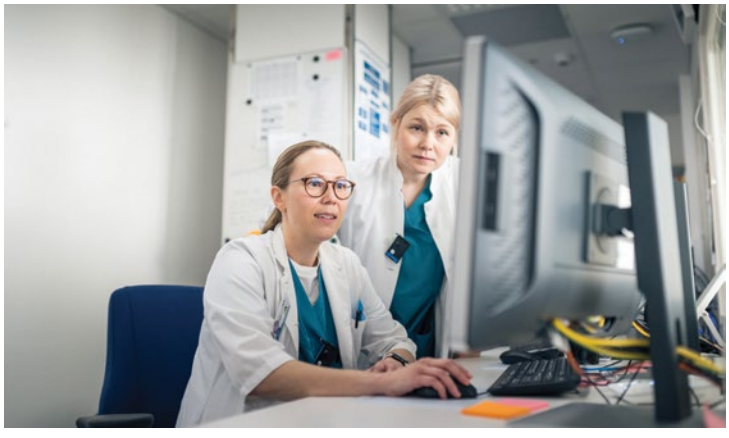

Reijonen and Ahtiainen collaborate on planning molecular radiotherapy, exemplifying the essential teamwork in cancer treatment.

Theranostics care pathway

Theranostics in comprehensive cancer care demands precision at every step of the patient care pathway. Learn more by visiting Siemens Healthineers Molecular Imaging's theranostics website. Explore our collection of case studies, videos, and product information.

Personalized treatment

Therapy response monitoring

Diagnosis and patient selection

Follow-up and survivorship monitoring

Our integrated value chain of precision oncology tools equips theranostics programs with state-of-the-art solutions at every step of the theranostics care pathway.

No matter where your institution is on its theranostics journey, we want to empower you with the tools you need to plan, implement, and expand your program. Together, let us set the standard in precision oncology to help patients get the right treatment at the right time.

Visit siemens-healthineers.com/clinical-specialities/theranostics or scan the QR code to learn more.

SCAN ME

SIEMENS Healthineers

Prof. Juhani Knuuti with Biograph Vision Quadra.
The radiowater generator used during water perfusion appears on the right.

The wisdom of water

Occasionally, technological progress opens the door for completely new realms of research. Such is the case at Turku PET Centre in Finland, where the Biograph Vision Quadra™ PET/CT is being used for total-body perfusion imaging—something that was simply not possible before.

By Philipp Grätzel von Grätz | Photography by Matti Immonen | Data courtesy of Turku PET Centre, Turku, Finland

PET imaging technology is very well suited to depict the function of a tissue. It does so by using radioactive substances, known as tracers. The best-known tracer is fludeoxyglucose injection F 18 (FDG)[a], a sugar-molecule that is enhanced with the radionuclide fluorine-18. It accumulates in sugar-hungry cancer tissue and is widely used to detect metastases. PET can also be used to image tissue perfusion. This is called perfusion imaging. Here, the aim is not to measure the blood flow in the big blood vessels, but rather how much blood is actually available in the periphery, in the tissues of the heart, the muscles, or any other organ.

Water as a tracer: In theory, almost perfect

"The PET tracers most commonly used for cardiac perfusion imaging are rubidium and ammonia," says Professor Juhani Knuuti, MD, from the PET Centre at Turku University. Rubidium is more comfortable to use, since it can be produced in a generator and does not require a particle accelerator, known as a cyclotron, on site. Both tracers have disadvantages, though, which is why Knuuti became interested in a different kind of tracer: radioactive water, or "radiowater." That was back in 1993 when Knuuti wrote his doctoral thesis on PET imaging and used radiowater as a tracer: "The images were terrible."

But terrible or not, the new tracer was there to stay. Radiowater is water that contains the isotope oxygen-15 (^{15}O). According to Knuuti, it has two distinct advantages over other tracers. "The clear benefit is that its half-life is short—only two minutes—meaning that the radiation dose for the patient becomes minimal. For a perfusion study, it is in the range of only 0.4 mSv, which is extremely low. You could basically repeat this examination as often as you liked without relevant risk."

Patients are scanned on Biograph Vision Quadra with the radiowater bolus infusion to a vein and with simultaneous adenosine stress infusion (syringe in the foreground).

Patient preparation is similar to any other perfusion study but radiowater delivery requires special equipment.

Prof. Knuuti examines total body perfusion images after the scan.

[a] Please see Indications and Important Safety Information for Fludeoxyglucose F 18 (^{18}F FDG) Injection on page 24. For full Prescribing Information, please see pages 70-72.

The second advantage of radiowater as a tracer is that it behaves like normal water. It is freely diffusible almost anywhere in the human body, making it—in theory—a nearly perfect tracer for perfusion images of the whole body. The downside of water's diffusivity is that perfusion cannot be visualized in the same way as with other tracers. "We need to do sophisticated image processing, and in order to do that properly, we need sensitive scanners and powerful software."

Making total-body perfusion a matter of minutes

In the late 1990s and early 2000s, PET scanners became more sensitive. As a result, the images generated by water perfusion PET imaging became "less bad." And this is how water as a tracer entered clinical routine, at least in some of the bigger PET centers with an on-site cyclotron—such as in Turku. "We started to use water in PET perfusion imaging of the heart routinely in 2005, and we have done thousands of scans since then," says Knuuti. In the meantime, medtech companies started to combine their PET scanners with CT scanners, transforming PET imaging into PET/CT imaging, which can depict tissue function and body anatomy at the same time.

These days, the PET Centre in Turku is taking another leap forward. A new Siemens Healthineers Biograph Vision Quadra PET/CT scanner was installed in May 2022. Knuuti is convinced that it has started an exciting new era in the 30 years history of water perfusion imaging. "So far, we have only been able to image individual organs, for example the heart or the brain. With Biograph Vision Quadra and water as a tracer, we can capture all other organs additionally for free. This scanner is so sensitive that we can do total-body water perfusion imaging within four minutes, without extra radiation."

Ongoing research on the interaction of heart and brain

Being able to analyze the perfusion in different parts of the body simultaneously is exciting because previously this was simply impossible, says Knuuti. "With total-body water

Located downstairs at the Centre, the particle accelerator makes the radioactive water.

The water is then pumped upstairs into the cylinder.

perfusion imaging, we are entering a new field of research. There are extremely interesting questions that we can ask now, for example about the impact of a disease on other parts of the body." In an ongoing research project, experts from the Turku PET Centre are looking into patients with myocardial ischemia, a disease with reduced perfusion of the heart muscle due to atherosclerosis. "We have no idea what happens in the other organs of these patients, specifically the brain or the kidneys. With total-body water perfusion imaging, we can now simply take a look."

Another example: It is well known that the brain and the heart interact in many ways, even in healthy individuals. But how exactly? And what does that mean for the oxygen supply and the oxygen distribution in the body in different situations? The question becomes clinically relevant, according to Knuuti, in patients who receive pharmacological stressors for diagnostic procedures. "Some patients feel very bad after these pharmaceuticals. Our hypothesis is that this might be related to perfusion changes in the brain—which is why we are looking into that in another research project."

With a little help from AI

Total-body water perfusion can be used in other medical specialties, too. In oncology, for example, standard total-body examinations with PET/CT can visualize glucose uptake in cancer cells, using the tracer FDG. But it could also be interesting to visualize tumor perfusion on a large scale. "Nobody has done that before because it wasn't possible. But let's see—it is a different dimension of information." Beyond total-body perfusion imaging with radiowater, Biograph Vision Quadra is also an interesting tool for research with other tracers. "In the European Biograph Vision Quadra consortium, different institutions use different types of tracers," says Knuuti. Some institutions are taking advantage of the low radiation doses made possible by Biograph Vision Quadra. Others use metabolic tracers to produce metabolic "maps" of the body for diseases in a way that was simply not feasible before.

"We have no idea what happens in the other organs of these patients, specifically the brain or the kidneys. With total-body water perfusion imaging, we can now simply take a look."

Professor Juhani Knuuti, MD, Turku PET Centre, Turku, Finland

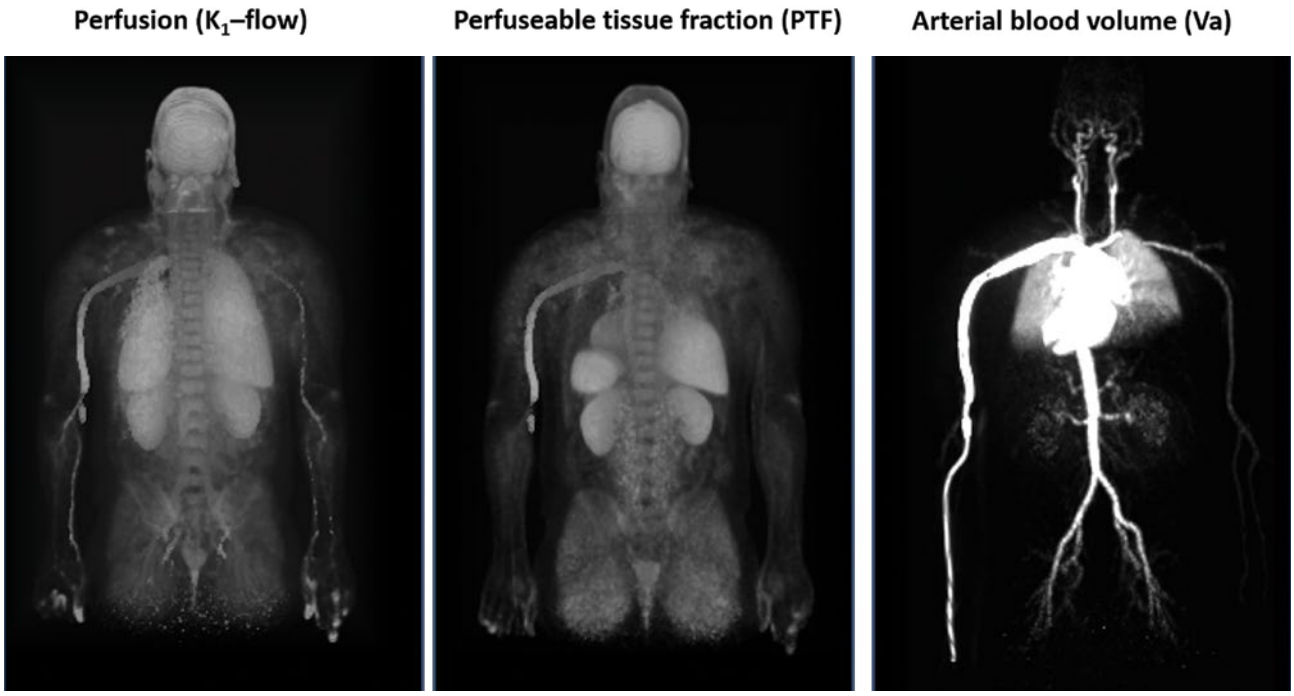

One of the first cases of total-body processed parametric images using ^{15}O-water as a tracer. The images are processed to three 3D parametric components: tissue perfusion, perfuseable tissue fraction, and arterial blood volume images. (Image created by Hidehiro Iida.)

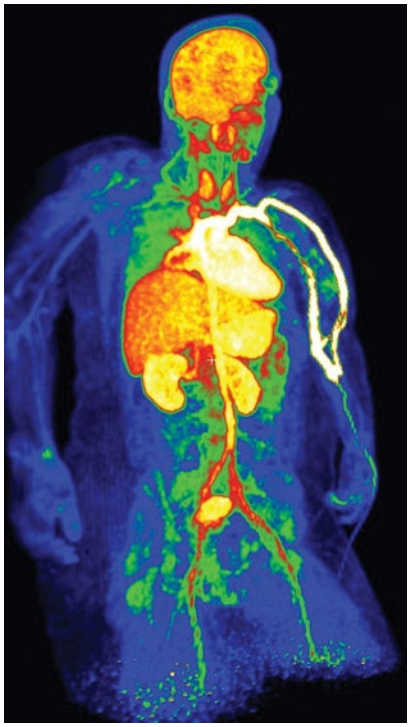

Summed dynamic 4-min ^{15}O-water MIP-image using total-body imaging with Biograph Vision Quadra. The tracer was injected into the arm vein located on the right side in the image. (Image created by Hidehiro Iida.)

Back to Turku: By end of February 2023, Knuuti and his team had already used total-body water perfusion imaging for more than 100 patients. Commercial water delivery devices are available to transfer the radiowater from the cyclotron swiftly to the patients. In terms of methodology, a mathematical modelling team is currently working on a segmentation software that relies heavily on artificial intelligence algorithms. "The idea is to automatically create a total-body perfusion map, so there is no need for any manual processing," says Knuuti. This work is well under way, and once tools like these are available, total-body water perfusion can be used in clinical routine. "I would be surprised if we didn't have a deliverable product soon. What will take longer is to fully understand how to read the scans." ●

Philipp Grätzel von Grätz lives and works as a freelance medical journalist in Berlin. His specialties are digitalization, technology, and cardiovascular therapy.

Biograph Vision Quadra is not commercially available in all countries. Due to regulatory reasons, its future availability cannot be guaranteed.

The statements by Siemens Healthineers customers described herein are based on results that were achieved in the customer's unique setting. Since there is no "typical" hospital and many variables exist (e.g., hospital size, case mix, level of IT adoption), there can be no guarantee that other customers will achieve the same results.

For More Information

siemens-healthineers.com/quadra

siemens-healthineers.com/molecular-imaging/news/biograph-vision-quadra-meet-and-greet

PETNET Solutions

Partnership Delivering Outcomes

MI PET Source

Helpful Information for everyday practice

PET knowledge for all

Expand your understanding of currently approved indications and applications in PET and PET/CT imaging:

- Oncology
- Neurology
- Cardiology
- Reimbursement information

Exclusive features for PETNET Solutions customers

Log in or register to access even more resources for practice growth:

- On-demand accredited webinars[1]
- Unbranded marketing toolkits
- New service checklists

And learn how PETNET Solutions can help you assess your market, design an action plan, and measure performance with our market data analysis program.

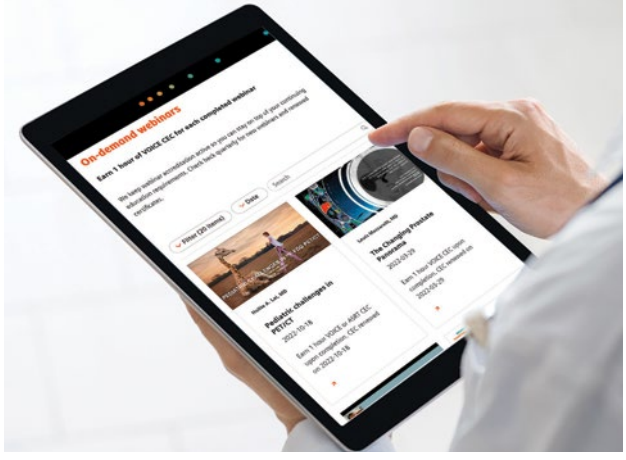

Visit today
MIPETSOURCE.COM

SIEMENS Healthineers

[1] *VOICE and ASRT accreditation available for select webinars*

Brazil and Argentina meet expanding patient needs with fast, low-dose PET/CT imaging

As populations grow around the world, safe and fast diagnostics and treatments are vital to meet patients' needs. Doctors in São Paulo, Brazil, and Buenos Aires, Argentina, discovered upgrading their PET/CT scanners enabled them to respond effectively to new patient demands and relieve scheduling pressures, and surpassed expectations by exploring new areas of care.

By Reinaldo Lopes | Photography by Ezequiel Scagnetti
Data courtesy of Cimed Diagnostic Imaging Center, La Plata, Argentina; and Dasa, São Paulo, Brazil.

La Plata, Argentina

Argentina and Brazil have a lot more in common than just their passion for football and the century-old World Cup rivalry it engendered. Between them, the two countries host more than half of South America's population. Both are now home to modern, intensely urbanized societies that have undergone a fast-paced demographic transition in the past few decades—with a growing proportion of middle-aged and elderly people in their midst. These rapid changes mean their need for high-quality, affordable healthcare will increase dramatically in the coming years.

New equipment for new challenges

Doctors in São Paulo, Brazil's largest metropolis, and La Plata, the charming capital city of Buenos Aires Province in Argentina, have found that the Biograph™ Horizon PET/CT scanner can be a powerful ally in coping with their new healthcare challenges. They have been able to achieve precise low-dose imaging quickly for patients with a variety of conditions, improving patient satisfaction as well as workflow.

"We were looking for a PET/CT system with time-of-flight technology, and Biograph Horizon was the perfect choice for us in terms of cost-benefit ratio," says Dalton Alexandre dos Anjos, MD, head of nuclear medicine and PET/CT at Dasa, a major diagnostic medicine company based in São Paulo. Dos Anjos is one of the directors of the Brazilian Society for Nuclear Medicine (SBMN). "In addition, the folks from our team had experience with the Biograph 16 PET/CT, so it was easier for them to adapt to this new system."

"Of course, it is a '*Formula One*' machine, but what made the most difference for us when choosing the PET/CT was the level of technical support available through our relationship with Siemens Healthineers," explains Mauro Piatti, MD, director of Cimed, a diagnostics clinic in La Plata. His team has been working with Biograph Horizon for the past six months.

Keeping pace with new challenges

Piatti's father, Gustavo Poggio, MD, led the founding of Cimed in 1991, and the clinic now receives about 15,000 patients a month for medical

The Cimed team, from left to right: Gustavo Poggio, MD, Cimed's founder; Mauro Piatti, MD, director, and Juan Cuesta, MD, radiologist and medical director, in front of Biograph Horizon.

Cimed Diagnostic Imaging Center in La Plata, Argentina.

Cuesta studying images from a Biograph Horizon PET/CT scan at Cimed, La Plata, Argentina.

imaging, from ultrasound and bone densitometry to PET/CT. "The referral is spontaneous—we are not associated with any hospital or medical group. Instead, many doctors choose to refer the patient to us," says Poggio.

According to Dos Anjos, one of the key ways to improve the patient experience in PET/CT is by reducing acquisition times. "The mean total scan time used to be about 20 minutes, and now we are scanning our patients in 15 minutes. It may seem like a small difference, but one needs to take into account the fact that most of them are oncologic patients who are suffering from pain," he explains. "Five minutes is actually a lot of time for them."

Another advantage of short acquisition times, according to Dos Anjos, is that there is less need to repeat scans due to inadvertent movements of tired patients—mainly in the region of the head—during longer sessions. He estimates that his team is now able to complete about three whole-body scans per hour. "The shorter acquisition times, lower doses, and fewer repetitions of the scans all add up to produce a great improvement to our patient workflow."

Importance of speed and image quality

"Speed is very important," agrees Poggio, "and so is imaging quality." The ability to detect smaller and smaller lesions has also been a marked improvement, says Dos Anjos. "I was skeptical about this before working with Biograph Horizon. Now we are performing some PSMA PET scans in which we are able to detect 5-millimeter lymph nodes with very sharp contours." The ability to identify such small lesions derives from Biograph Horizon's small LSO crystals and its true time-of-flight technology, enabling high spatial resolution and better signal-to-noise ratio than prior to using the technology.

Patients in La Plata are also being scanned in 15 minutes or even less time, says Juan Cuesta, MD, a radiologist and Cimed's medical director. He explains he and his colleagues do their utmost to wed

"We were looking for a PET/CT system with time-of-flight technology, and Biograph Horizon was the perfect choice for us in terms of cost-benefit ratio."

Dalton Alexandre dos Anjos, MD, head of nuclear medicine and PET/CT at Dasa, São Paulo, Brazil

this technological efficiency with the culture of personalized care that Cimed has always emphasized.

"One thing that we try to do differently here is to have the doctors always stay close to the patients, from the time they arrive until the end of the scan, asking detailed questions about their condition and explaining the process," says Cuesta. "The patient is not left alone at any time, being accompanied warmly, respectfully—and that makes a huge difference," adds Poggio. This approach has also been helpful when the need to scan pediatric patients arises. He adds that in most cases, the team has managed to do this without the need to anesthetize those patients.

Reduced radiation treatments

In Brazil, Dos Anjos' team at Dasa has seen a marked reduction in the dosage of radioisotopes, such as fludeoxyglucose F 18 (FDG)[a], in their routine exams. "We usually had to inject a dose with about 1.5 millicurie per kilogram of FDG to achieve good imaging. Now, we are down to about 0.8 to 1.0 millicuries—an almost 50% reduction," he continues. "Some of the oncologic patients are scanned every two to three months, so we are talking about a significant exposure to radiation. It's great if you can find ways to reduce it."

Although PET/CT scans in both centers are mainly focused on oncological treatments, Biograph Horizon has shown its usefulness for other specialties as well, such as neurology. "Five months ago, we

[a] Please see Indications and Important Safety Information for Fludeoxyglucose F 18 (^{18}F FDG) Injection on page 31. For full Prescribing Information, please see pages 70-72.

"One thing that we try to do differently here is to have the doctors always stay close to the patients, from the time they arrive until the end of the scan, asking detailed questions about their condition and explaining the process."

Juan Cuesta, MD, radiologist and medical director at Cimed, La Plata, Argentina

started to perform amyloid PET scans that are now commercially available in Brazil, and it's amazing," says Dos Anjos. "In the older population, it's not that specific to detect Alzheimer's disease, since about 30% of elderly people have a positive amyloid PET scan without having Alzheimer's. Now it's starting to become very useful in detecting the early stages of the disease in patients who are younger."

His Argentinian counterparts are doing similar work with Alzheimer's and neurodegenerative diseases like Parkinson's and epilepsy. According to Dos Anjos, there are also interesting possibilities to explore in cardiology. "The referral for endocarditis investigation is increasing, and it's amazing how we can detect small defects in the heart." The members of the La Plata team have also used their PET/CT capabilities to look for the causes of different medical conditions that have not been discovered by other methods.

Novel radioisotopes

Dos Anjos foresees exciting future research and clinical possibilities applying PET/CT, including the use of novel radioisotopes. "We are seeing a

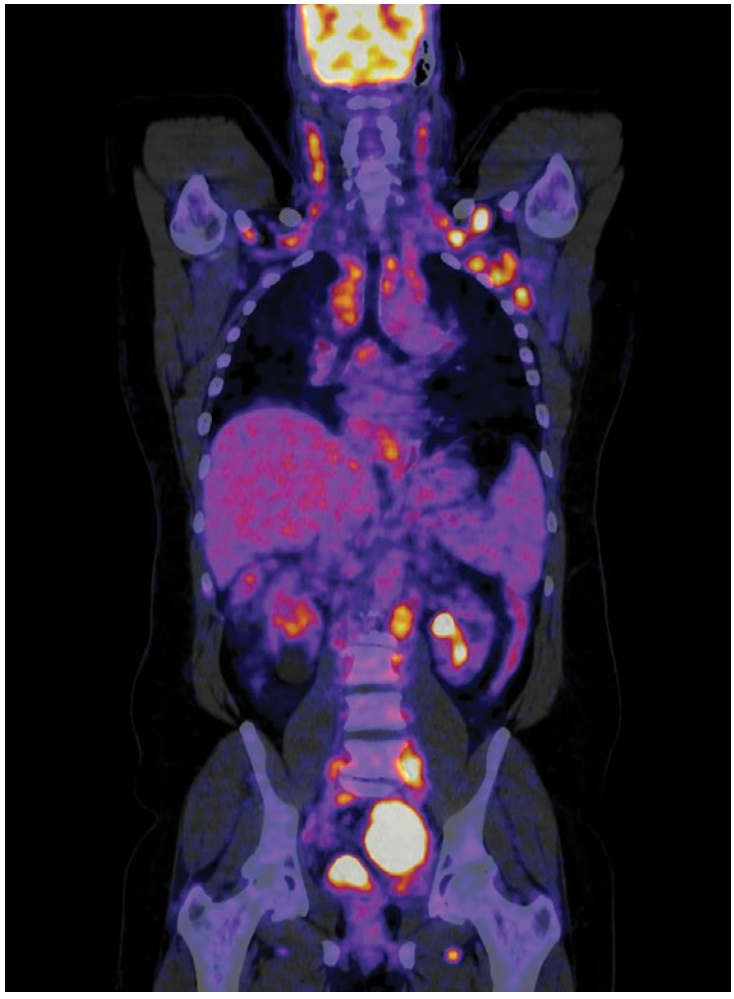

PET/CT-fused coronal image. Patient with follicular lymphoma diagnosed after incidental axillary lymphadenopathy. Staging ^{18}F FDG PET/CT scan to assess disease extent showed extensive nodal involvement, affecting cervical, axillary, mediastinal, and retroperitoneal lymph nodes. Data courtesy of Cimed, La Plata, Argentina.

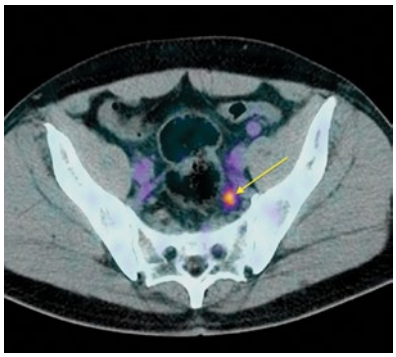

CT and PET/CT-fused axial images. A 59-year-old male patient with prostate adenocarcinoma underwent a PET/CT with 18F-PSMA-1007 for biochemical recurrence. PET/CT image showed a very small pelvic lymph node (5 mm) with high radiotracer uptake. Data courtesy of Dasa, São Paulo, Brazil.

PET maximum intensity projection (MIP) image. Data courtesy of Dasa, São Paulo, Brazil.

lot of clinical trials testing PSMA-lutetium in association with other drugs in the earlier clinical stage of prostate cancer. PET images are being used more and more in these clinical trials, and I think they will be essential to patient selection and to treatment risk monitoring."

Dos Anjos and his colleagues are also using Biograph Horizon to monitor treatments via radioembolization, using labeled microspheres. After the treatment, the patients receive a PET scan. "It's a very nice way of making sure that the microspheres have been correctly delivered to tumors," he explains. "Imaging is fundamental to monitor any treatment." ●

Reinaldo José Lopes is a science and health writer at *Folha de S. Paulo*, Brazil's leading daily newspaper, and is the author of several books.

For More Information

siemens-healthineers.com/BiographHorizon

siemens-healthineers.com/retropharyngeal-case

siemens-healthineers.com/mi-pet-source

siemens-healthineers.com/tamaki

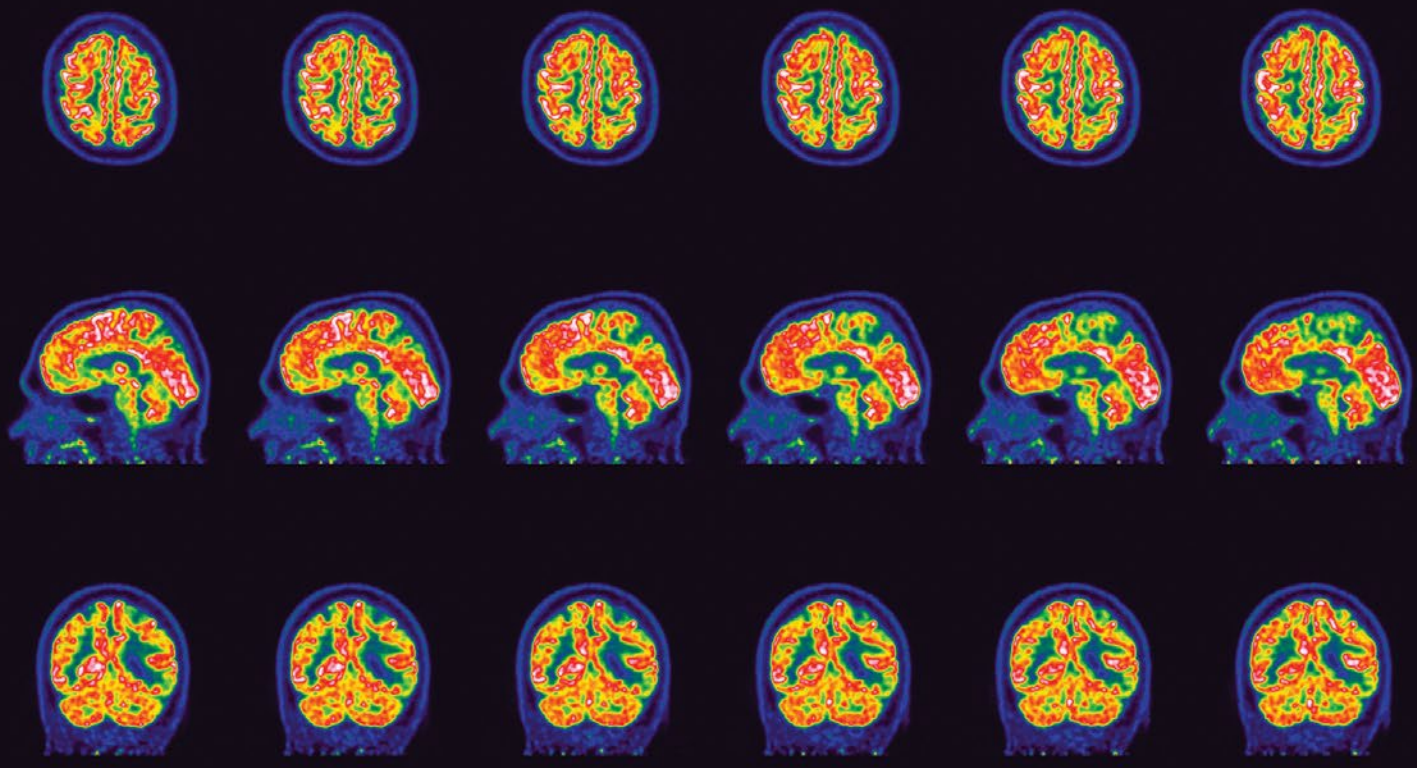

Data courtesy of Main Line Health, Pennsylvania, USA.

Image-based selection of Alzheimer's disease therapy

PET imaging and emerging immunotherapy candidates are beginning to enable image-based therapy personalization for dementia.

By Takeshi Shimizu, PhD

A growing number of senior citizens across the globe, as well as the spectrum of society, are affected by dementia due to Alzheimer's disease (AD). According to the World Health Organization, currently more than 55 million people live with some form of dementia worldwide, 60-70% of which is attributed to AD.[1] At first, the onset of cognitive decline can be as subtle as a change in mood or irritability. Many start to suffer from symptoms, such as impairment in linguistic skills, much sooner than receiving their official diagnoses of dementia.

"Accumulation of senile plaques in the brain is the first recognizable sign of Alzheimer's dementia, followed by neuroinflammation and tauopathy. Beyond that, it starts to affect brain anatomy by neurodegeneration," says Babak Tousi, MD, a neuro-geriatrician at a world-renowned brain health center based in the midwestern United States. Conventional diagnosis of AD requires exclusion of other potential underlying conditions, making distinctions of similar dementia symptoms and cognitive profiles difficult. Recently, biological factors were added to the AD definition, such as the presence of a specific protein abnormalities in the brain. More specifically, these abnormalities include extracellular deposition of amyloid plaques and aggregation of intracellular neurofibrillary tangles due to hyperphosphorylated tau proteins. Amyloid is a generic name of protein debris. In the case of AD, a receptor protein on the neuron called amyloid precursor protein (APP) breaks down into small peptide fragments, and the delayed clearance and aggregation of such debris would cause functional impairment in neurons.[2]

"We're talking about breakdown of APP, releasing monomers, monomers attaching to each other to form oligomers, and oligomers to protofibrils and ending up as amyloid plaques. These senile plaques then set out the inflammatory process and tau fibrils," Tousi explains. This idea of disease progression, wherein amyloid accumulation triggers the cascade of neurodegenerative events, is called amyloid hypothesis.[3] "Over the last couple of decades, most of the research for discovery of disease-modifying therapies was focused on somehow manipulating the cycle of events associated with amyloid pathology. For example, some of those developments focused on beta-secretase and gamma-secretase, enzymes that break down amyloid precursor proteins. Unfortunately, these studies were unsuccessful."

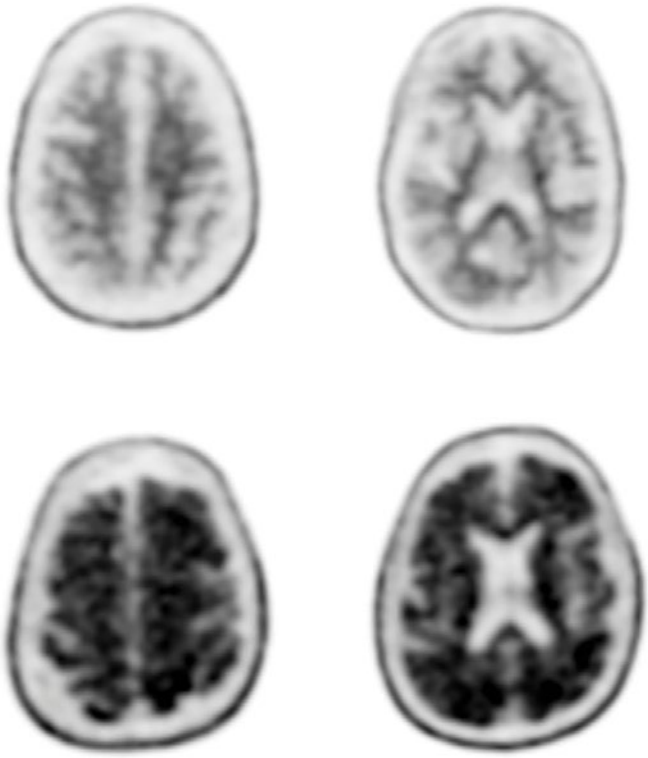

Examples of amyloid-PET scans. Top: amyloid negative scan. Bottom: amyloid positive scan. Data courtesy of University of Tennessee Medical Center, Knoxville, Tennessee, USA.

Drug discovery and clinical development

This lack of pharmacological intervention, progressive devastation in quality of life, and the associated social costs have propelled the recent drug discovery and clinical development in AD. "There are three different types of pharmacological therapies currently available for Alzheimer's disease: cognitive enhancers like the cholinesterase inhibitor family and an N-methyl-D-aspartic acid (NMDA) receptor antagonist, medications for management of neuropsychiatric symptoms, and more recently disease-modifying monoclonal antibodies that most of our current research is focused on," explains Tousi.

The loss of neuronal communication mediated by a neurotransmitter acetylcholine is often observed in the Alzheimer's brain. "First of all, drugs that can prevent the degradation of acetylcholine in the synapse are shown to provide modest improvement in cognition. The second category is antipsychotic or antidepressants. Such drugs may be administered to manage behavioral symptoms, such as depression, irritability, and agitation, but they will not reverse or slow down the progression of the disease," Tousi explains. "The third category is about disease-modifying therapeutics. Recently, a therapeutic agent was approved based on the fact that it can decrease amyloid plaques in the brain. We continue to do more trials for this agent as a part of open label study and a new randomized clinical trial, so there's going to be more safety and efficacy data."

Many of these disease-modifying therapeutics belong to a class of macro-protein agents called monoclonal antibodies. Monoclonal antibodies are antibodies that are made by selected cultured immune cells that bind to a specific epitope. In the case of AD, the target molecule is a various soluble and insoluble species of APP. When bound by antibodies, these amyloid debris can be recognized by the immune cells and get cleared away.[4] Clinical trials showed that treatment with these monoclonal antibodies can reduce amyloid plaques in patients' brains.[5,6]

Biomarkers for specific targets

In positron emission tomography (PET) brain imaging, radioactive imaging agent for specific targets—or biomarkers—are injected into the patient's bloodstream, and in vivo accumulation of the biomarker is imaged under a PET camera. As such, the first signs of neuropathological changes can be detected without removal of the brain biopsy specimen. For cognitive disease related to AD, there are two kinds of PET biomarkers approved for clinical use. The first biomarker is an imaging agent used to estimate amyloid neuritic plaque density. Currently, there are three approved amyloid PET imaging biomarkers. The second biomarker targets aggregation of intracellular neurofibrillary tangles due to

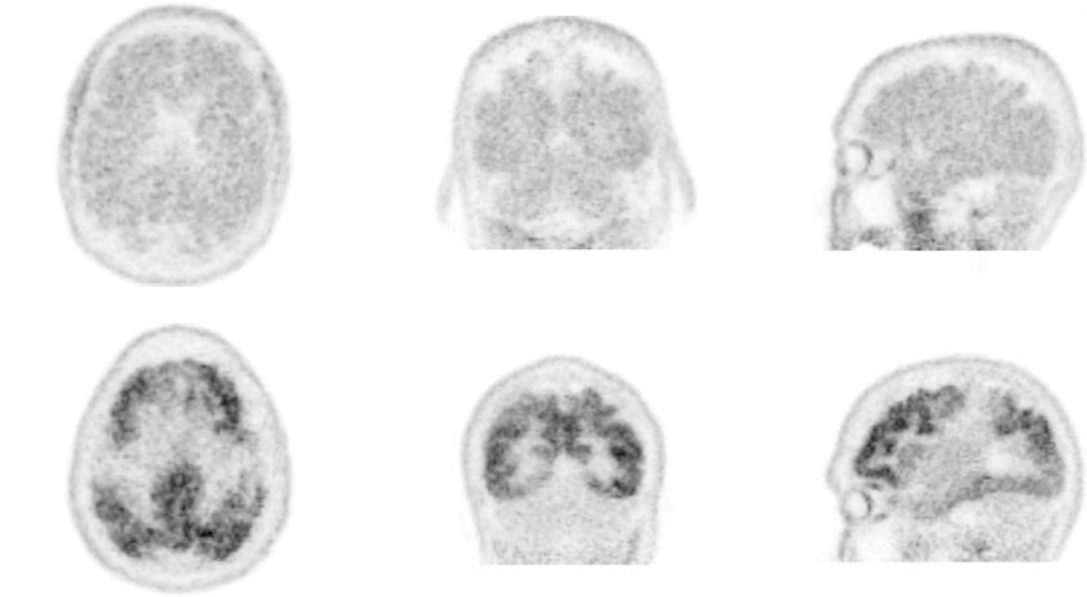

Examples of tau PET scans. Top: tau negative scan. Bottom: tau positive scan. Data courtesy of ADNI database.

hyperphosphorylated tau proteins. The U.S. Food and Drug Administration (FDA) approved one such biomarker in May 2020.[7]

In current clinical trials, these Alzheimer's imaging biomarkers are used for selecting the suitable patient population that may benefit from investigational drugs being tested. "Clinical trial participants undergo cognitive testing, but aside from that, they undergo amyloid imaging," explains Tousi. "Based on how much amyloid plaque they have in their brains, they may be qualified to participate in trials to receive anti-amyloid therapy."

The PET biomarker for tau neurofibrillary tangles may have additional value. "Having more amyloid plaque in the brain doesn't mean that the person is more forgetful than others, simply put. But it seems that the more tau spreading you see, the more likely a person declines in cognition. We have enough study to show that tau PET may reflect cognitive stages across the AD spectrum," Tousi reports.

Therapeutic trials across the spectrum

The current Alzheimer's therapeutic trials are enrolling people with a very wide spectrum of cognitive states. "We have some trials for anti-amyloid therapy agent for patients with mild cognitive impairment and earlier stage of Alzheimer's dementia. We also have another multicenter trial in which a drug candidate is tested in healthy, at-risk subjects." Tousi continues. "These are participants who may only have concerns about their memory problems because of their family history. Even before their symptoms start, they want to explore preventive treatments. For most trials, it is usually a requirement to have PET imaging to confirm the involvement of Alzheimer's pathologies. Recent studies use amyloid imaging or tau imaging or a combination of both." Imaging biomarkers therefore serve as a key tool to select target clinical trial participants.

The concept of image-based therapy personalization has been discussed for many years. In oncology, thyroid cancer, neuroendocrine tumors, and prostate cancer are good examples of how imaging can confirm pathologies and contribute to therapy planning. It is curious whether PET imaging also plays a role in determining the patient eligibility for AD therapeutic agents.

"We never had a treatment for AD that required more accurate diagnosis. But if there's a treatment focused on amyloid pathology, then I think it's more important to confirm such a problem exists before we start giving treatments," Tousi says. "It brought up to the surface the fact that we need a biomarker for a diagnosis of Alzheimer's. Biomarkers have not been a part of clinical diagnostic criteria." Recently, the International Working Group for the clinical diagnosis of AD proposed including biomarker evidence of Alzheimer's pathology for clinical diagnosis of AD.[8] "We certainly know that there is a vascular component, inflammatory component, and comorbidities from synucleinopathy. A large percentage of patients with Lewy Body dementia may also have Alzheimer's pathology in autopsy. DaTScan™ is another biomarker that we use to differentiate dementia of Lewy bodies and other types of dementia. If there are more selective biomarkers, they can be helpful."

Many initial trials targeting removal of cerebral amyloid accumulation failed, leading many to question the validity of amyloid hypothesis. "I see some promising results with new anti-amyloid antibody agents under trial," Tousi asserts. "These agents

"I see some promising results with new anti-amyloid antibody agents under trial."

Babak Tousi, MD
Neuro-geriatrician based in the midwestern United States

seem to remove amyloid plaques and show promising results in cognitive improvement. So, there is some validation coming for the amyloid hypothesis. I think we had the right hypothesis but didn't have the right targets in the past."

It appears that the recent development in PET imaging and antibody therapy agents are beginning to enable image-based therapy personalization for dementia. In particular, imaging may help stratify patients who are likely to respond to the treatment from those who do not. In combination with other biomarkers that can indicate the metabolic patterns of the brain or other confounding etiologies of neurodegenerative states, physicians now have a few more tools to make more specific diagnosis and to plan the most suitable treatment for AD. ●

Takeshi Shimizu, PhD, is a molecular imaging clinical marketing specialist at Siemens Healthineers. He holds a PhD in biochemistry, microbiology, and molecular biology and worked as a molecular imaging collaboration scientist for Siemens Healthineers in Japan for 10 years prior to assuming his current role.

For More Information

siemens-healthineers.com/molecular-imaging/news/mso-nuclear-neurology-japan.html

siemens-healthineers.com/molecular-imaging/trends-innovations/pet-imaging-for-alzheimers

The interview for this article was first conducted on January 26, 2022. Since that date, the article has been adjusted to reflect ever-changing developments in this area.

References

1 https://www.who.int/news-room/fact-sheets/detail/dementia

2 Scheuner, D., et al. (1996). Secreted amyloid beta-protein similar to that in the senile plaques of Alzheimer's disease is increased in vivo by the presenilin 1 and 2 and APP mutations linked to familial Alzheimer's disease. Nat Med, 2(8), 864-70.

3 Hardy J, & Selkoe, D.J. (2002). The amyloid hypothesis of Alzheimer's disease: progress and problems on the road to therapeutics. Science, 297, 353–56.

4 Morgan, D. (2011). Immunotherapy for Alzheimer's disease. J Intern Med, 269(1), 54-63.

5 Sevigny, J., et al. (2016). The antibody aducanumab reduces Aβ plaques in Alzheimer's disease. Nature, 537(7618), 50-56.

6 Lowe, S.L., et al. (2021). Donanemab (LY3002813) Phase 1b Study in Alzheimer's Disease: Rapid and Sustained Reduction of Brain Amyloid Measured by Florbetapir F18 Imaging. J Prev Alzheimers Dis, 8(4),414-424.

7 U.S. Food and Drug Administration (2021, July 7). FDA Grants Accelerated Approval for Alzheimer's Drug. https://www.fda.gov/news-events/press-announcements/fda-grants-accelerated-approval-alzheimers-drug

8 Dubois, B., et al. (2021). Clinical diagnosis of Alzheimer's disease: recommendations of the International Working Group. Lancet Neurol, 20(6), 484-496.

9 Centers for Medicare & Medicaid Services (2022, April 7). CMS Finalizes Medicare Coverage Policy for Monoclonal Antibodies Directed Against Amyloid for the Treatment of Alzheimer's Disease. https://www.cms.gov/newsroom/press-releases/cms-finalizes-medicare-coverage-policy-monoclonal-antibodies-directed-against-amyloid-treatment

Fast, quantitative SPECT/CT acquisition following multiple therapy cycles of ^{177}Lu-PSMA-617 enables response assessment in a patient with metastatic prostate cancer

By Andrés Ricaurte Fajardo, MD,[1] Joseph Osborne, MD, PhD,[1] Lady Sawoszczyk, BS, CNMT[2]
Data and images courtesy of New York-Presbyterian Hospital/Weill Cornell Medical Center, New York, New York, USA

History

A male in his 70s with a history of prostate-specific membrane antigen (PSMA)-positive metastatic castration-resistant prostate cancer (mCRPC) underwent ^{177}Lu-PSMA-617 treatment 14 years after his initial diagnosis. When prostate-specific antigen (PSA) levels began to rise, the patient was unsuccessfully treated with androgen deprivation therapy (ADT) and multiple lines of systemic chemotherapy. As the disease progressed, the patient received treatment with ^{223}Ra-dichloride, docetaxel, and cabazitaxel with no significant improvement. The patient also completed a palliative course of radiotherapy (30 Gy in 10 fractions) without any treatment complications.

[1] Department of Molecular Imaging and Therapeutics, New York-Presbyterian Hospital/Weill Cornell Medicine, New York, New York, USA
[2] Siemens Healthineers Molecular Imaging, Hoffman Estates, Illinois, USA

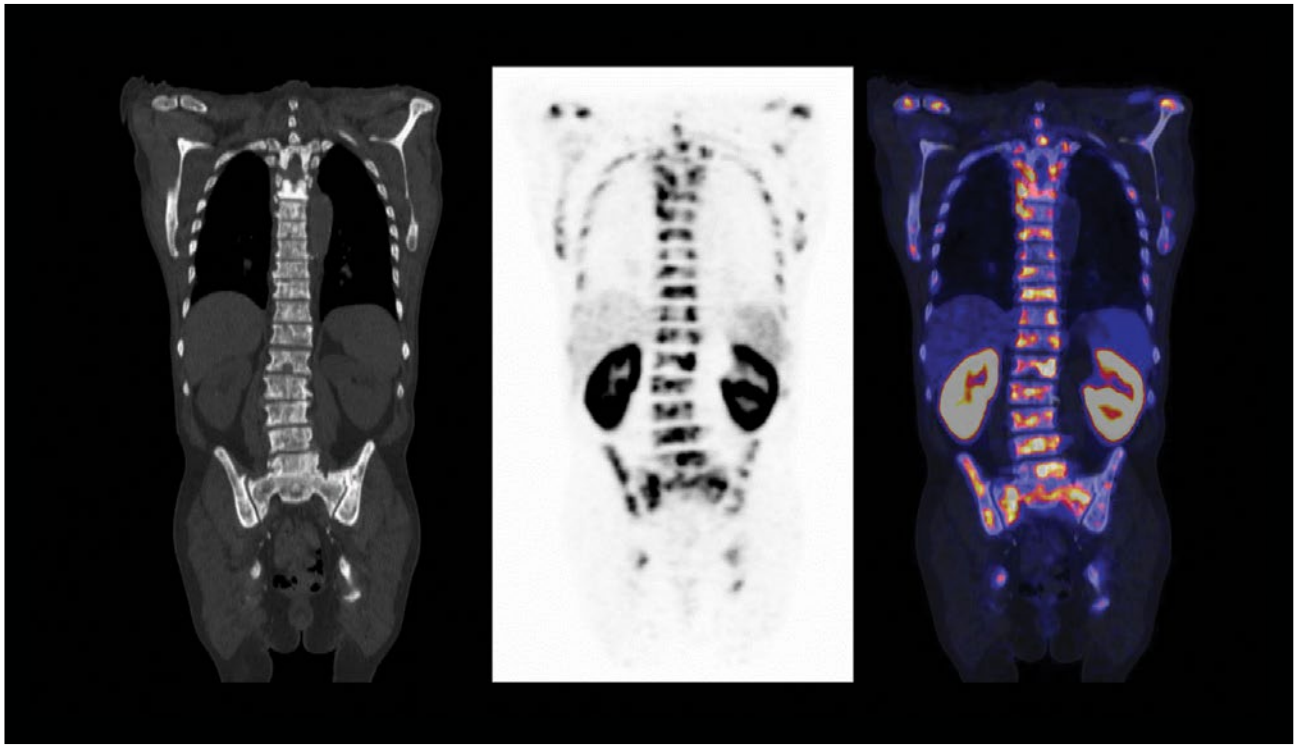

1 **Coronal CT, ^{68}Ga-PSMA-11 PET, and PET/CT images confirm PSMA expression in metastatic disease and qualify the patient for ^{177}Lu-PSMA-617 treatment.**

Findings

A routine ^{68}Ga-PSMA-11 PET/CT was performed to qualify the patient for ^{177}Lu-PSMA-617 treatment. PET/CT findings confirmed PSMA expression in the tumors. The patient was administered with 3.76 mCi (139.12 MBq) intravenous (IV) injection of ^{68}Ga-PSMA-11, and approximately 1 hour later, a single-scan, whole-body acquisition was conducted on Biograph mCT Flow™ PET/CT.

As observed in Figures 1-3, ^{68}Ga-PSMA-11 PET/CT images demonstrate an increased extent of PSMA-avid osseous metastasis within the T3-T7 vertebrae with extension into the neural foramen and ventral epidural space suspected at the T4-T6 levels.

2 **Sagittal CT, ^{68}Ga-PSMA-11 PET, and PET/CT images demonstrate the extent of metastatic disease prior to ^{177}Lu-PSMA-617 treatment.**

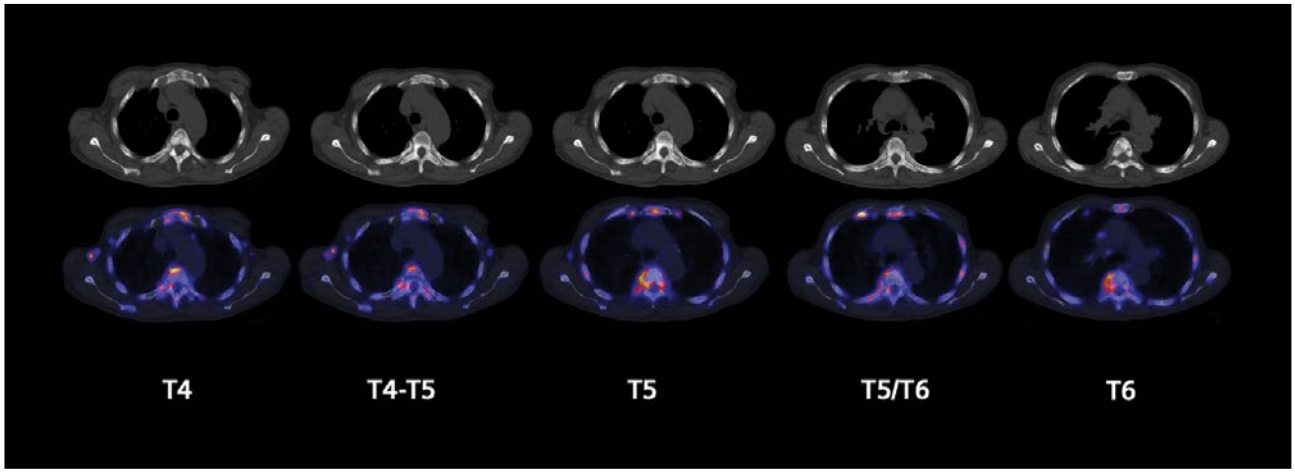

3 **Axial CT and ^{68}Ga-PSMA-11 PET/CT images demonstrate the extent of metastatic disease in the T4-T6 vertebrae.**

There is an overall increased extent of PSMA-avid cervical, thoracic, and abdominopelvic nodal metastasis.

The patient underwent 6 cycles of ^{177}Lu-PSMA-617 therapy; each cycle was delivered every 6-8 weeks. Multi-bed, quantitative SPECT/CT imaging was conducted on Symbia Intevo Bold™ with xSPECT Quant™ after each treatment cycle. The 3-bed, quantitative SPECT/CT study was acquired at 60 stops per detector with 5 seconds per stop. Total scan time was 15 minutes. Following CT attenuation correction (CTAC), the corrected SPECT data was fused with CT data for visual interpretation.

Due to the patient's neutropenia, which was based on absolute neutrophil count (ANC) values in between cycles, the recommended dose of 200 mCi (7.4 GBq) was modified by 20% to 160 mCi (5.9 GBq). Therapy response continued to be monitored via PSA values and quantitative SPECT/CT imaging.

Treatment cycle	^{177}Lu-PSMA-617 dose	Prostate-specific antigen (PSA) values (ng/mL)	Absolute neutrophil count (ANC) (Normal ANC range: 2,500-6,000 cells/µL)
1	203 mCi (7.5 GBq)	2,009	2,540
2	160 mCi (5.92 GBq)	1,514.29	1,000
3	193.5 mCi (7.1 GBq)	934.73	800
4	160.6 mCi (5.94 GBq)	658.83	1,220
5	156.9 mCi (5.8 GBq)	618.36	800
6	165.2 mCi (6.11GBq)	374.46	1,300

As observed in Figures 4 and 5, the SPECT/CT with xSPECT Quant images demonstrate a normal biodistribution of ^{177}Lu-PSMA-617 and foci of increased uptake compatible with the expected distribution of targeted PSMA in concordance with findings from the preceding PSMA PET (Figures 1 and 2).

4 **Sagittal CT through the thoracic and lumbar spine shows extensive sclerosis in the vertebral bodies reflecting metastatic disease with particularly dense sclerosis in the T5 vertebral body. Cycle 2 image shows significant decrease in mid-thoracic vertebral uptake compared to that of low thoracic and lumbar vertebrae, which can be explained by additional mid-thoracic external beam radiation delivered throughout the ^{177}Lu-PSMA therapy regimen. Cycle 3 images acquired 7 days post injection demonstrate lower bladder uptake when increasing time lapse post injection. High uptake in the lower thoracic and lumbar vertebrae is visualized after cycles 2 and 3 but shows considerable decrease after cycles 4 and 6, which clearly demonstrates tumor response.**

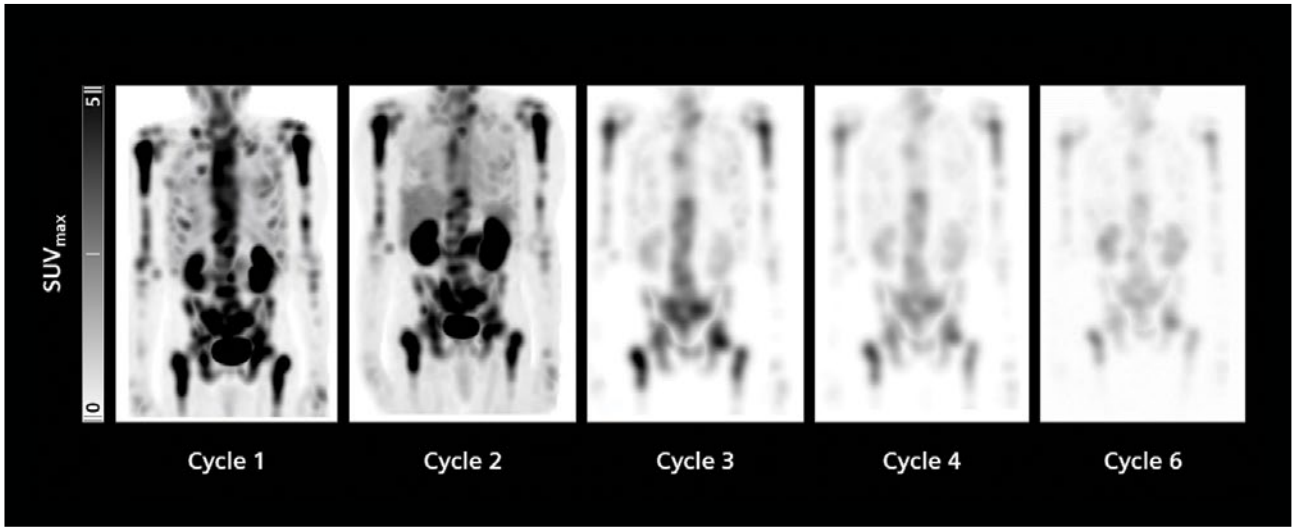

5 **^{177}Lu-PSMA-617 SPECT maximum intensity projection (MIP) images demonstrate positive treatment response. Cycle 1 and 2 images acquired 2 hours post injection. Cycle 3, 4, and 6 images acquired 7 days post injection. Comparison of cycle 1 and cycle 6 SPECT MIP images reveals decreased uptake through the axial skeleton and pelvis as well as the left and right humerus.**

Discussion

This case demonstrates the clinical advantage of using quantitative SPECT/CT with ^{177}Lu-PSMA-617 treatment for therapy monitoring. The confirmation of positive or negative treatment response plays a critical role in disease management, and SPECT/CT with xSPECT Quant images helped confirm that the tumors visualized on the ^{68}Ga-PSMA-11 PET/CT were the same tumors being treated with ^{177}Lu-PSMA-617. The large field of view available on Symbia Intevo Bold SPECT/CT enabled a 15-minute, 3-bed-position imaging protocol, which covered vertex to thigh and allowed the routine use of post-treatment, image-based ^{177}Lu-PSMA-617 uptake assessment. As shown in Figure 5, a progressive reduction of ^{177}Lu-PSMA-617 uptake demonstrated the efficacy of this treatment. Furthermore, the method of imaging after each treatment cycle enabled quality control checks that helped ensure that the treatment was irradiating the tumors as expected.

Conclusion

^{177}Lu-PSMA-617 treatment plays a critical role in patients with mCRPC who have a history of unsuccessful response to hormone therapy and chemotherapy. The ability to perform fast, multi-bed, quantitative SPECT/CT imaging on Symbia Intevo Bold with xSPECT Quant provides high sensitivity to assess ^{177}Lu-PSMA-617 therapy response. Thus, post-treatment imaging is critical for quality control evaluation to confirm PSMA-avid tumors are being treated properly.

Examination protocol

Scanners: Biograph mCT Flow PET/CT and Symbia Intevo Bold SPECT/CT

^{68}Ga-PSMA-11 PET

Injected dose	3.76 mCi (139.12 MBq)
Post-injection delay	60 minutes
Acquisition	1.0 mm/s FlowMotion™ continuous bed motion
Reconstruction	200 x 200 matrix

CT

Tube voltage	100 kV
Tube current	74 mAs
Slice collimation	3.0 mm
Slice thickness	3.0 mm

^{177}Lu-PSMA-617 SPECT (Cycle 6)

Injected dose	165.2 mCi (6.11 GBq)
Post-injection delay	7 days
Acquisition	3 bed positions/5 seconds per view, 60 views per detector Total scan time: 15 minutes (5 minutes per bed)
Reconstruction	256 x 256 matrix, xSPECT Zoom 1.0

CT

Tube voltage	110 kV
Tube current	12 mAs
Slice collimation	3.0 mm
Slice thickness	3.0 mm

The outcomes achieved by the Siemens Healthineers customers described herein were achieved in the customer's unique setting. Since there is no "typical" hospital and many variables exist (eg, hospital size, case mix, level of IT adoption) there can be no guarantee that others will achieve the same results.

Localization of infection site in femoral stabilization pin using SPECT/CT with radiolabeled leukocytes

By Partha Ghosh, MD, Siemens Healthineers, Hoffman Estates, Illinois, USA
Data and images courtesy of Queen Elizabeth Hospital Birmingham, Birmingham, United Kingdom

History

An approximately 70-year-old female with history of trauma with bilateral femoral fractures was treated with intramedullary rod insertions. The right femur was stabilized using an intramedullary rod with external fixation plate and screw, and the left femur had an intramedullary rod with a dynamic hip screw through the femoral neck and trochanter. The patient complained of severe pain in the right femoral fixation screws along with slight wound discharge. In view of the possibility of prosthetic infection, a ^{99m}Tc HMPAO-labeled leukocyte study was performed on Symbia Pro.specta™[a] SPECT/CT.

The patient was administered 8.91 mCi (330 MBq) of ^{99m}Tc-HMPAO-labeled leukocytes and then the planar and SPECT/CT acquisition was performed after 3 hours. Initial CT scan performed with 110 kV and 150 reference mAs and 32 x 0.7 mm collimation. 1-mm slices were reconstructed with iterative metal artifact reduction (iMAR)[b] in order to ensure virtually artifact-free, thin-slice CT images.

The SPECT study was acquired at 60 stops per detector with 20 seconds per stop. Data was reconstructed using OSEM3D with 5 iterations, 15 subsets, and a 128 x 128 matrix. Following CT attenuation correction (CTAC), the corrected SPECT data was fused with iMAR CT data for visual interpretation.

1 An anterior X-ray shows right-sided intramedullary femoral nail which appears displaced with extrusion of fixation screws. The lateral external plate also shows displacement with extrusion of screws especially in the lower part. The femoral intramedullary nails for the shaft and the neck of the left femur appear to be properly positioned.

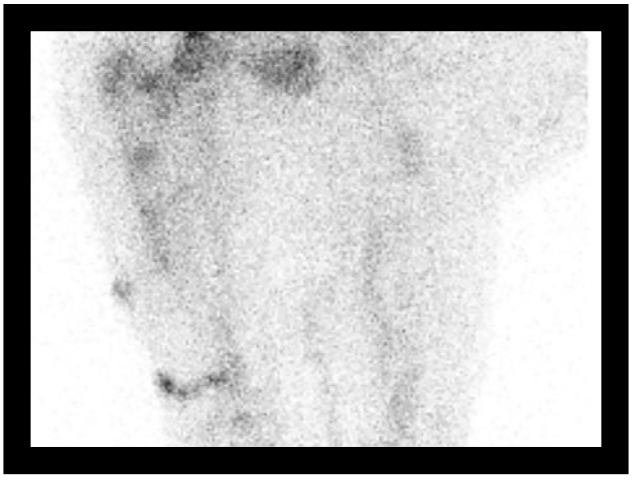

2 Delayed static planar images acquired 3 hours following injection of ^{99m}Tc-HMPAO-labeled leukocytes. The image shows considerable accumulation of labeled leukocytes along the lateral plate as well as the upper part of the intramedullary femoral nail suggestive of active infection. There is accumulation in a sinus tract from the lower part of the femoral shaft to the skin of the lateral thigh, reflecting infection throughout the entire intramedullary nail. The left femoral nail does not show any abnormal leukocyte accumulation.

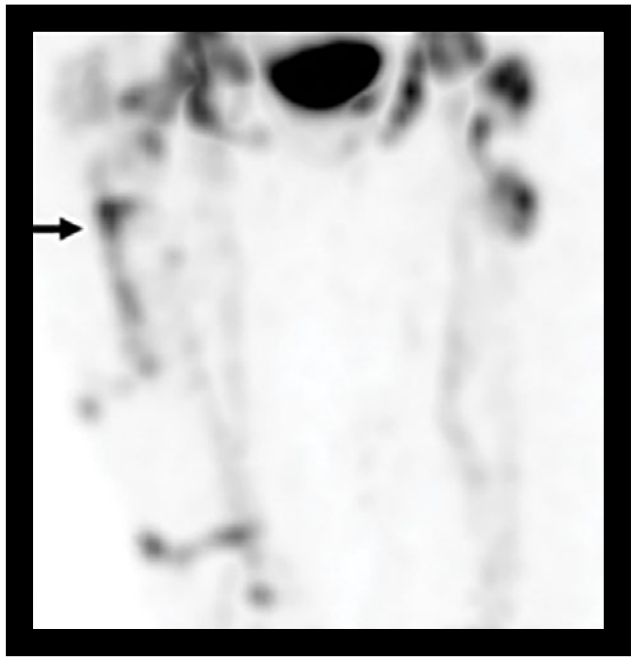

3 SPECT maximium intensity projection (MIP) shows abnormal accumulation of ^{99m}Tc-HMPAO-labeled white blood cells (WBCs) along the entire right lateral plate with maximum uptake at a focal area localizing to the second fixation screw (arrow) suggesting presence of active infection. There is also an accumulation of labeled leukocytes in a tract from the lower edge of the lateral nail to the exterior, which is indicative of a soft-tissue collection draining externally. Additionally, there is also tracer accumulation in the upper part of the right femoral intramedullary nail and attached screws. Milder uptake extends along the entire length of the right femoral intramedullary nail suggesting an infection throughout the femoral marrow cavity. Additional accumulation of leukocytes along the sinus tract from the lower part of the femoral shaft to the skin laterally indicates draining exudate.

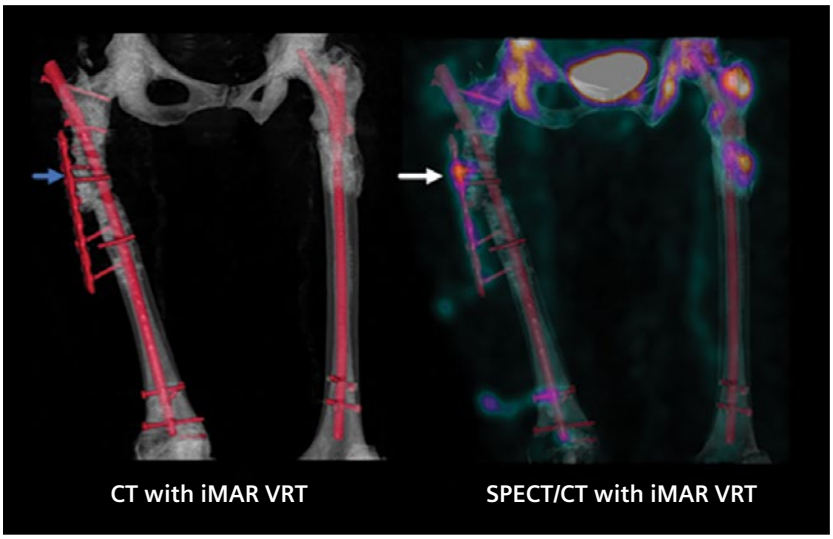

4 **A volume-rendered CT image with iMAR shows artifact-free depiction of the displaced right femoral intramedullary nail with extruded fixation screws—many of which are bent. The lateral plate is also displaced, especially in the lower part with extruded screws as well. There is significant sclerosis in the trochanteric region and upper half of the shaft of the right femur, which is possibly reflective of sequestrum formation secondary to osteomyelitis. The intramedullary nails in the shaft and neck of the right femur are in proper position. There is sclerosis in the upper third of the left femoral shaft, which reflects fusion following fracture in absence of any displacement of prosthesis.**

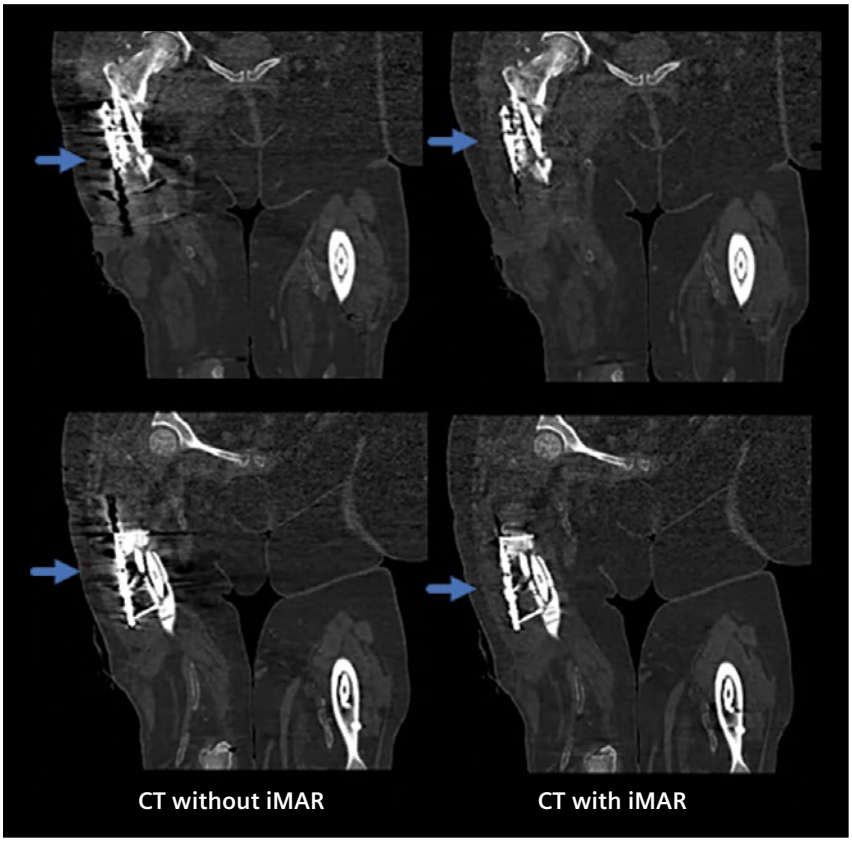

5 **Comparisons of coronal CT slices with and without iMAR show the reduction of metal-related beam-hardening artifacts lateral to the lateral fixation plate (arrows) as well as the medial to the femoral intramedullary nail, which enables artifact-free visualization of the nail, lateral plate, and the extruded fixation screws.**

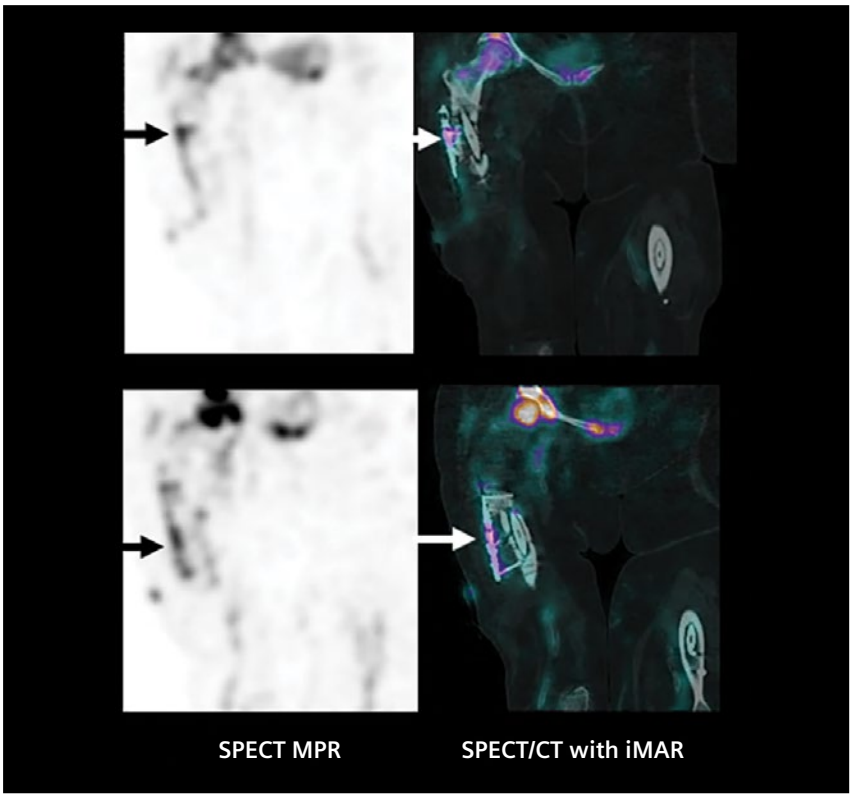

6 Coronal SPECT multiplanar reconstruction (MPR) and SPECT/CT with iMAR images show the accumulation of ^{99m}Tc-HMPAO-labeled leukocytes along the entire length of the lateral plate with focal areas of intense accumulation exactly at the location of the fixation screws attaching the lateral plate to the femoral shaft. Note the extrusion of the lower screws with major lateral displacement of the lateral plate.

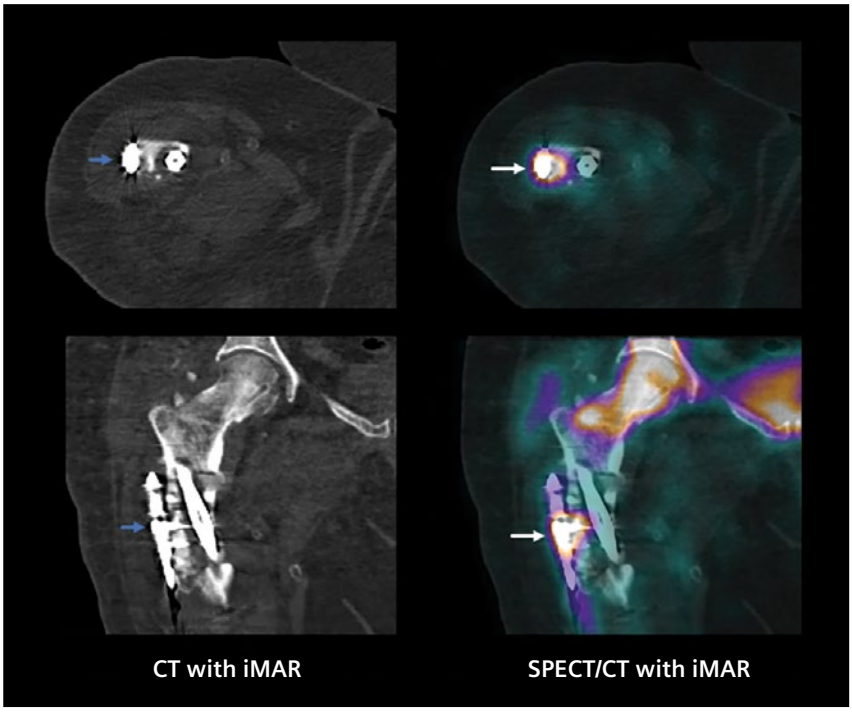

7 Axial and coronal CT and SPECT/CT images show the high focal accumulation of radiolabeled leukocytes in the lateral plate at the level of the second fixation screw (arrows), which suggests a collection of infective exudate at that level.

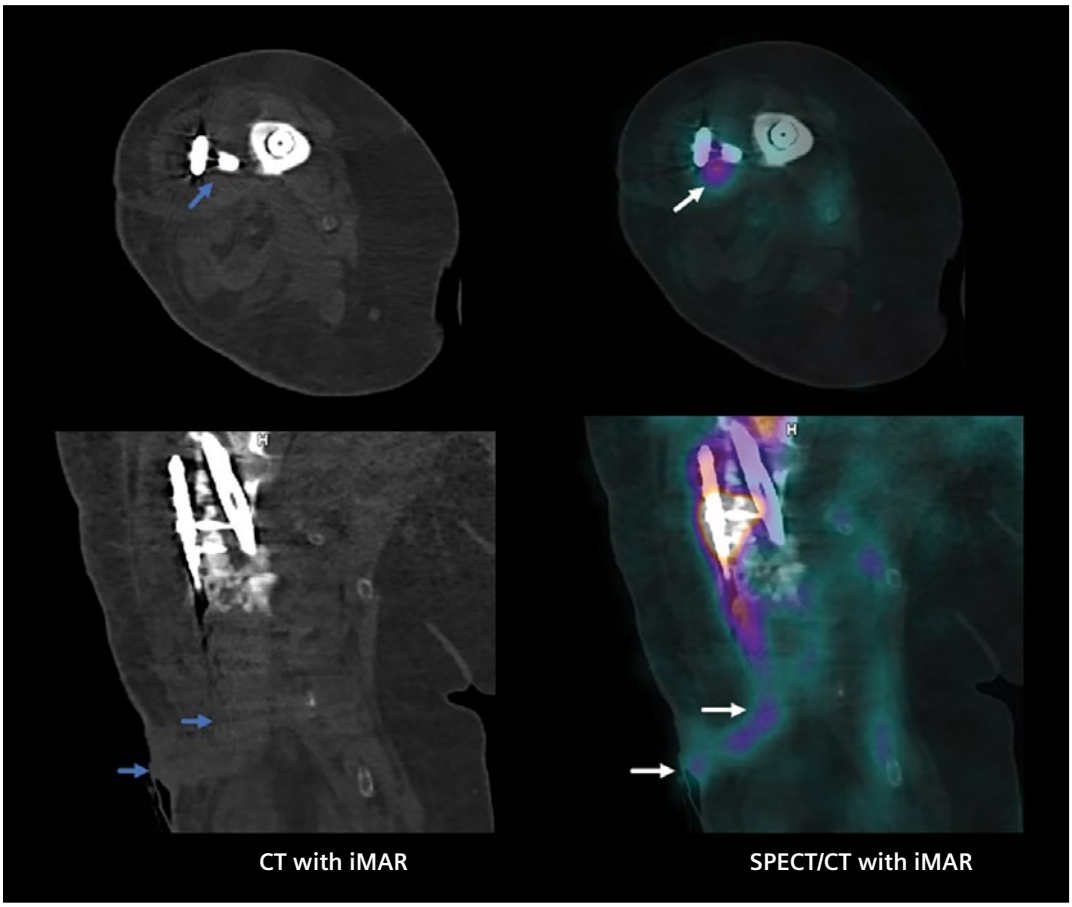

8 Axial and coronal CT and SPECT/CT images show the accumulation of radiolabeled leukocytes in the lower end of the lateral fixation plate and along the sinus tract draining into the skin laterally (arrows). There is also associated collection within the adjacent soft tissue.

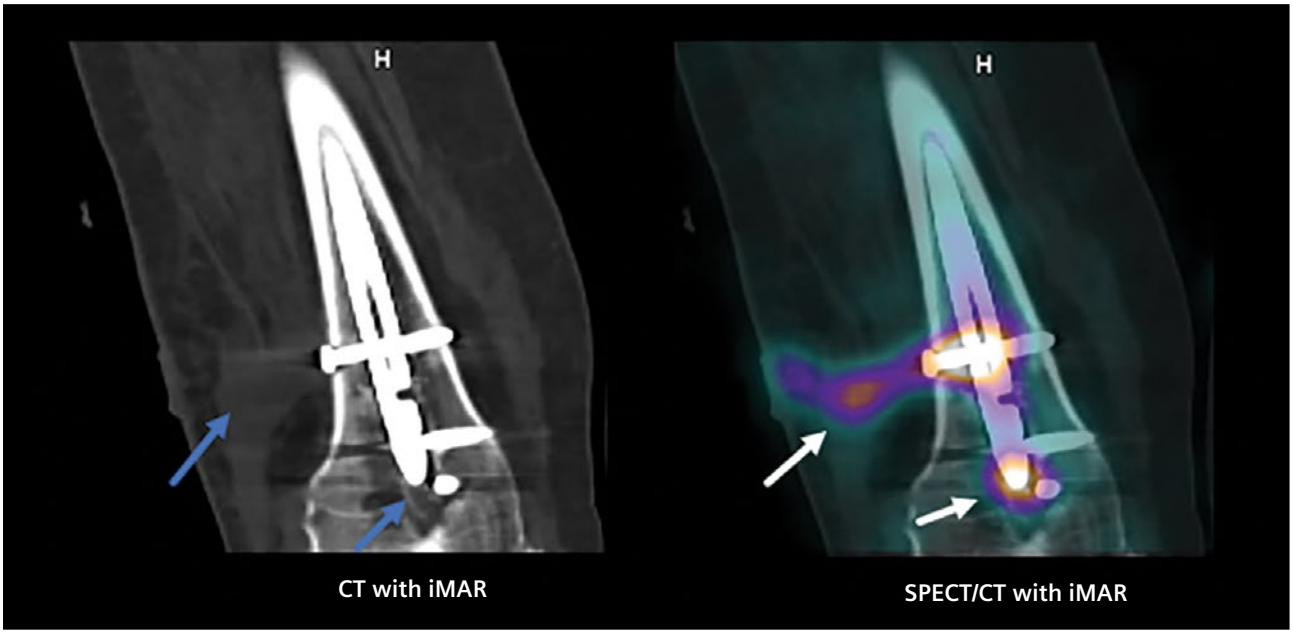

9 Coronal CT and SPECT/CT images show intense accumulation of radiolabeled leukocytes in the lower fixation screws attached to the lower third of the femoral intramedullary plate (arrow) with activity within the sinus tract draining into the skin laterally (arrow). There is also tracer accumulation at the lower tip of the intramedullary nail (arrow) representing a dependent collection of infective exudate.

Findings

As seen in Figure 4, volume rendering of SPECT/CT data shows an accumulation of radiolabeled leukocytes along the entire length of the right lateral fixation plate as well as the femoral intramedullary nail with focal area of intense accumulation localized to the first fixation screw of the lateral plate (arrows). There is also a clear visualization of the leukocyte accumulation in the sinuses draining from the lower end of the lateral plate to the skin laterally as well as the lower third of the femoral intramedullary rod, which suggests a sinus tract in the lower third of the thigh as well.

As evident from the SPECT/CT images, the study shows increased uptake reflecting accumulation of radiolabeled leukocytes along the entire length of the lateral femoral plate. The uptake appears to be partly extruded from underlying bone with maximum focal uptake in the second fixation screw, which appears to be the site of maximum infective exudate. There is extrusion of the most distal fixation screws of the lateral plate with lucency surrounding the tip of the other remaining distal screws. This represents both a shear strain on the fixation plate due to malunion of the fractured femoral shaft as well as the osteolysis related to infection. There is also a soft-tissue collection at the lower end of the lateral plate with a sinus tract draining to the skin laterally.

Furthermore, there is accumulation of radiolabeled leukocytes throughout the entire length of the femoral intramedullary nail representing infection throughout the entire prosthesis. The intramedullary nail also shows significant osteolysis surrounding its distal tip with fractures of the lowermost screw and the most proximal of the distal screws. The low-grade increased activity at the tip suggests active infection along with dependent collection of infective exudate. Linear increased accumulation of radiolabeled leukocytes along the proximal end of most of the distal screws represents focal infection at and around the screws and at the site of its attachment with the intramedullary plate, which extends along the subcutaneous sinus tract and appears to open onto the skin surface along the lateral right thigh. The left intramedullary nail in the femoral shaft as well as in the neck show complete union of the left subtrochanteric fracture without any evidence of active infection in the left femur or hip.

Discussion

This case example demonstrates the clinical advantage of using SPECT/CT with radiolabeled leukocytes to exactly localize the site of abnormal accumulation of leukocytes and differentiate physiological leukocyte accumulation in the bone marrow from foci of infection. The CT component of the SPECT/CT is key for proper evaluation of the prosthesis, especially when evaluating the alignment, displacement, fracture or extrusion, periosteal reaction, bone sclerosis, bony cortical fractures, and the soft-tissue collections and sinus tracts associated with such infections.

Symbia Pro.specta SPECT/CT enables a 32-slice acquisition with 0.7-mm collimation, which enables a reconstructed slice thickness of 1 mm with high image quality at a low dose. This enables high-quality coronal and sagittal reconstructions as well as volume rendering for optimal interpretation of the bony and prosthetic joint pathologies. In this case, the iMAR feature available on the CT of Symbia Pro.specta provided sharp, virtually artifact-free visualization of the intramedullary nail, lateral plate, and associated interlocking screws. This visualization was key in interpreting the displacement and extrusion, localizing the site, and determining the extent of abnormal accumulation of radiolabeled leukocytes, especially at the sites of the screw insertions. High-quality CT also enabled the localization of the sinus tract with retained radiolabeled leukocytes and the adjacent collections of infective exudate.

Infection is the most serious complication after external or internal fixation with nails or plates for fracture or total- or partial-joint replacement with prosthesis. This occurs in 1.5-2.5% of primary procedures and up to 20% for revision surgeries.[1]

Implanted devices and the presence of any foreign body is associated with a higher susceptibility for infection. Skin-derived bacteria are most often the ones to colonize an implant during surgery. Microorganisms form biofilms around the implant which protects the bacteria within the biofilm from phagocytes. The indolent nature of prosthetic joint infections may be due to the development of such protective biofilms on the surface of the infected implants, and very often, the infection cannot be controlled unless the implant is removed. The chemotactic factors secreted by the infective pathogens cause neutrophil recruitment at the site of infection, which is the basis of the effectiveness of infection imaging with radiolabeled leukocytes. In this case, the presence of radiolabeled leukocytes throughout the entire length of the lateral plate and intramedullary rod may reflect the presence of such biofilms harboring infective microorganisms.

Although in this case there is minimal hematopoietic bone marrow within the femoral shaft due to the presence of the intramedullary rod, it is to be noted that radiolabeled leukocytes do accumulate in normal

marrow and need to be differentiated from abnormal accumulations related to infection based on the location of such accumulation. Thus, the CT component of SPECT/CT is key for such localization. The CT performance of Symbia Pro.specta with thin-slice reconstruction with iMAR for metal-artifact-free visualization of the intramedullary plates and screws was instrumental in the correct assessment of the degree of extrusion as well as periprosthetic lucency associated with infection and sinus tracts, which was then accurately coregistered to the abnormal focal leukocyte accumulations.

Conclusion

The clinical evaluation of CT, SPECT, and SPECT/CT images suggests infection of the right lateral femoral plate throughout the length of the intramedullary femoral nail, especially at the proximal and distal ends, along with an infected sinus tract extending from the lower end of the femoral plate and intramedullary nail to the skin surface in the right distal thigh.

The high-quality, thin-slice CT with iMAR made possible by the CT performance of Symbia Pro.specta was instrumental in the proper assessment of the degree of displacement, extrusion, and fracture of the lateral femoral plate, the interlocking screws and femoral intramedullary nail, as well as the localization of the focal accumulation of radiolabeled leukocytes, infective exudates, collections, and related sinus tracts.

From the clinical impression of extensive infection within the femoral implants, along with the malunion of the fracture site and osteolysis associated with the periprosthetic bone, a total removal of the prosthesis with re-insertion of new stabilization rods with antibiotic beads would be a recommended approach to management. ●

Examination protocol

Scanner: Symbia Pro.specta

SPECT	
Injected dose	8.91 mCi (330 MBq) ^{99m}Tc-HMPAO-labeled leukocytes
Post-injection delay:	3 hours
Acquisition	60 stops per detector, 20 seconds per stop
Image reconstruction	128 x 128 matrix, OSEM3D 5i15s

CT	
Tube voltage	110 kV
Tube current	150 ref mAs
Slice collimation	32 x 0.7 mm
Slick thickness	1 mm

The outcomes achieved by the Siemens Healthineers customers described herein were achieved in the customer's unique setting. Since there is no "typical" hospital and many variables exist (eg, hospital size, case mix, level of IT adoption) there can be no guarantee that others will achieve the same results.

References

[1] Glaudemans AW, Galli F, Pacilio M, Signore A. Leukocyte and bacteria imaging in prosthetic joint infection. *Eur Cell Mater.* 2013;25:61-77. doi:10.22203/ecm.v025a05.

[a] Symbia Pro.specta is not commercially available in all countries. Future availability cannot be guaranteed.

[b] The amount of metal artifact reduction and corresponding improvement in image quality depends on a number of factors including: composition and size of the metal object, patient size, anatomical location and clinical practice. It is recommended to perform reconstruction with iMAR enabled in addition to conventional reconstruction without iMAR.

Facet arthropathy along with fracture of spinal stabilization rod defined on ^{99m}Tc-HMDP bone SPECT/CT in a patient with pain following thoracolumbar spinal fusion surgery

By Partha Ghosh, MD, Siemens Healthineers, Hoffman Estates, Illinois, USA
Data and images courtesy of Queen Elizabeth Hospital Birmingham, Birmingham, United Kingdom

History

An approximately 75-year-old male with history of posterior spinal stabilization surgery presented with severe lower back pain. Routine X-rays were inconclusive, and the patient was referred for a ^{99m}Tc-HMDP bone SPECT/CT study to determine the site of bone stress and related pathology.

The study was performed on Symbia Pro.specta™[a] SPECT/CT 3 hours following 20.9 mCi (776 MBq) intravenous (IV) injection of ^{99m}Tc-HMDP. Following anterior and posterior planar whole-body acquisitions, multibed SPECT/CT acquisition of the entire cervical, thoracic, and lumbar spine as well as the pelvis was performed.

CT was performed with 130 kV with 30 reference mAs. 1.5-mm-reconstructed CT slices were obtained for evaluation and fusion with SPECT. Three-bed SPECT was performed with 60 stops per detector and 10 seconds per stop. SPECT was reconstructed using OSEM3D 7i15s with 128 x 128 matrix. SPECT/CT data was reviewed using *syngo*.via.

1 Routine X-ray of the lower thoracic and lumbar vertebrae shows bilateral spinal stabilization rod and screws without any clear evidence of displacement or fracture.

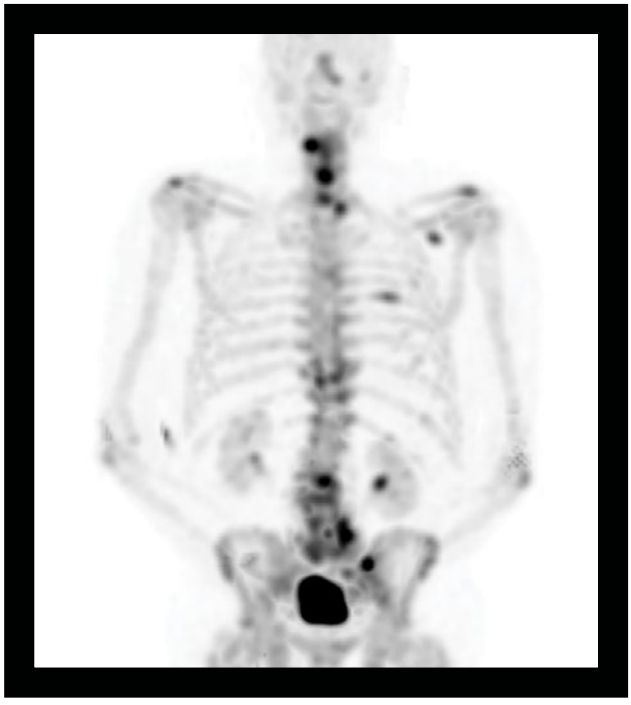

2 Posterior planar static image of the spine shows focal areas of increased uptake in the left lateral L5 vertebrae and left sacroiliac joint. It is not possible to conclude the cause of the hypermetabolism or whether it is related to loosening of the spinal screw or degenerative changes from planar studies alone. Minor degenerative changes are also visualized in the lower thoracic vertebrae.

3 Anterior SPECT maximum intensity projection (MIP) shows intense focal uptake of tracer in the left pedicle of the L5 vertebrae, left sacroiliac joint, as well as the left aspect of the L2 and L3 vertebral bodies. Significant scoliosis of the lumbar spine is apparent. Lower thoracic vertebrae also show focal hypermetabolism at the laminar levels.

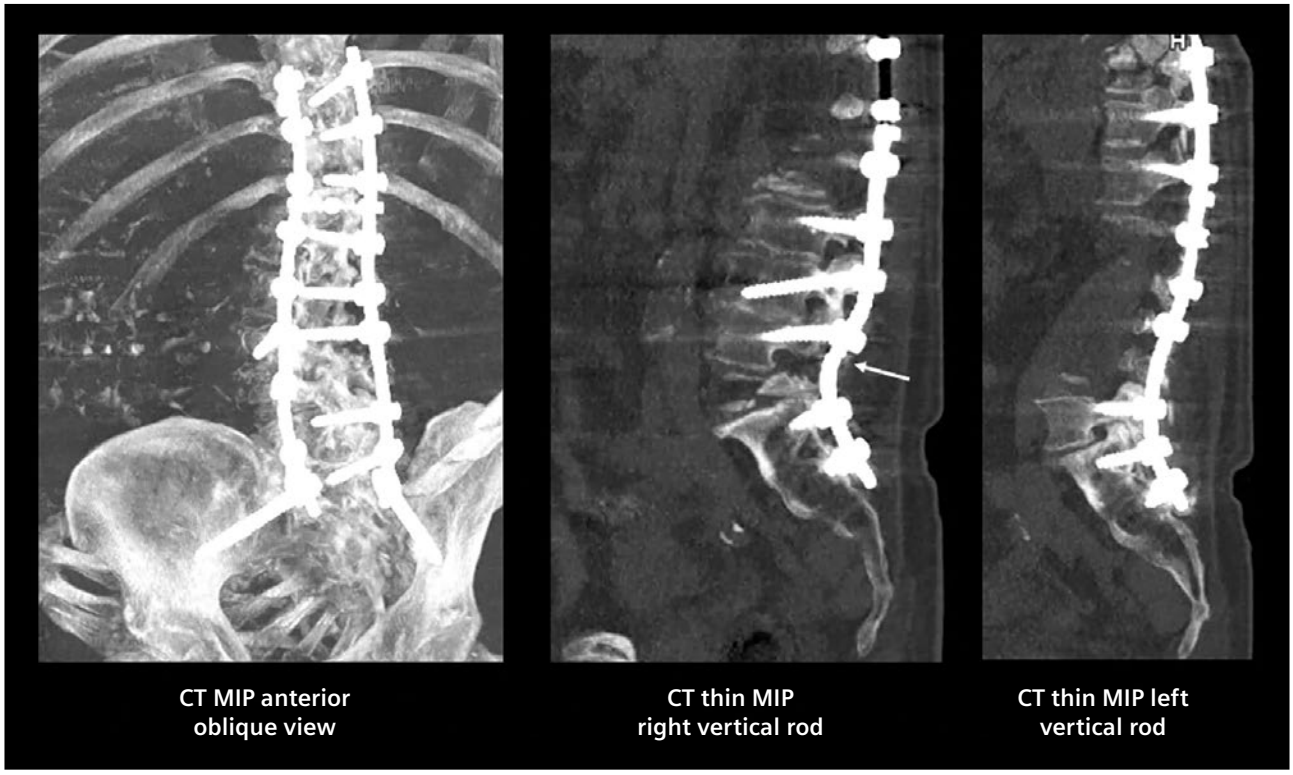

4 **CT MIP images show left and right vertical stabilization rods and fixation screws. The distortion of the left vertical rod related to the scoliosis is apparent from the image. Sagittal CT thin-MIP views show the right vertical stabilization rod and defines a fracture of the rod at the mid-vertebral body level of L4 (arrow) without significant displacement. CT thin-MIP image of the left vertical rod shows no fracture.**

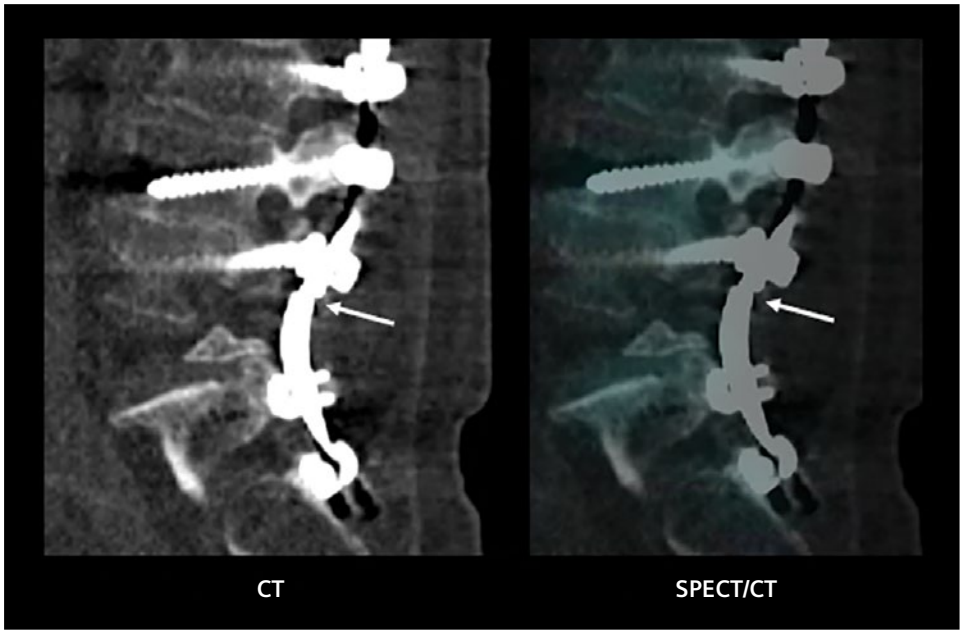

5a **Sagittal CT and SPECT/CT images at the level of the right vertical stabilization rod show a fracture of the rod at the level of the mid-vertebral body of the L4 vertebrae (arrow), which does not show significant hypermetabolism in the adjacent bone reflecting the absence of significant displacement or related instability.**

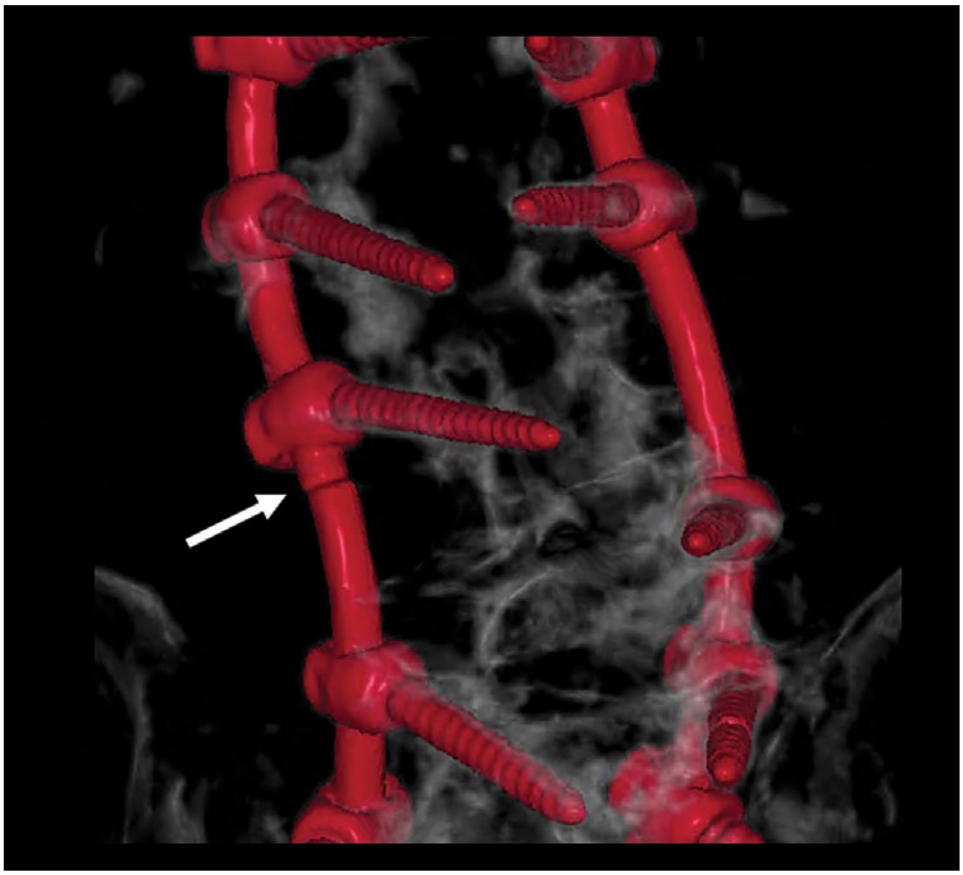

5b Volume rendering of the CT with zoomed visualization of the spinal vertical stabilization rods shows the fracture of the right vertical rod (arrow) at the mid-L4 vertebral level. However, the displacement of the rod at the fracture site is minimal.

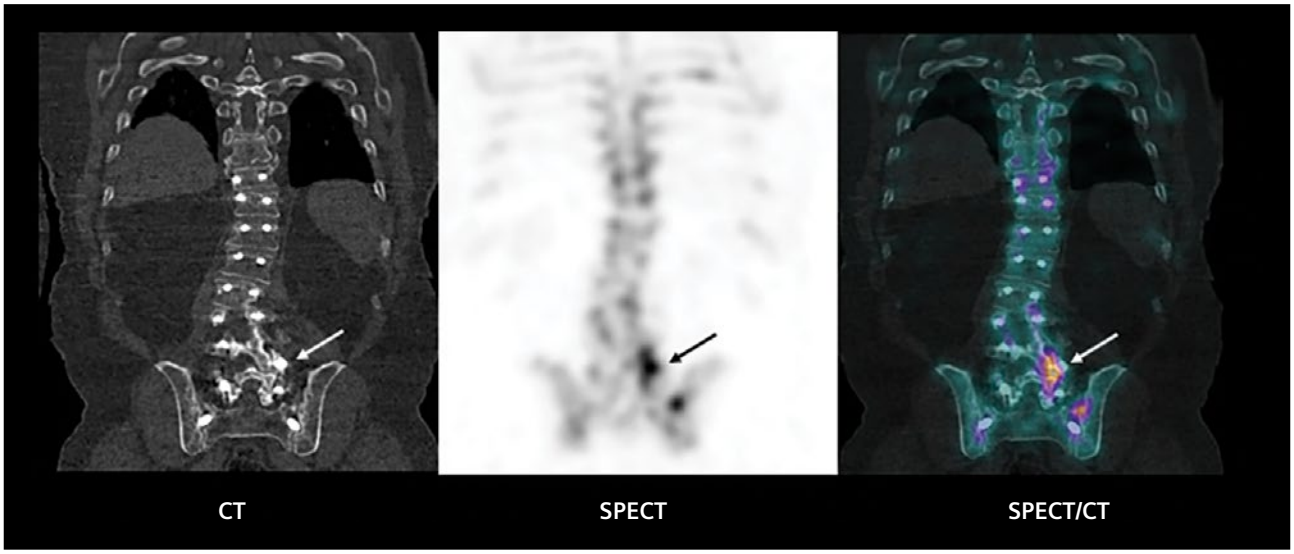

6 Coronal CT, SPECT, and SPECT/CT views through the lower lumbar spine and sacroiliac joints show hyperintensities on CT related to the spinal fixation screws with focal increase in tracer uptake seen on SPECT and SPECT/CT images corresponding to the left L4/L5 vertebral facet adjacent and medial to the fixation screw.

7 **Sagittal CT and SPECT/CT views through the lumbar vertebrae show the left vertical spinal stabilization rod with focal hypermetabolism surrounding the L4 fixation screw. The lower thoracic and lumbar fixation screws show normal tracer uptake.**

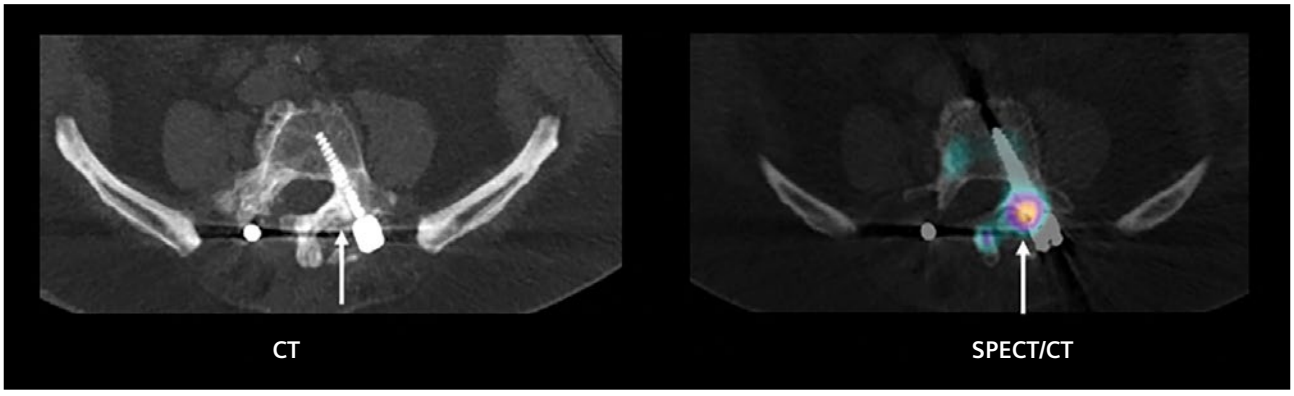

8 **Axial CT thin-MIP and SPECT/CT views at the level of L4 vertebrae show sclerosis adjacent and medial to the left fixation screw (arrow) that attaches the left vertical stabilization rod to the L4 vertebral body through the lamina. SPECT/CT images show focal hypermetabolism in the vertebral pedicle around the base of the fixation screw reflecting bone stress related to scoliosis and related instability.**

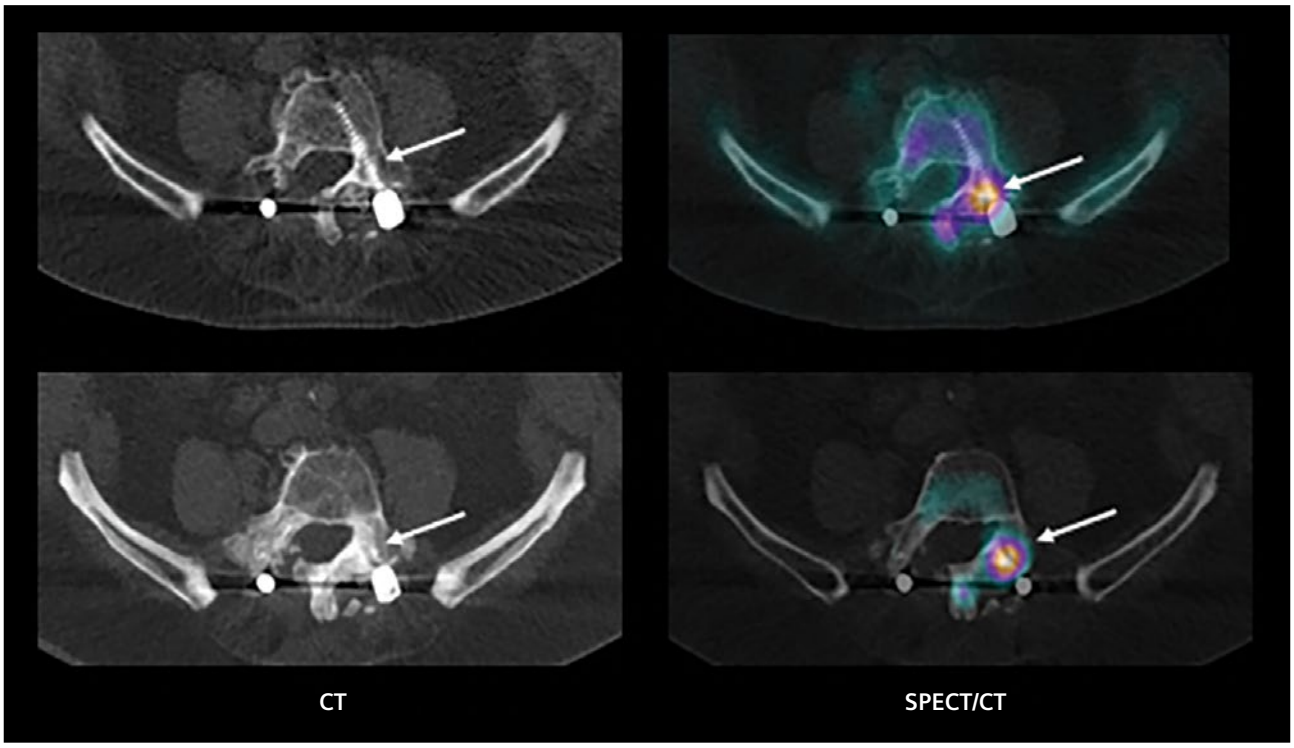

9 **Axial CT and SPECT/CT images show focal uptake around the base of the left L4 fixation screw and the adjacent L5 facet joint, which shows intense uptake of bone stress at the left L4 facet joint, related to instability of the fixation screw and associated severe facet arthropathy.**

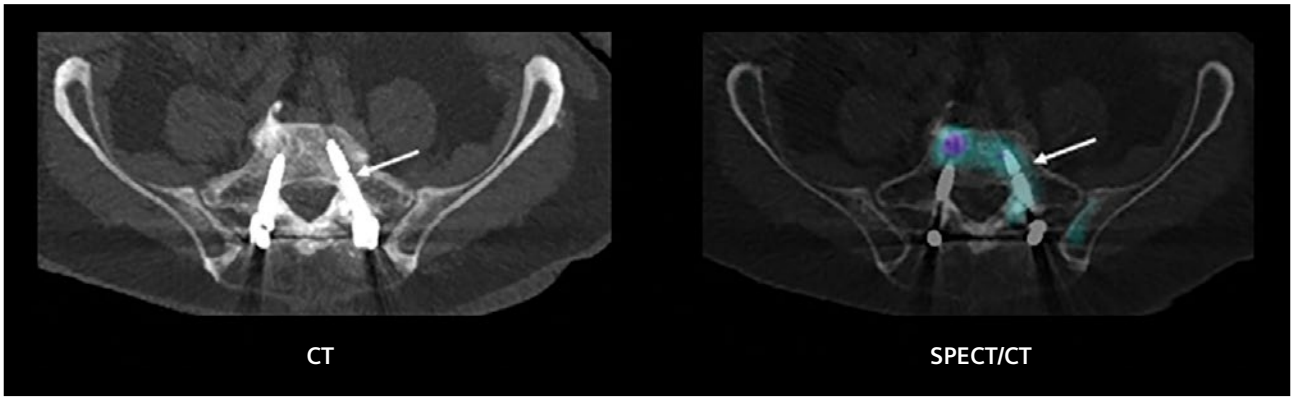

10a **Axial CT thin-MIP and SPECT/CT images at the level of the upper sacrum show a fracture at the middle of the left sacral fixation screw at S1 level. However, there is no displacement or osteolysis around the screw, and SPECT/CT images show absence of significant hypermetabolism around the screw.**

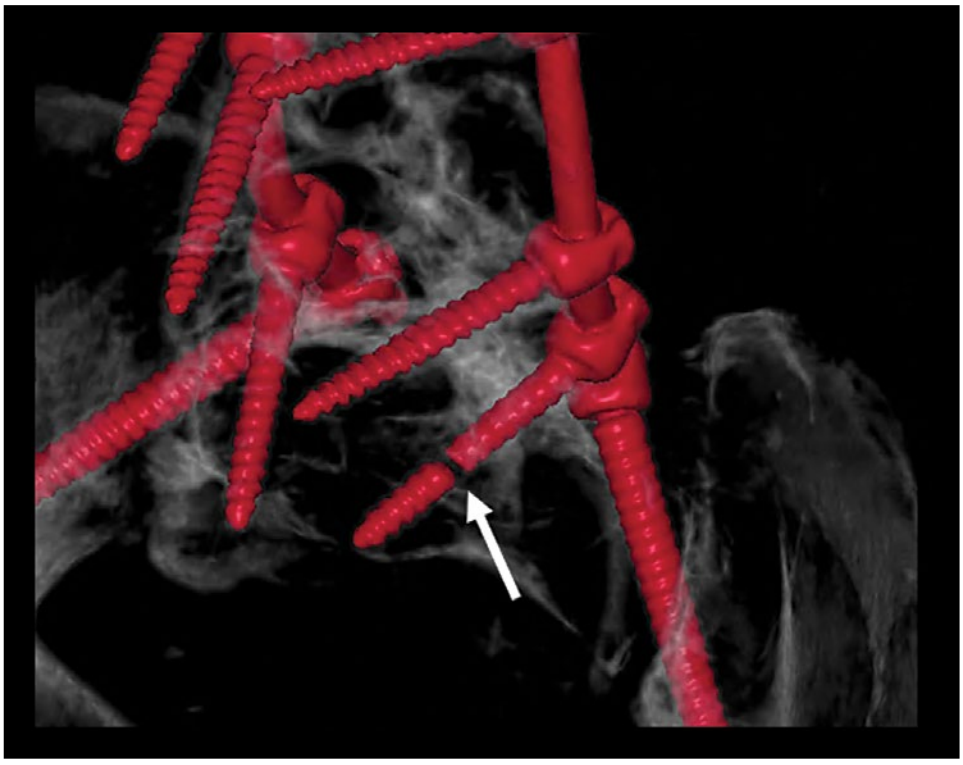

10b Volume rendering of CT provides zoomed 3D display of S1 fixation screw with fracture site at the middle of the screw within the vertebral body (arrow).

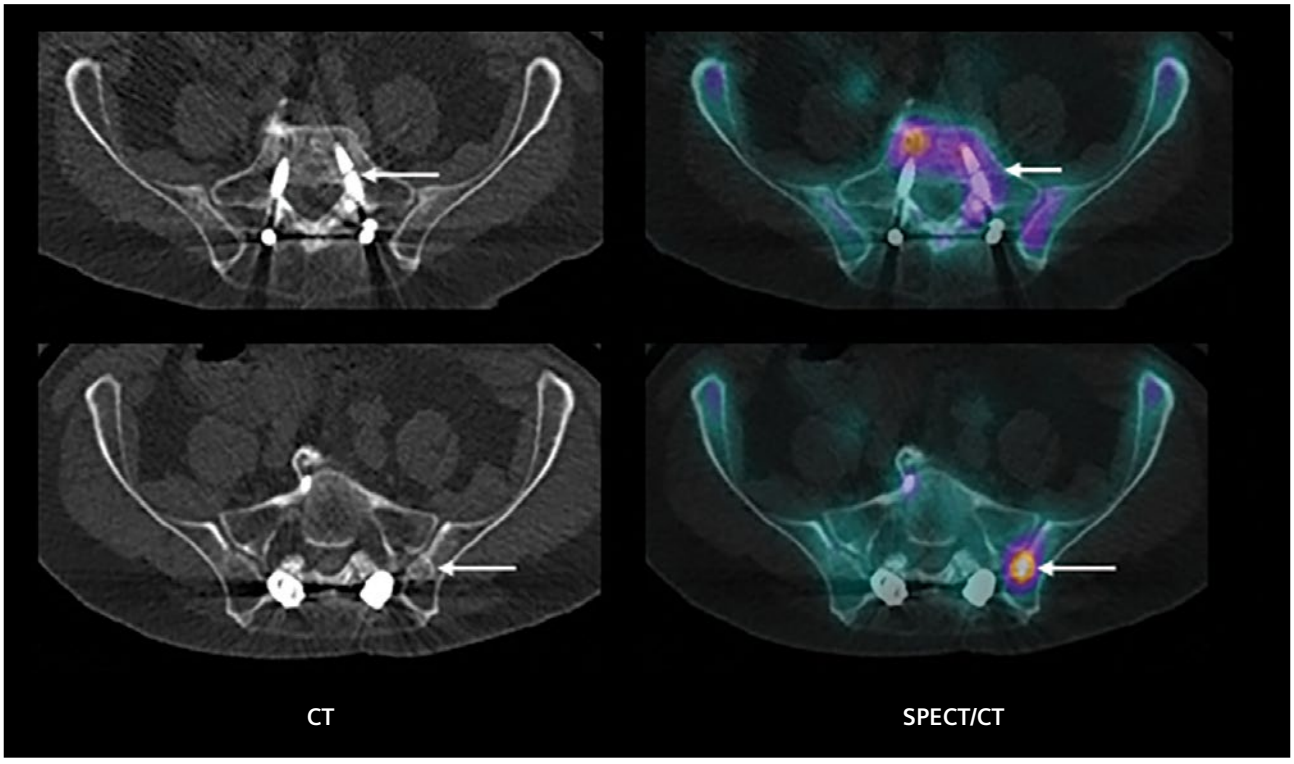

11 Axial CT and SPECT/CT images show fracture of the left S1 vertebral fixation screw (top-row arrow) without significant hypermetabolism at the fracture site. There is another focal area of increased uptake within a small lytic area in the left ilium adjacent to the sacroiliac joint (bottom-row arrow) associated with subchondral lucency with sclerosis in the lesion margins, which probably represents a subchondral bone cyst or geode.

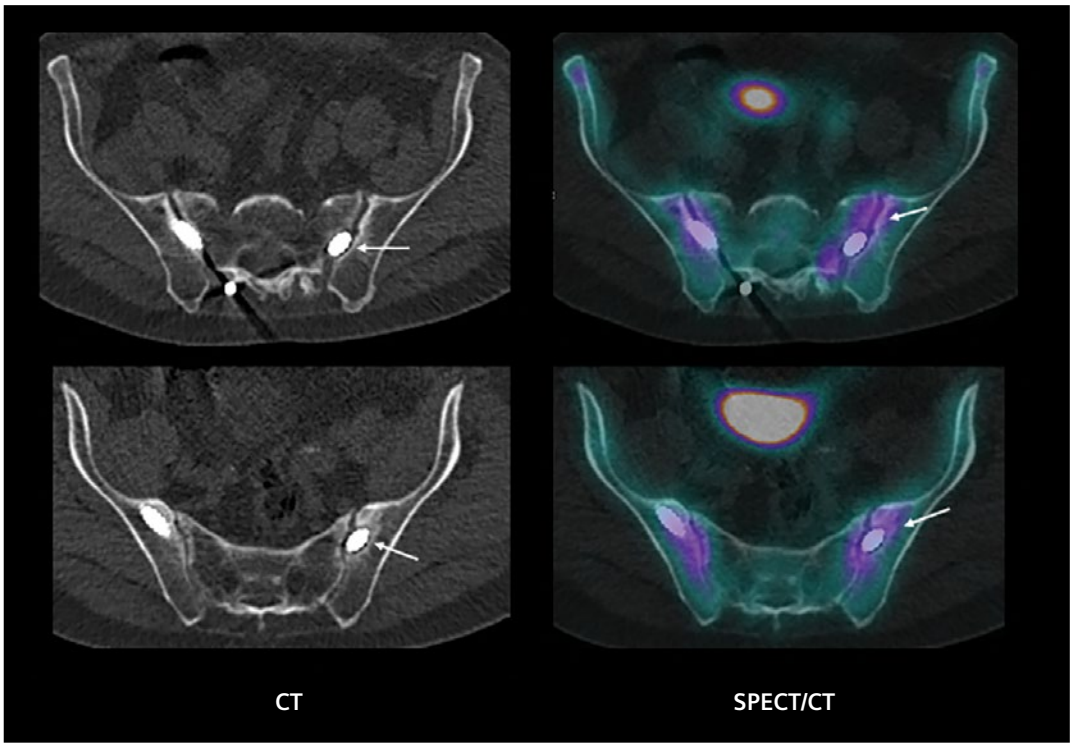

12 **Axial CT and SPECT/CT images at the level of sacroiliac joints show lucency surrounding the screw across the left sacroiliac joint (arrow) suggestive of loosening. The low-grade uptake visualized around the distal end of the screw also reflects abnormal motion related to loosening.**

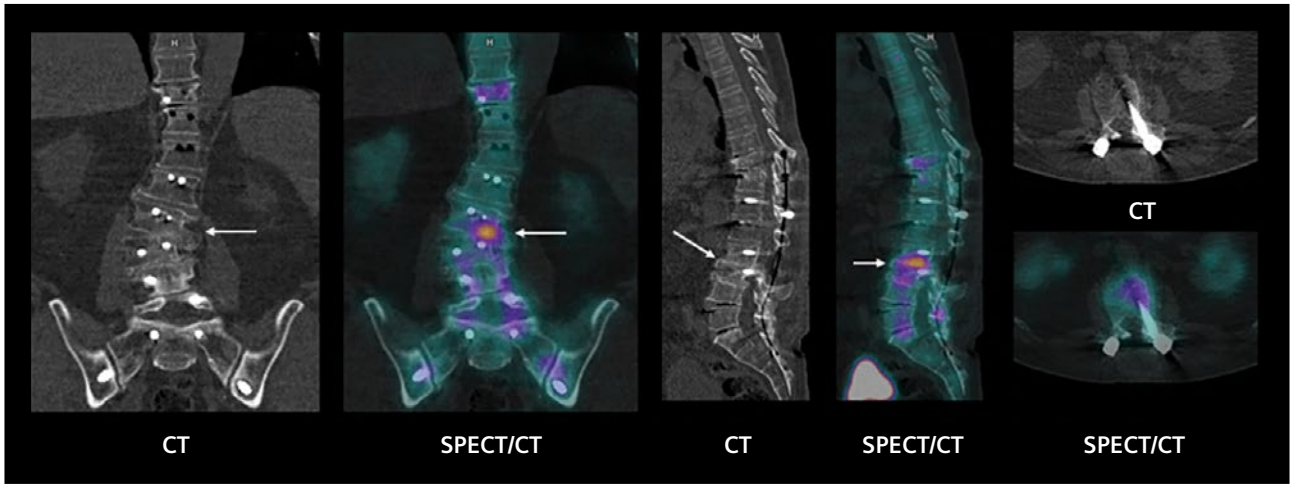

13 **Coronal and sagittal CT and SPECT/CT images show hypermetabolism at the level of the endplates and osteophytes at L2 and L3 disc-space levels, which reflects severe degenerative changes associated with significant scoliosis. However, the fixation screws and stabilization rods in the mid- and upper-lumbar vertebrae do not show evidence of loosening or pathological motion due to instability.**

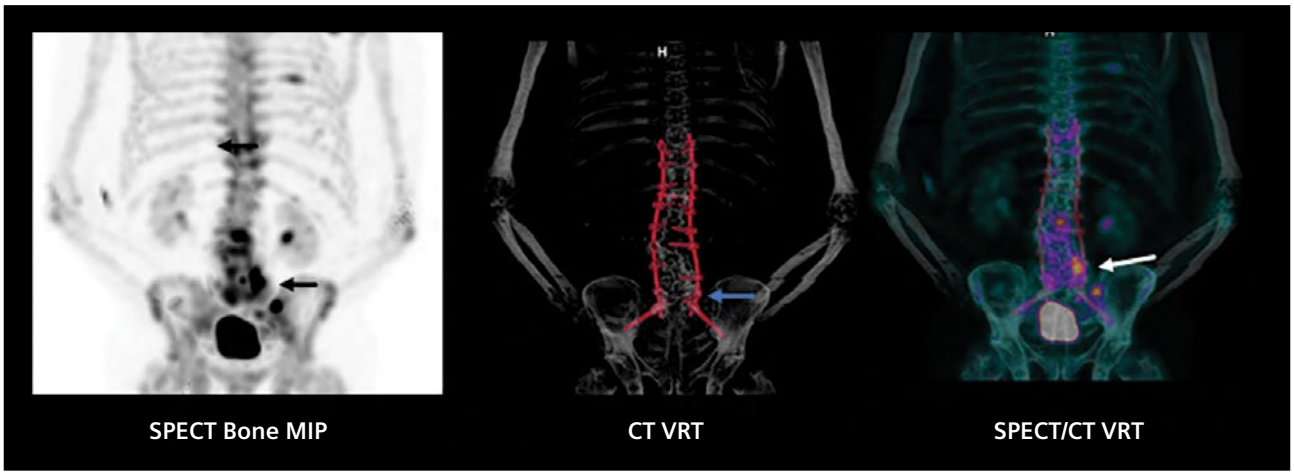

14 **SPECT MIP, volume-rendered CT, and SPECT/CT images show the position of the spinal stabilization rods and fixation screws with focal areas of significant hypermetabolism at the level of the left L4 and L5 vertebral pedicles and degenerative changes in the L2 disk space, as well as the lower thoracic vertebrae.**

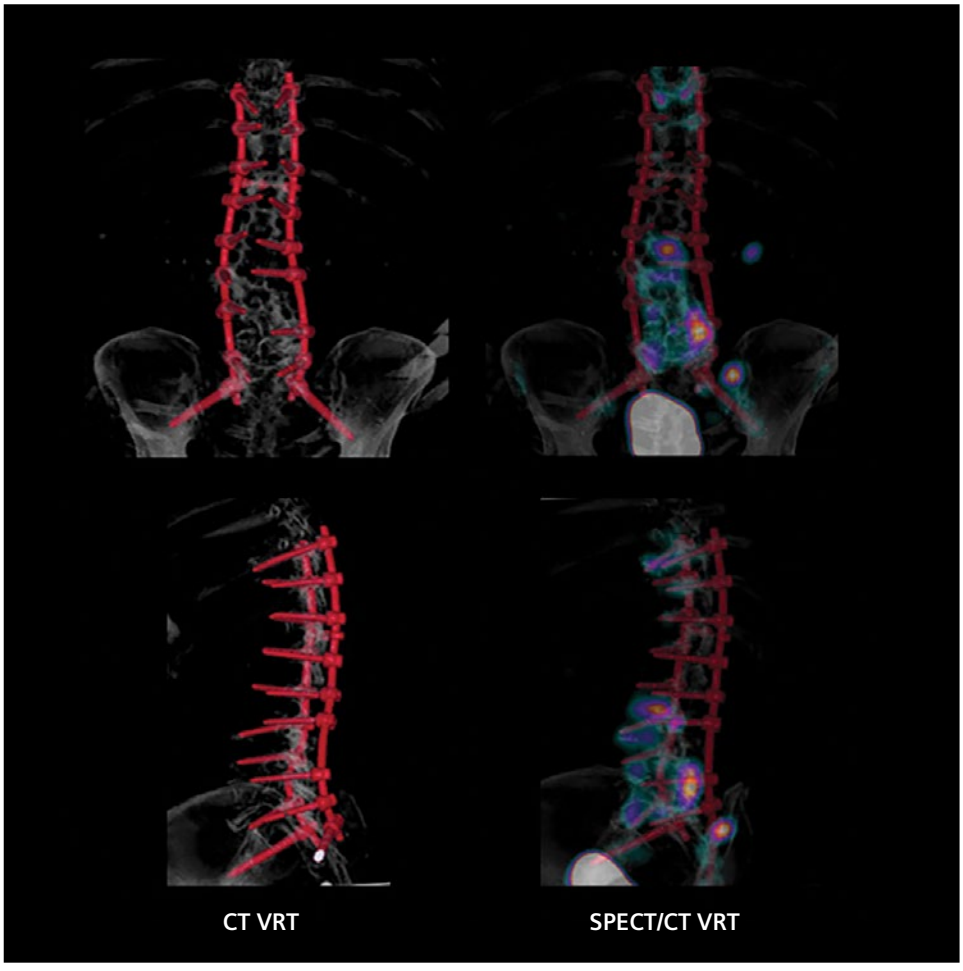

15 **Volume-rendered CT and SPECT/CT images in various orientations demonstrate the slight distortion of the left vertical spinal stabilization rod related to the scoliosis and fracture of the right vertical rod at the L4 level and fracture of left fixation screw at S1 level, along with the focal hypermetabolism at L4-L5 facet joint secondary to instability due to scoliosis-related shear stress, as well as the related instability of the left vertical rod and fixation screw at that level. The small focal hot area lateral to the left sacroiliac joint corresponds to a subchondral bone cyst.**

Findings

These findings clearly highlight the importance of high-quality CT with accurate SPECT fusion to enable the accurate interpretation of bone SPECT/CT in situations of spinal stabilization prosthesis fracture, instability, or loosening.

Thin-slice CT images and volume rendering sharply define the left and right posterior spinal stabilization rods and the fixation screws attaching the rod to the vertebral bodies, extending from T10 to S2. Although Symbia Pro.specta is capable of CT metal-artifact reduction (iMAR)[b], it was not applied with this patient. However, the high-quality, thin-slice CT provided optimum diagnostic information without excessive metal-related beam hardening, especially regarding the sites of fracture of the right spinal stabilization rod and the left S1 fixation screw and adjacent facet joints, particularly the sclerosis and focal lysis adjacent to the prosthesis.

CT images show fracture of the right vertical rod at the level of the mid-L4 vertebral body without significant displacement. There is no related hypermetabolism, suggesting absence of any instability on the right side due to this fracture. However, the scoliosis and instability related to the fracture of the left S1 fixation screw is the cause of severe L4-L5 facet arthropathy and associated bone stress around the fixation screw, which is reflected as focal hypermetabolism on SPECT images. The left vertical rod appears intact. The fracture of the left S1 screw distally within the vertebral body is sharply defined on thin-slice CT, although there appears to be no displacement or loosening. Increased uptake within a small lytic area in the left ilium adjacent to the sacroiliac joint associated with subchondral lucency with margin sclerosis likely represents a subchondral bone cyst or geode. Other transpedicular screws show normal alignment and absence of abnormal focal hypermetabolism, which suggests an absence of loosening. The lucency surrounding the left trans-sacroiliac joint screw is suggestive of early loosening. The low-grade uptake at the distal end of the screw reflects abnormal motion of the screw related to loosening.

Discussion

Spinal arthrodesis involving the fixation of vertebrae using metallic rods or plates with pedicular screws inserted within vertebral bodies through vertebral pedicles and lamina, often with intervertebral disc cages, are common surgical procedures for treating spinal instability in various spinal pathologies such as disc degeneration, spondylolisthesis and scoliosis, or kyphosis. A substantial percentage of patients experience recurrent pain following spine stabilization surgery with surgical re-intervention rates around 14% over 4-year follow-up.[1] Common conditions causing post-spinal-fusion-surgery pain are loosening and fracture of stabilization rods and screws, vertebral non-union, pseudoarthrosis, adjacent facet arthropathy, vertebral disk degeneration, and infection.

^{99m}Tc-HMDP bone SPECT/CT has been shown to have a high accuracy in the detection of the cause of post-spinal-surgery pain and instrumentation failure. Hudyana et al demonstrated a sensitivity of 100% and specificity of 89.7% for bone SPECT/CT for lumbar vertebral prosthesis loosening.[2] Overall, loosening was seen in 18.8% of patients undergoing lumbar stabilization surgery. However, in nearly 50% of patients with pain without evidence of loosening, SPECT/CT revealed other causes of symptoms including facet arthropathy, disc degeneration, and sacroiliac joint-degenerative arthropathy.

In this patient, SPECT/CT was instrumental in defining the exact cause of patient symptoms with clear visualization of fracture of the right vertical rod and left S1 pedicular screw. Symbia Pro.specta provided high-quality CT with 32-slice per sub-second rotation (0.33 seconds per rotation) at a collimation of 0.7 mm. The 1.5-mm-reconstructed CT slices with different kernels provided optimum visualization of fracture of the stabilization rods and pedicular screws, as well as the lucency and sclerosis around the screws. The lucency around the trans-sacroiliac joint screw on the left side visualized by the thin-slice CT together with the mild hypermetabolism around the screw was instrumental in detecting the early loosening of the screw. The presence of an osteolytic cyst lateral to the left sacroiliac joint with intense hypermetabolism and sclerotic margins is suggestive of a subchondral bone cyst, which is typically associated with severe sacroiliac joint degenerative changes.

The sclerosis medial to the insertion of the left L4 pedicular screw to the left-sided vertical stabilization rod visualized with thin-slice CT was precisely the region of hypermetabolism seen on SPECT/CT images, reflecting reactive bone stress due to instability, although there was no sign of loosening of the L4 pedicular screw. The intense hypermetabolism in the left L4/L5 facet joint associated with increased facet joint space and periarticular sclerosis reflects the actual cause of pain, which is related to the bone stress on the facet joint due to scoliosis, peri-prosthetic

bone loss, and instability related to abnormal motion from the left-side screw fracture and loosening. Other degenerative changes in L2 and L4-L5 disc spaces are also related to the scoliosis and instability.

Bone scintigraphy after lumbar fusion surgery can show hypermetabolism at the operative site for up to 1 year following surgery. However, the high intensity of uptake at the facet joint clearly identifies the site of active arthropathy to be the origin of the pain. The exact localization and characterization of multiple coexisting pathologies in this patient, including fracture of stabilization rod and screw, facet arthropathy, degenerative-disk disease, transsacroiliac screw loosening, and associated sacroiliac joint degenerative changes, is achieved through a combination of high-quality CT and SPECT with the exact co-registration of both leading to optimum visual and interpretational clarity.

Conclusion

This case demonstrates ^{99m}Tc-HMDP bone SPECT/CT imaging in the evaluation of pain following thoracolumbar spinal fusion surgery to identify facet arthropathy along with fracture of the spinal stabilization rod. The high-quality CT provided by Symbia Pro.specta was instrumental in defining prosthetic fractures, and when paired with the co-registered SPECT, resulted in SPECT/CT findings that provided clear evidence of the facet arthropathy being the cause of symptoms. ●

Examination protocol

Scanner: Symbia Pro.specta

SPECT	
Injected dose	20.9 mCi (776 MBq) ^{99m}Tc-HMDP
Post-injection delay	3 hours
Acquisition	3 bed positions/60 stops per detector, 10 seconds per stop
Image reconstruction	128 x 128 matrix, OSEM3D 7i15s

CT	
Tube voltage	130 kV
Tube current	30 ref mAs
Slice collimation	32 x 0.7 mm
Slick thickness	1.5 mm

The outcomes achieved by the Siemens Healthineers customers described herein were achieved in the customer's unique setting. Since there is no "typical" hospital and many variables exist (eg, hospital size, case mix, level of IT adoption) there can be no guarantee that others will achieve the same results.

References

[1] Martin BI, Mirza SK, Comstock BA, Gray DT, Kreuter W, Deyo RA. Are lumbar spine reoperation rates falling with greater use of fusion surgery and new surgical technology? *Spine* (Phila Pa 1976). 2007;32(19):2119-26. doi:10.1097/BRS.0b013e318145a56a.

[2] Hudyana H, Maes A, Vandenberghe T, Fidlers L, Sathekge M, Nicolai D, Van de Wiele C. Accuracy of bone SPECT/CT for identifying hardware loosening in patients who underwent lumbar fusion with pedicle screws. *Eur J Nucl Med Mol Imaging*. 2016;43(2):349-354. doi:10.1007/s00259-015-3158-7.

[a] Symbia Pro.specta is not commercially available in all countries. Future availability cannot be guaranteed.

[b] The amount of metal artifact reduction and corresponding improvement in image quality depends on a number of factors including: composition and size of the metal object, patient size, anatomical location and clinical practice. It is recommended to perform reconstruction with iMAR enabled in addition to conventional reconstruction without iMAR.

^{18}F FDG PET/CT delineation of diffuse large B-cell lymphoma involving lower spinal cord and spinal nerve roots

By Partha Ghosh, MD, Siemens Healthineers, Hoffman Estates, IL, USA
Data and images courtesy of Osaka City University Hospital, Osaka, Japan

History

A 50-year-old female with progressive weakness in both legs underwent PET/CT imaging to evaluate a spinal pathology. The study was conducted on a Biograph Vision™ 450 scanner using Fludeoxyglucose F 18 (^{18}F FDG) Injection.[a]

Approximately 51 minutes following the intravenous (IV) injection of 4.6 mCi (173 MBq) of ^{18}F FDG and completion of the initial low-dose CT, a dynamic whole-body PET acquisition was performed with FlowMotion™ continuous-bed-motion technology. A total of 6 consecutive whole-body passes were acquired at 3 minutes and 19 seconds per pass and subsequently summed into a single PET dataset. The individual dynamic whole-body PET acquisitions, as well as the summed PET data, were evaluated on a *syngo*.via workstation.

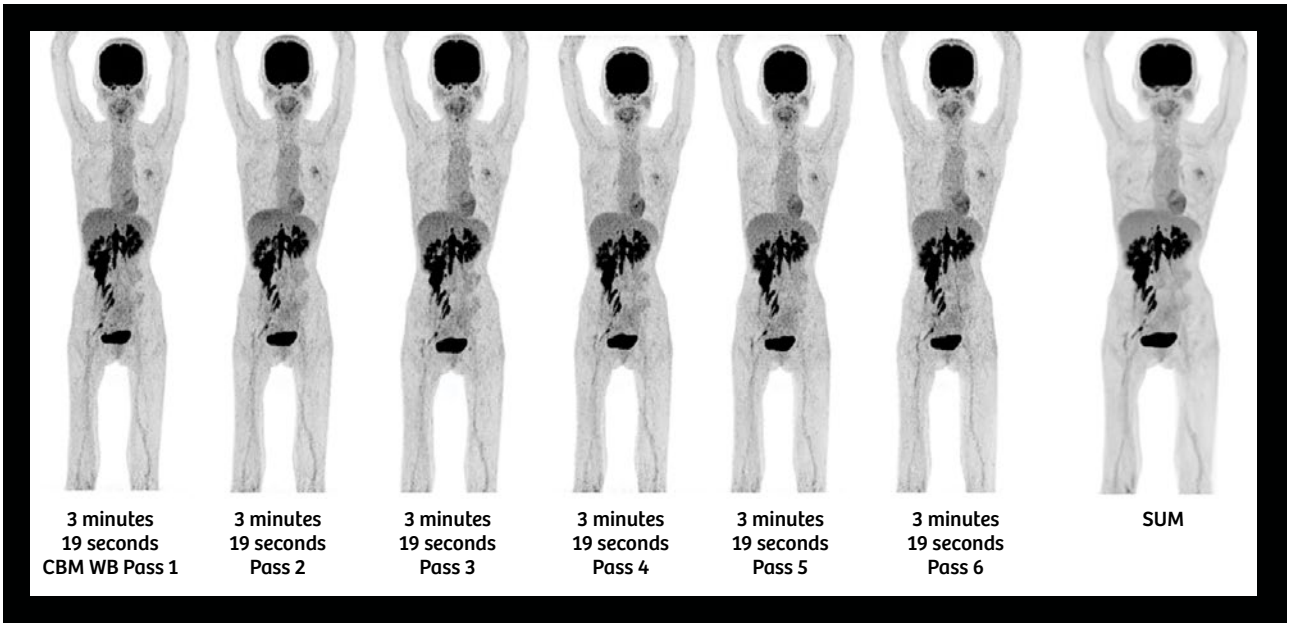

1 **Whole-body PET maximum intensity projection (MIP) images of 6 sequential whole-body PET FlowMotion acquisitions, acquired at 3 minutes and 19 seconds per pass (20-minute total scan time), along with the summed PET image.**

[a] Please see Indications and Important Safety Information for Fludeoxyglucose F 18 (^{18}F FDG) Injection on page 63. For full Prescribing Information, please see pages 70-72.

Fludeoxyglucose F 18 Injection

INDICATIONS AND USAGE

Fludeoxyglucose F 18 Injection is indicated for positron emission tomography (PET) imaging in the following settings:

- **Oncology:** For assessment of abnormal glucose metabolism to assist in the evaluation of malignancy in patients with known or suspected abnormalities found by other testing modalities, or in patients with an existing diagnosis of cancer.
- **Cardiology:** For the identification of left ventricular myocardium with residual glucose metabolism and reversible loss of systolic function in patients with coronary artery disease and left ventricular dysfunction, when used together with myocardial perfusion imaging.
- **Neurology:** For the identification of regions of abnormal glucose metabolism associated with foci of epileptic seizures.

IMPORTANT SAFETY INFORMATION

- **Radiation Risks:** Radiation-emitting products, including Fludeoxyglucose F 18 Injection, may increase the risk for cancer, especially in pediatric patients. Use the smallest dose necessary for imaging and ensure safe handling to protect the patient and health care worker.
- **Blood Glucose Abnormalities:** In the oncology and neurology setting, suboptimal imaging may occur in patients with inadequately regulated blood glucose levels. In these patients, consider medical therapy and laboratory testing to assure at least two days of normoglycemia prior to Fludeoxyglucose F 18 Injection administration.
- **Adverse Reactions:** Hypersensitivity reactions with pruritus, edema and rash have been reported; have emergency resuscitation equipment and personnel immediately available.

DOSAGE FORMS AND STRENGTHS

Multiple-dose 30 mL and 50 mL glass vial containing 0.74 to 7.40 GBq/mL (20 to 200 mCi/mL) of Fludeoxyglucose F 18 Injection and 4.5 mg of sodium chloride with 0.1 to 0.5% w/w ethanol as a stabilizer (approximately 15 to 50 mL volume) for intravenous administration.

Fludeoxyglucose F 18 Injection is manufactured by PETNET Solutions, a Siemens Healthineers Company, 810 Innovation Drive, Knoxville, TN 39732.

Findings

The visual evaluation of the sequential dynamic whole-body PET acquisitions, as well as the summed PET image comprised of data acquired over 20 minutes, shows intense ^{18}F FDG uptake in the lower spinal cord, lumbar spinal nerve roots, and cauda equina. In addition, a linear mass in the region of right psoas muscle, which includes the sacral spinal nerve roots within the pelvis is evident.

As depicted in Figures 4-9, the ^{18}F FDG PET/CT shows hypermetabolic and enlarged lower spinal cord and spinal nerve roots in bilateral L1 and L2, L4 and L5, and S1 and S2. The large right psoas mass appears to be an enlarged extension of the hypermetabolic right L2 nerve root. The right sacral nerve roots also show an extension of hypermetabolism along the neural sheath.

The pattern of such hypermetabolism—including the involvement of the spinal cord with continuous extension into spinal nerve roots seen in the lower spinal cord and L1 and L2 spinal nerve roots, as well as discontinuous involvement of right L4 and L5 and S1 and S2 nerve roots with extension along nerve tracts—suggests a primary spinal cord lesion with diffuse extension along nerve sheaths, which indicates the possibility of a primary spinal cord lymphoma or leukemia.

The patient underwent resection of the psoas lesion and a biopsy was performed on a surgical specimen of the involved nerve roots. The histopathology report revealed diffuse large B-cell lymphoma (DLBCL), and the patient was diagnosed with primary central nervous system DLBCL derived from the lumbar spinal cord.

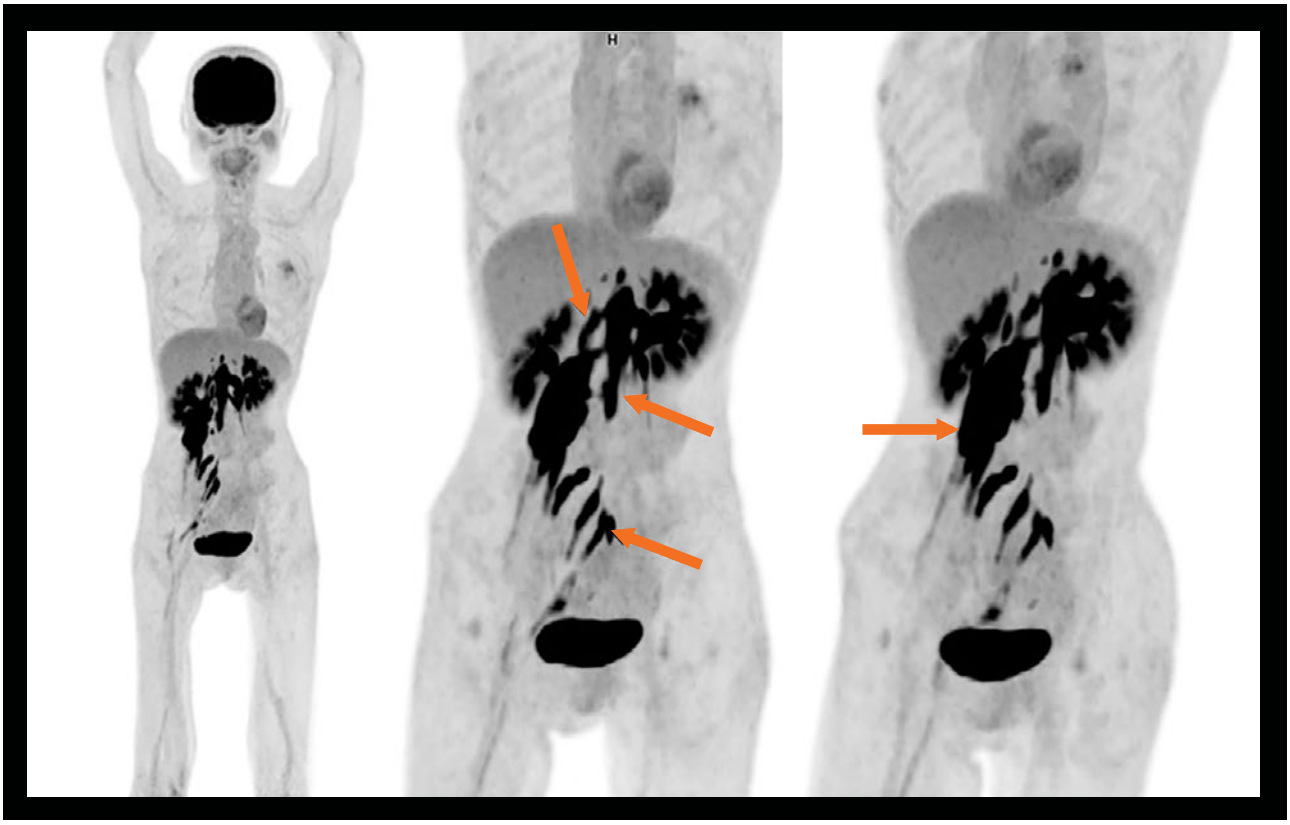

2 A MIP of summed whole-body PET/CT image shows intense ^{18}F FDG uptake in the spinal cord at the T12-L4 vertebral bodies (arrow), as well as at the spinal nerve roots of L1 and L2 vertebrae bilaterally (arrow). Intense uptake in the right L2 spinal nerve root expands into a large hypermetabolic mass within the right psoas muscle (arrow). Right lumbosacral trunk (L4 and L5 spinal nerve roots) as well as right S1 and S2 nerve roots are also enlarged and show hypermetabolic activity.

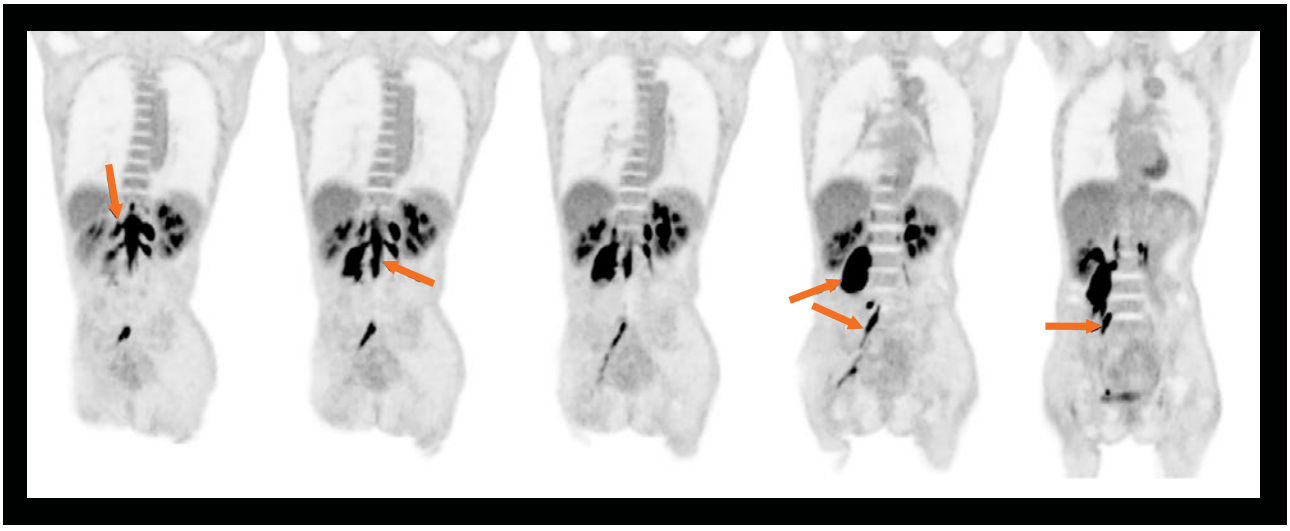

3 The coronal thin MIP of the summed PET image (left to right, posterior to anterior) visualizes an enlarged and hypermetabolic lower spinal cord from T12-L4 (arrow) along with bilaterally enlarged and hypermetabolic L1 (arrow) and L2 spinal nerve roots. An enlarged hypermetabolic psoas mass (arrow) is shown arising from the right L2 spinal nerve root. The enlarged hypermetabolic lumbosacral trunk (L4 and L5 spinal nerve roots) and S1 spinal nerve roots show hypermetabolism (arrows). The S1 spinal nerve depicts hypermetabolism along the entire nerve fiber.

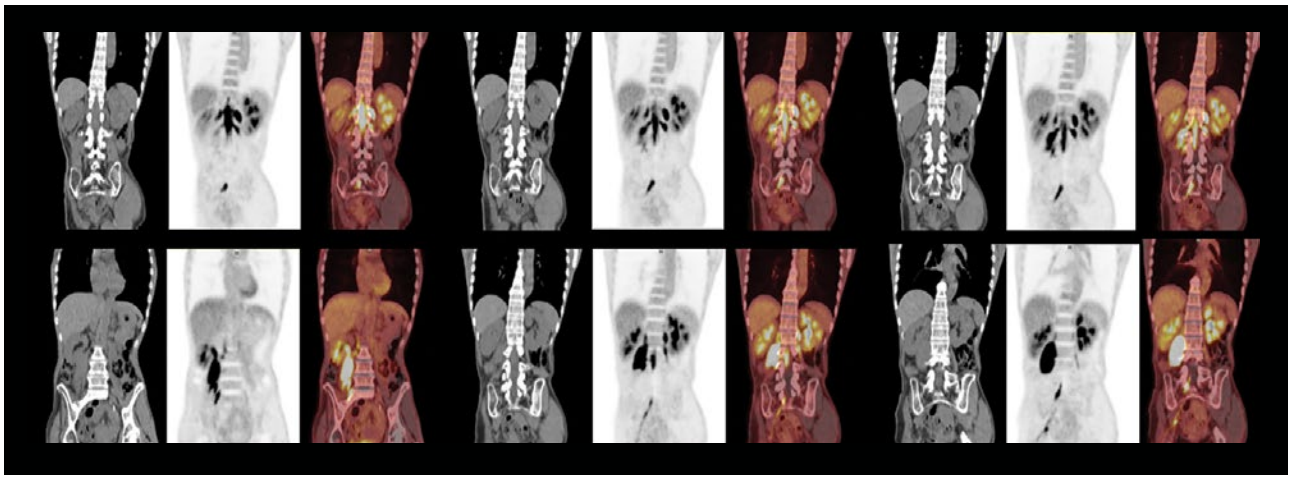

4 Coronal views of CT, PET, and fused images demonstrate spinal cord and spinal nerve enlargement and hypermetabolism. The hypermetabolic psoas mass arising from the right L2 spinal nerve root measures 9 cm x 3.3 cm and appears to be a lymphomatous expansion of the spinal nerve passing along the psoas muscle.

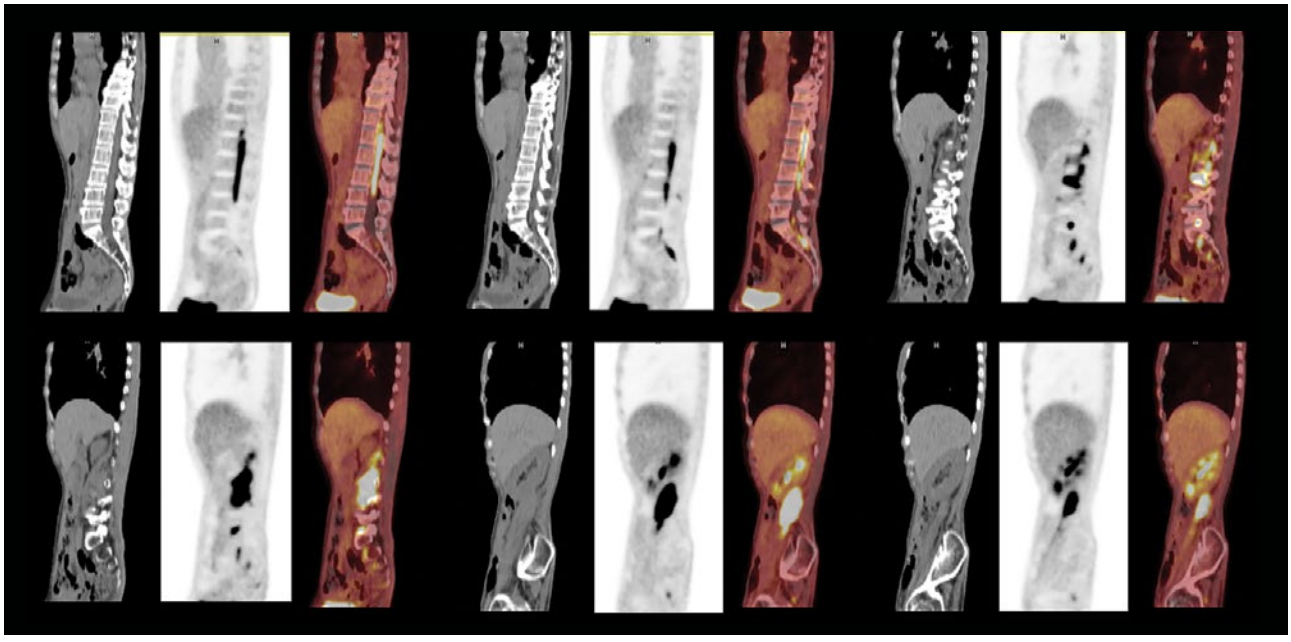

5 Sagittal views of CT, PET, and fused images show an enlarged hypermetabolic lower spinal cord from T1-L4, which reveals involvement of spinal nerve roots, enlarged psoas mass, and sacral nerve roots.

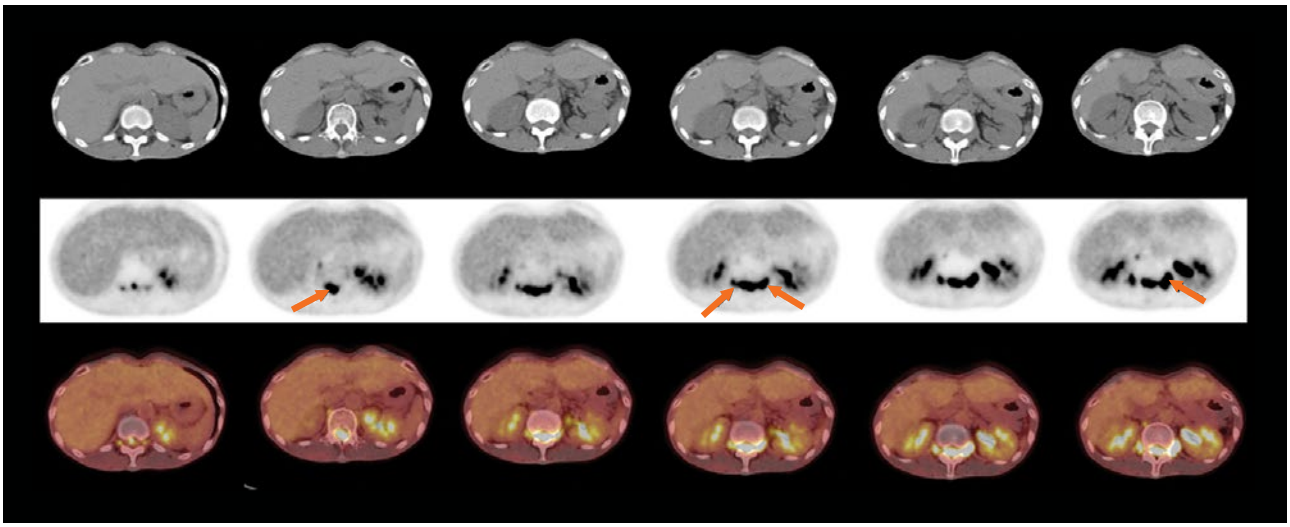

6 Axial views of CT, PET, and fused images from the level at lower end of the T12 vertebra to the L2 vertebrae show a hypermetabolic spinal cord (arrow) with enlarged hypermetabolic bilateral L1 and L2 spinal nerve roots (arrows).

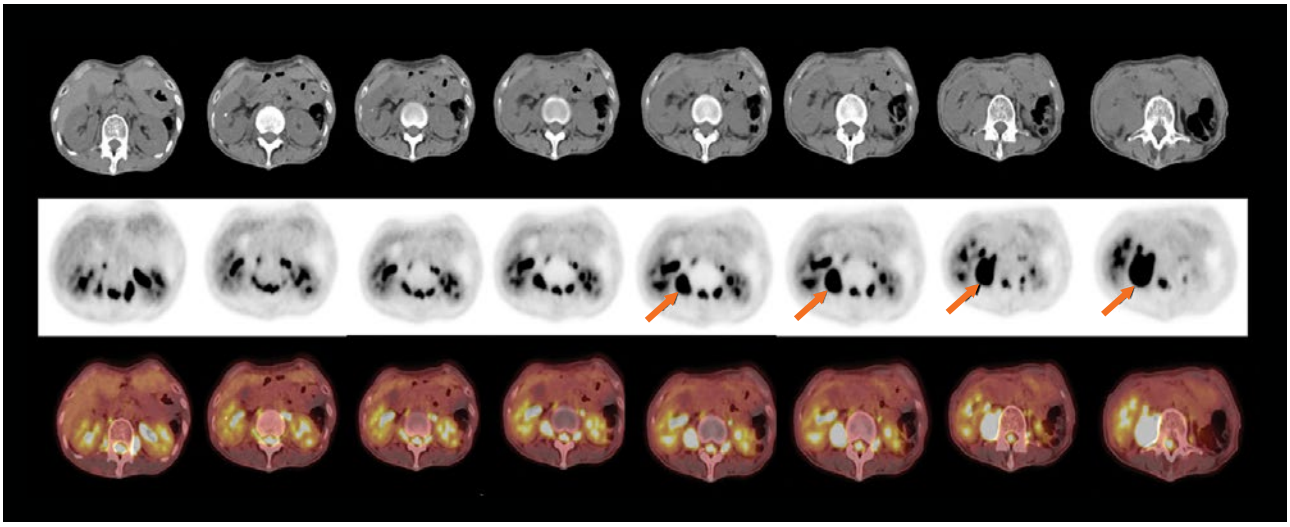

7 Axial views of CT, PET, and fused images from L2-L4 show hypermetabolic spinal cord and spinal nerve roots in addition to a hypermetabolic mass in the region of the right psoas muscle (arrows) measuring 3.9 cm x 3.83 cm maximum dimension in the axial section.

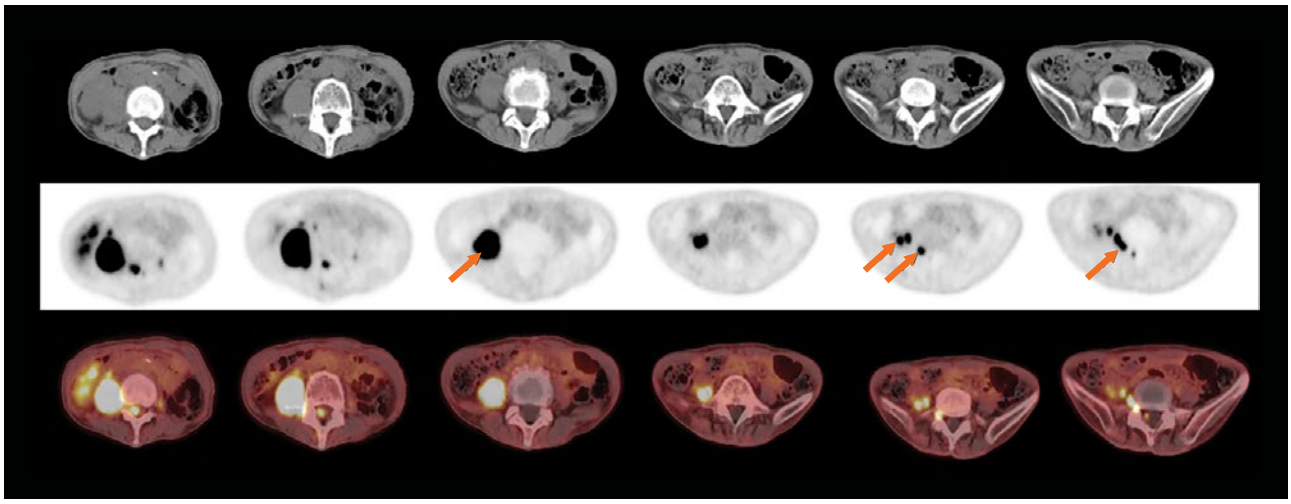

8 Axial views of CT, PET, and fused images from L4-S1 show an enlarged hypermetabolic psoas mass (arrow), which bifurcates further into the pelvic nerve roots (arrow). A hypermetabolic right lumbosacral nerve root (L4 and L5 spinal nerve root combined) exiting from the right L5-S1 spinal canal is also visualized (arrow).

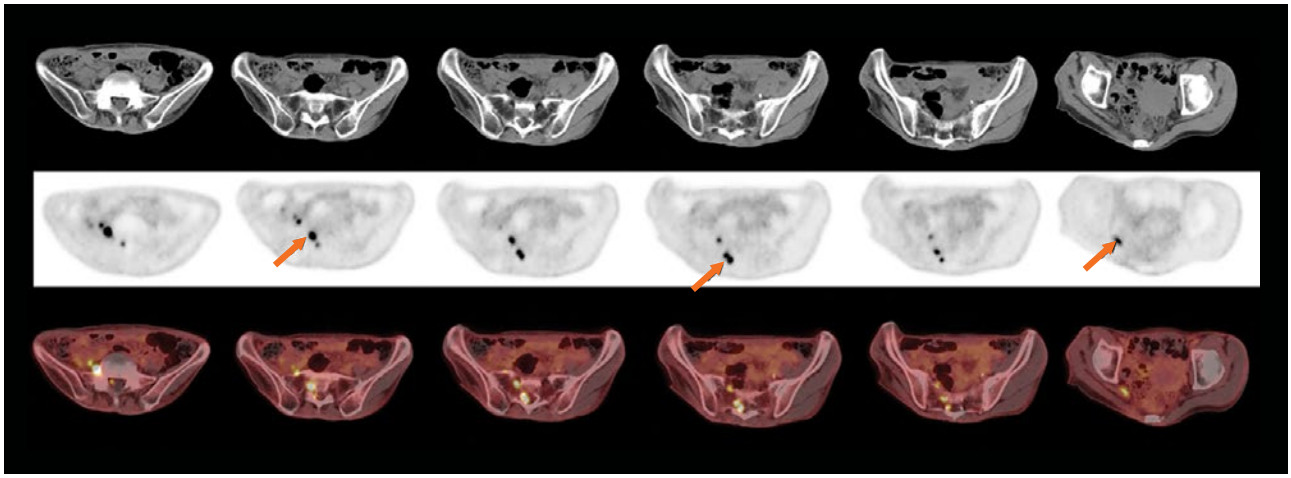

9 Axial views of CT, PET, and fused images through the sacrum and pelvis demonstrate a hypermetabolic enlarged sacral nerve roots on the right side (arrows), specifically the lumbosacral S1 and S2 nerve roots.

Discussion

Primary central nervous system B-cell lymphoma accounts for 4-6% of all malignant lymphomas.[1] There is increased incidence in immunocompromised individuals, including acquired immunodeficiency syndrome and transplant recipients. Direct infiltration of the cauda equina is rare and is usually in the form of a primary localized or disseminated form of central nervous system (CNS) lymphoma. Most common presentations are muscular weakness, paraparesis or paraplegia, and radiculopathy. Magnetic resonance imaging (MRI) findings include swelling of the involved spinal cord and nerve roots, which is either hypo- or iso-intense to the normal spinal cord in both T1 and T2 with enhancement following contrast. ^{18}F FDG PET/CT shows increased tracer accumulation in the involved areas with the SUV being lower than that of general DLBCL. In a case report of lower spinal cord and cauda equina DLCBL, the calculated SUV_{max} in two lesions at 9.6 and 4.9 were deemed lower than those reported for non-neurological DLBCL.[1] In this particular case, the SUV_{max} were much higher, although consideration should be given to the Biograph Vision 450 PET/CT system and its 214-picosecond time-of-flight (TOF) performance with high-resolution PET acquisition, which results in higher SUV_{max} levels.

Intense accumulation of ^{18}F FDG in the lower spinal cord from T12-L4, as well as the spinal nerve roots seen in the present case are typical of spinal cord DLBCL. The enlargement of the involved nerve roots seen on both CT and PET correlates with typical MRI findings in similar clinical situations. The large, intensely hypermetabolic mass in the right psoas region, which arises from the involved right L2 spinal nerve root may be an affected paravertebral ganglion. In the absence of any non-nervous system involvement, the right psoas mass was evaluated as the primary neurological origin, and the biopsy revealed it to be a primary CNS large B-cell lymphoma.

Conclusion

This case illustrates how a comprehensive PET/CT evaluation of nervous system lymphoma helps delineate the extent of disease infiltration. The high resolution of the Biograph Vision 450 system paired with the high contrast-to-background ratio achieved due to high TOF performance helps achieve sharp definition with high contrast within nerve tract lesions, as seen in the involved pelvic nerves arising from the S1 and S2 nerve roots that are clearly defined on PET/CT. ●

Examination protocol

Scanner: Biograph Vision 450

PET		CT	
Injected dose	4.6 mCi (173 MBq)	Tube voltage	120 kV
Post-injection delay	51 minutes	Tube current	100 ref mAs
Acquisition	6 whole-body passes acquired with FlowMotion technology	Slice collimation	64 x 0.6 mm
Scan time	Total scan time of 20 minutes: 3 minutes and 19 seconds per pass	Slice thickness	1.5 mm reconstructed
		Reconstruction kernel	B31f

The outcomes achieved by the Siemens Healthineers customer described herein were achieved in the customer's unique setting. Since there is no "typical" hospital and many variables exist (eg, hospital size, case mix, level of IT adoption) there can be no guarantee that others will achieve the same results.

References

[1] Suzuki K, Yasuda T, Hiraiwa T, et al. Primary cauda equina lymphoma diagnosed by nerve biopsy: A case report and literature review. *Oncology Letters.* 2018;16(1):623-631. doi:10.3892/ol.2018.8629.

Imprint

Publisher
Siemens Medical Solutions USA, Inc.
2501 N. Barrington Road
Hoffman Estates, IL 60192-2061
USA
Phone: +1 847-304-7700
siemens-healthineers.com/mi

Editor
Catherine Joyce
catherine.joyce@siemens-healthineers.com

Journalists
Sameh Fahmy
Claudette Lew
Reinaldo Lopes
Takeshi Shimizu
Philipp Grätzel von Grätz

Photographers
Jonathan Browning
James Farrell
Matti Immonen
Ezequiel Scagnetti

Illustrations
Zeichen und Zeit GmbH

Text & Photographic Contribution
Primafila AG, Zurich, Switzerland/
Primafila Correspondents

Layout
Clint Poy Design, Georgia, USA

Printer
The YGS Group, York, Pennsylvania, USA

***Imaging Life* is available online:**
siemens-healthineers.com/NMNS

Some of the imaging biomarkers in this publication are not currently recognized by the U.S. Food and Drug Administration (FDA) or other regulatory agencies as being safe and effective, and Siemens Healthineers does not make any claims regarding their use.

DISCLAIMERS: *Imaging Life*: "The information presented in this magazine is for illustration only and is not intended to be relied upon by the reader for instruction as to the practice of medicine. Healthcare practitioners reading this information are reminded that they must use their own learning, training and expertise in dealing with their individual patients. This material does not substitute for that duty and is not intended by Siemens Healthcare GmbH to be used for any purpose in that regard." Contrast agents: "The drugs and doses mentioned herein are consistent with the approved labeling for uses and/or indications of the drug. The treating physician bears the sole responsibility for the diagnosis and treatment of patients, including drugs and doses prescribed in connection with such use. The operating instructions must always be strictly followed when operating your Siemens system. The source for the technical data is the corresponding data sheets." Trademarks: "All trademarks mentioned in this document are property of their respective owners." Results: "The outcomes achieved by the Siemens customers described herein were achieved in the customer's unique setting. Since there is no "typical" hospital and many variables exist (e.g., hospital size, case mix, level of IT adoption), there can be no guarantee that others will achieve the same results."

SIEMENS Healthineers

HIGHLIGHTS OF PRESCRIBING INFORMATION

These highlights do not include all the information needed to use Fludeoxyglucose F 18 Injection safely and effectively. See full prescribing information for Fludeoxyglucose F 18 Injection.

Fludeoxyglucose F 18 Injection, USP
For intravenous use
Initial U.S. Approval: 2005

INDICATIONS AND USAGE

Fludeoxyglucose F 18 Injection is indicated for positron emission tomography (PET) imaging in the following settings:

- Oncology: For assessment of abnormal glucose metabolism to assist in the evaluation of malignancy in patients with known or suspected abnormalities found by other testing modalities, or in patients with an existing diagnosis of cancer.
- Cardiology: For the identification of left ventricular myocardium with residual glucose metabolism and reversible loss of systolic function in patients with coronary artery disease and left ventricular dysfunction, when used together with myocardial perfusion imaging.
- Neurology: For the identification of regions of abnormal glucose metabolism associated with foci of epileptic seizures (1).

DOSAGE AND ADMINISTRATION

Fludeoxyglucose F 18 Injection emits radiation. Use procedures to minimize radiation exposure. Screen for blood glucose abnormalities.

- In the oncology and neurology settings, instruct patients to fast for 4 to 6 hours prior to the drug's injection. Consider medical therapy and laboratory testing to assure at least two days of normoglycemia prior to the drug's administration (5.2).
- In the cardiology setting, administration of glucose-containing food or liquids (e.g., 50 to 75 grams) prior to the drug's injection facilitates localization of cardiac ischemia (2.3).

Aseptically withdraw Fludeoxyglucose F 18 Injection from its container and administer by intravenous injection (2).

The recommended dose:

- for adults is 5 to 10 mCi (185 to 370 MBq), in all indicated clinical settings (2.1).
- for pediatric patients is 2.6 mCi in the neurology setting (2.2).

Initiate imaging within 40 minutes following drug injection; acquire static emission images 30 to 100 minutes from time of injection (2).

DOSAGE FORMS AND STRENGTHS

Multi-dose 30mL and 50mL glass vial containing 0.74 to 7.40 GBq/mL (20 to 200 mCi/mL) Fludeoxyglucose F 18 Injection and 4.5mg of sodium chloride with 0.1 to 0.5% w/w ethanol as a stabilizer (approximately 15 to 50 mL volume) for intravenous administration (3).

CONTRAINDICATIONS

None.

WARNINGS AND PRECAUTIONS

- Radiation risks: use smallest dose necessary for imaging (5.1).
- Blood glucose adnormalities: may cause suboptimal imaging (5.2).

ADVERSE REACTIONS

Hypersensitivity reactions have occurred; have emergency resuscitation equipment and personnel immediately available (6).

To report SUSPECTED ADVERSE REACTIONS, contact PETNET Solutions, Inc. at 877-473-8638 or FDA at 1-800-FDA-1088 or www.fda.gov/medwatch.

USE IN SPECIFIC POPULATIONS

- Lactation: Temporarily discontinue breastfeeding. A lactating woman should pump and discard breastmilk for 9 hours after Fludeoxyglucose F 18 Injection (8.2).
- Pediatric Use: Safety and effectiveness in pediatric patients have not been established in the oncology and cardiology settings (8.4).

See 17 for PATIENT COUNSELING INFORMATION

Revised: 10/2019

FULL PRESCRIBING INFORMATION: CONTENTS*

* Sections or subsections omitted from the full prescribing information are not listed.

FULL PRESCRIBING INFORMATION

1 INDICATIONS AND USAGE

Fludeoxyglucose F 18 Injection is indicated for positron emission tomography (PET) imaging in the following settings:

1.1 Oncology

For assessment of abnormal glucose metabolism to assist in the evaluation of malignancy in patients with known or suspected abnormalities found by other testing modalities, or in patients with an existing diagnosis of cancer.

1.2 Cardiology

For the identification of left ventricular myocardium with residual glucose metabolism and reversible loss of systolic function in patients with coronary artery disease and left ventricular dysfunction, when used together with myocardial perfusion imaging.

1.3 Neurology

For the identification of regions of abnormal glucose metabolism associated with foci of epileptic seizures.

2 DOSAGE AND ADMINISTRATION

Fludeoxyglucose F 18 Injection emits radiation. Use procedures to minimize radiation exposure. Calculate the final dose from the end of synthesis (EOS) time using proper radioactive decay factors. Assay the final dose in a properly calibrated dose calibrator before administration to the patient *[see Description (11.2)]*.

2.1 Recommended Dose for Adults

Within the oncology, cardiology and neurology settings, the recommended dose for adults is 5 to 10 mCi (185 to 370 MBq) as an intravenous injection.

2.2 Recommended Dose for Pediatric Patients

Within the neurology setting, the recommended dose for pediatric patients is 2.6 mCi, as an intravenous injection. The optimal dose adjustment on the basis of body size or weight has not been determined *[see Use in Special Populations (8.4)]*.

2.3 Patient Preparation

- To minimize the radiation absorbed dose to the bladder, encourage adequate hydration. Encourage the patient to drink water or other fluids (as tolerated) in the 4 hours before their PET study.
- Encourage the patient to void as soon as the imaging study is completed and as often as possible thereafter for at least one hour.
- Screen patients for clinically significant blood glucose abnormalities by obtaining a history and/or laboratory tests *[see Warnings and Precautions (5.2)]*. Prior to Fludeoxyglucose F 18 PET imaging in the oncology and neurology settings, instruct patient to fast for 4 to 6 hours prior to the drug's injection.
- In the cardiology setting, administration of glucose-containing food or liquids (e.g., 50 to 75 grams) prior to Fludeoxyglucose F 18 Injection facilitates localization of cardiac ischemia.

2.4 Radiation Dosimetry

The estimated human absorbed radiation doses (rem/mCi) to a newborn (3.4 kg), 1-year old (9.8 kg), 5-year old (19 kg), 10-year old (32 kg), 15-year old (57 kg), and adult (70 kg) from intravenous administration of Fludeoxyglucose F 18 Injection are shown in Table 1. These estimates were calculated based on human[2] data and using the data published by the International Commission on Radiological Protection[4] for Fludeoxyglucose ^{18}F. The dosimetry data show that there are slight variations in absorbed radiation dose for various organs in each of the age groups. These dissimilarities in absorbed radiation dose are due to developmental age variations (e.g., organ size, location, and overall metabolic rate for each age group). The identified critical organs (in descending order) across all age groups evaluated are the urinary bladder, heart, pancreas, spleen, and lungs.

Table 1. Estimated Absorbed Radiation Doses (rem/mCi) After Intravenous Administration of Fludeoxyglucose F 18 Injection[a]

Organ	Newborn (3.4 kg)	1-year old (9.8 kg)	5-year old (19 kg)	10-year old (32 kg)	15-year old (57 kg)	Adult (70 kg)
Bladder wall[b]	4.3	1.7	0.93	0.60	0.40	0.32
Heart wall	2.4	1.2	0.70	0.44	0.29	0.22
Pancreas	2.2	0.68	0.33	0.25	0.13	0.096
Spleen	2.2	0.84	0.46	0.29	0.19	0.14
Lungs	0.96	0.38	0.20	0.13	0.092	0.064
Kidneys	0.81	0.34	0.19	0.13	0.089	0.074
Ovaries	0.80	0.8	0.19	0.11	0.058	0.053
Uterus	0.79	0.35	0.19	0.12	0.076	0.062
LLI wall *	0.69	0.28	0.15	0.097	0.060	0.051
Liver	0.69	0.31	0.17	0.11	0.076	0.058
Gallbladder wall	0.69	0.26	0.14	0.093	0.059	0.049
Small intestine	0.68	0.29	0.15	0.096	0.060	0.047
ULI wall **	0.67	0.27	0.15	0.090	0.057	0.046
Stomach wall	0.65	0.27	0.14	0.089	0.057	0.047
Adrenals	0.65	0.28	0.15	0.095	0.061	0.048
Testes	0.64	0.27	0.14	0.085	0.052	0.041
Red marrow	0.62	0.26	0.14	0.089	0.057	0.047
Thymus	0.61	0.26	0.14	0.086	0.056	0.044
Thyroid	0.61	0.26	0.13	0.080	0.049	0.039
Muscle	0.58	0.25	0.13	0.078	0.049	0.039
Bone surface	0.57	0.24	0.12	0.079	0.052	0.041
Breast	0.54	0.22	0.11	0.068	0.043	0.034
Skin	0.49	0.20	0.10	0.060	0.037	0.030
Brain	0.29	0.13	0.09	0.078	0.072	0.070
Other tissues	0.59	0.25	0.13	0.083	0.052	0.042

[a] MIRDOSE 2 software was used to calculate the radiation absorbed dose.
[b] The dynamic bladder model with a uniform voiding frequency of 1.5 hours was used.
* LLI = lower large intestine; ** ULI = upper large intestine

2.5 Radiation Safety – Drug Handling

- Use waterproof gloves, effective radiation shielding, and appropriate safety measures when handling Fludeoxyglucose F 18 Injection to avoid unnecessary radiation exposure to the patient, occupational workers, clinical personnel and other persons.
- Radiopharmaceuticals should be used by or under the control of physicians who are qualified by specific training and experience in the safe use and handling of radionuclides, and whose experience and training have been approved by the appropriate governmental agency authorized to license the use of radionuclides.
- Calculate the final dose from the end of synthesis (EOS) time using proper radioactive decay factors. Assay the final dose in a properly calibrated dose calibrator before administration to the patient *[see Description (11.2)]*.
- The dose of Fludeoxyglucose F 18 used in a given patient should be minimized consistent with the objectives of the procedure, and the nature of the radiation detection devices employed.

2.6 Drug Preparation and Administration

- Calculate the necessary volume to administer based on calibration time and dose.
- Aseptically withdraw Fludeoxyglucose F 18 Injection from its container.
- Inspect Fludeoxyglucose F 18 Injection visually for particulate matter and discoloration before administration, whenever solution and container permit.
- Do not administer the drug if it contains particulate matter or discoloration; dispose of these unacceptable or unused preparations in a safe manner, in compliance with applicable regulations.
- Use Fludeoxyglucose F 18 Injection within 12 hours from the EOS.

2.7 Imaging Guidelines

- Initiate imaging within 40 minutes following Fludeoxyglucose F 18 Injection administration.
- Acquire static emission images 30 to 100 minutes from the time of injection.

3 DOSAGE FORMS AND STRENGTHS

Multiple-dose 30 mL and 50 mL glass vial containing 0.74 to 7.40 GBq/mL (20 to 200 mCi/mL) of Fludeoxyglucose F 18 Injection and 4.5 mg of sodium chloride with 0.1 to 0.5% w/w ethanol as a stabilizer (approximately 15 to 50 mL volume) for intravenous administration.

4 CONTRAINDICATIONS

None.

5 WARNINGS AND PRECAUTIONS

5.1 Radiation Risks

Radiation-emitting products, including Fludeoxyglucose F 18 Injection, may increase the risk for cancer, especially in pediatric patients. Use the smallest dose necessary for imaging and ensure safe handling to protect the patient and health care worker *[see Dosage and Administration (2.5)]*.

5.2 Blood Glucose Abnormalities

In the oncology and neurology setting, suboptimal imaging may occur in patients with inadequately regulated blood glucose levels. In these patients, consider medical therapy and laboratory testing to assure at least two days of normoglycemia prior to Fludeoxyglucose F 18 Injection administration.

6 ADVERSE REACTIONS

Hypersensitivity reactions with pruritus, edema and rash have been reported in the post-marketing setting. Have emergency resuscitation equipment and personnel immediately available.

7 DRUG INTERACTIONS

The interactions of Fludeoxyglucose F 18 Injection with other drugs taken by patients undergoing PET imaging has not been studied.

8 USE IN SPECIFIC POPULATIONS

8.1 Pregnancy

Risk Summary

Data from published case series and case reports describe Fludeoxyglucose F 18 Injection crossing the placenta with uptake by the fetus (see Data). All radiopharmaceuticals have the potential to cause fetal harm depending on the fetal stage of development and the magnitude of the radiation dose. However, published studies that describe Fludeoxyglucose F 18 Injection use in pregnant women have not identified a risk of drug-associated major birth defects, miscarriage, or adverse maternal or fetal outcomes. If considering Fludeoxyglucose F 18 Injection administration to a pregnant woman, inform the patient about the potential for adverse pregnancy outcomes based on the radiation dose from Fludeoxyglucose F 18 Injection and the gestational timing of exposure. The estimated background risk of major birth defects and miscarriage for the indicated population is unknown. All pregnancies have a background risk of birth defect, loss, or other adverse outcomes. In the U.S. general population, the estimated background risk of major birth defects and miscarriage in clinically recognized pregnancies are 2-4% and 15-20%, respectively.

Data

Human Data

Data from published case series and case reports describe Fludeoxyglucose F 18 Injection crossing the placental barrier and visualization of radioactivity throughout the body of the fetus. The estimated fetal absorbed radiation dose from the maximum labeled dose (370 MBq) of Fludeoxyglucose F 18 was 10 mGy with first trimester exposure to PET alone and 20 mGy with first trimester exposure to PET/CT scan combination. Long-term adverse radiation effects to a child exposed to Fludeoyxglucose F 18 Injection in utero are unknown. No adverse fetal effects or radiation-related risks have been identified for diagnostic procedures involving less than 50 mGy, which represents less than 20 mGy fetal doses.

8.2 Lactation

Risk Summary

A published case report and case series show the presence of Fludeoxyglucose F 18 Injection in human milk following administration. There are no data on the effects of Fludeoxyglucose F 18 Injection on the breastfed infant or the effects on milk production. Exposure of Fludeoxyglucose F 18 Injection to a breastfed infant can be minimized by temporary discontinuation of breastfeeding (see Clinical Considerations). The developmental and health benefits of breastfeeding should be considered along with the mother's clinical need for Fludeoxyglucose F 18 Injection, any potential adverse effects on the breastfed child from Fludeoxyglucose F 18 Injection or from the underlying maternal condition.

Clinical Considerations

To decrease radiation exposure to the breastfed infant, advise a lactating woman to pump and discard breastmilk and avoid close (breast) contact with the infant for at least 9 hours after the administration of Fludeoxyglucose F 18 Injection.

8.4 Pediatric Use

The safety and effectiveness of Fludeoxyglucose F 18 Injection in pediatric patients with epilepsy is established on the basis of studies in adult and pediatric patients. In pediatric patients with epilepsy, the recommended dose is 2.6 mCi. The optimal dose adjustment on the basis of body size or weight has not been determined. In the oncology or cardiology settings, the safety and effectiveness of Fludeoxyglucose F 18 Injection have not been established in pediatric patients.

11 DESCRIPTION

11.1 Chemical Characteristics

Fludeoxyglucose F 18 Injection is a positron emitting radiopharmaceutical that is used for diagnostic purposes in conjunction with positron emission tomography (PET) imaging. The active ingredient 2-deoxy-2-[^{18}F]fluoro-D-glucose has the molecular formula of $C_6H_{11}{}^{18}FO_5$ with a molecular weight of 181.26, and has the following chemical structure:

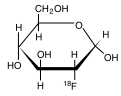

Fludeoxyglucose F 18 Injection is provided as a ready to use sterile, pyrogen free, clear, colorless solution. Each mL contains between 0.740 to 7.40GBq (20.0 to 200 mCi) of 2-deoxy-2-[^{18}F]fluoro-D-glucose at the EOS, 4.5 mg of sodium chloride and 0.1 to 0.5% w/w ethanol as a stabilizer. The pH of the solution is between 4.5 and 7.5. The solution is packaged in a multiple-dose glass vial and does not contain any preservative.

11.2 Physical Characteristics

Fluorine F 18 has a physical half-life of 109.7 minutes and decays to Oxygen O 16 (stable) by positron decay. The principal photons useful for imaging are the dual 511 keV "annihilation" gamma photons, that are produced and emitted simultaneously in opposite direction when the positron interacts with an electron (Table 2).

Table 2. Principal Radiation Emission Data for Fluorine F 18

Radiation/Emission	% Per Disintegration	Mean Energy
Positron (β+)	96.73	249.8 keV
Gamma (±)*	193.46	511.0 keV

*Produced by positron annihilation

From: Kocher, D.C. Radioactive Decay Tables DOE/TIC-I 1026, 89 (1981)

The specific gamma ray constant (point source air kerma coefficient) for fluorine F 18 is 5.7 R/hr/mCi (1.35 x 10^{-6} Gy/hr/kBq) at 1 cm. The half-value layer (HVL) for the 511 keV photons is 4 mm lead (Pb). The range of attenuation coefficients for this radionuclide as a function of lead shield thickness is shown in Table 3. For example, the interposition of an 8 mm thickness of Pb, with a coefficient of attenuation of 0.25, will decrease the external radiation by 75%.

Table 3. Radiation Attenuation of 511 keV Photons by lead (Pb) shielding

Shield thickness (Pb) mm	Coefficient of attenuation
0	0.00
4	0.50
8	0.25
13	0.10
26	0.01
39	0.001
52	0.0001

For use in correcting for physical decay of this radionuclide, the fractions remaining at selected intervals after calibration are shown in Table 4.

Table 4. Physical Decay Chart for Fluorine F 18

Minutes	Fraction Remaining
0*	1.000
15	0.909
30	0.826
60	0.683
110	0.500
220	0.250

*calibration time

12 CLINICAL PHARMACOLOGY

12.1 Mechanism of Action

Fludeoxyglucose F 18 is a glucose analog that concentrates in cells that rely upon glucose as an energy source, or in cells whose dependence on glucose increases under pathophysiological conditions. Fludeoxyglucose F 18 is transported through the cell membrane by facilitative glucose transporter proteins and is phosphorylated within the cell to [^{18}F] FDG-6-phosphate by the enzyme hexokinase. Once phosphorylated it cannot exit until it is dephosphorylated by glucose-6-phosphatase. Therefore, within a given tissue or pathophysiological process, the retention and clearance of Fludeoxyglucose F 18 reflect a balance involving glucose transporter, hexokinase and glucose-6-phosphatase activities. F 18 is used to assess glucose metabolism.

In comparison to background activity of the specific organ or tissue type, regions of decreased or absent uptake of Fludeoxyglucose F 18 reflect the decrease or absence of glucose metabolism. Regions of increased uptake of Fludeoxyglucose F 18 reflect greater than normal rates of glucose metabolism.

12.2 Pharmacodynamics

Fludeoxyglucose F 18 Injection is rapidly distributed to all organs of the body after intravenous administration. After background clearance of Fludeoxyglucose F 18 Injection, optimal PET imaging is generally achieved between 30 to 40 minutes after administration.

In cancer, the cells are generally characterized by enhanced glucose metabolism partially due to (1) an increase in activity of glucose transporters, (2) an increased rate of phosphorylation activity, (3) a reduction of phosphatase activity or, (4) a dynamic alteration in the balance among all these processes. However, glucose metabolism of cancer as reflected by Fludeoxyglucose F 18 accumulation shows considerable variability. Depending on tumor type, stage, and location, Fludeoxyglucose F 18 accumulation may be increased, normal, or decreased. Also, inflammatory cells can have the same variability of uptake of Fludeoxyglucose F 18.

In the heart, under normal aerobic conditions, the myocardium meets the bulk of its energy requirements by oxidizing free fatty acids. Most of the exogenous glucose taken up by the myocyte is converted into glycogen. However, under ischemic conditions, the oxidation of free fatty acids decreases, exogenous glucose becomes the preferred myocardial substrate, glycolysis is stimulated, and glucose taken up by the myocyte is metabolized immediately instead of being converted into glycogen. Under these conditions, phosphorylated Fludeoxyglucose F 18 accumulates in the myocyte and can be detected with PET imaging.

In the brain, cells normally rely on aerobic metabolism. In epilepsy, the glucose metabolism varies. Generally, during a seizure, glucose metabolism increases. Interictally, the seizure focus tends to be hypometabolic.

12.3 Pharmacokinetics

Distribution: In four healthy male volunteers, receiving an intravenous administration of 30 seconds induration, the arterial blood level profile for Fludeoxyglucose F 18 decayed triexponentially. The effective half-life ranges of the three phases were 0.2 to 0.3 minutes, 10 to 13 minutes with a mean and standard deviation (STD) of 11.6 (±) 1.1 min, and 80 to 95 minutes with a mean and STD of 88 (±) 4 min.

Plasma protein binding of Fludeoxyglucose F 18 has not been studied.

Metabolism: Fludeoxyglucose F 18 is transported into cells and phosphorylated to [^{18}F]-FDG-6-phosphate at a rate proportional to the rate of glucose utilization within that tissue. [^{18}F]-FDG-6-phosphate presumably is metabolized to 2-deoxy-2-[^{18}F]fluoro-6-phospho-D-mannose([^{18}F]FDM-6-phosphate).

Fludeoxyglucose F 18 Injection may contain several impurities (e.g., 2-deoxy-2-chloro-D-glucose (ClDG)). Biodistribution and metabolism of ClDG are presumed to be similar to Fludeoxyglucose F 18 and would be expected to result in intracellular formation of 2-deoxy-2-chloro-6-phospho-D-glucose (ClDG-6-phosphate) and 2-deoxy-2-chloro-6-phospho-D-mannose (ClDM-6-phosphate). The phosphorylated deoxyglucose compounds are dephosphorylated and the resulting compounds (FDG, FDM, ClDG, and ClDM) presumably leave cells by passive diffusion. Fludeoxyglucose F 18 and related compounds are cleared from non-cardiac tissues within 3 to 24 hours after administration. Clearance from the cardiac tissue may require more than 96 hours. Fludeoxyglucose F 18 that is not involved in glucose metabolism in any tissue is then excreted in the urine.

Elimination: Fludeoxyglucose F 18 is cleared from most tissues within 24 hours and can be eliminated from the body unchanged in the urine. Within 33 minutes, a mean of 3.9% of the administrated radioactive dose was measured in the urine. The amount of radiation exposure of the urinary bladder at two hours post-administration suggests that 20.6% (mean) of the radioactive dose was present in the bladder.

Special Populations:

The pharmacokinetics of Fludeoxyglucose F 18 Injection have not been studied in renally-impaired, hepatically impaired or pediatric patients. Fludeoxyglucose F 18 is eliminated through the renal system. Avoid excessive radiation exposure to this organ system and adjacent tissues.

The effects of fasting, varying blood sugar levels, conditions of glucose intolerance, and diabetes mellitus on Fludeoxyglucose F 18 distribution in humans have not been ascertained [*see Warnings and Precautions (5.2)*].

13 NONCLINICAL TOXICOLOGY

13.1 Carcinogenesis, Mutagenesis, Impairment of Fertility

Animal studies have not been performed to evaluate the Fludeoxyglucose F 18 Injection carcinogenic potential, mutagenic potential or effects on fertility.

14 CLINICAL STUDIES

14.1 Oncology

The efficacy of Fludeoxyglucose F 18 Injection in positron emission tomography cancer imaging was demonstrated in 16 independent studies. These studies prospectively evaluated the use of Fludeoxyglucose F 18 in patients with suspected or known malignancies, including non-small cell lung cancer, colo-rectal, pancreatic, breast, thyroid, melanoma, Hodgkin's and non-Hodgkin's lymphoma, and various types of metastatic cancers to lung, liver, bone, and axillary nodes. All these studies had at least 50 patients and used pathology as a standard of truth. The Fludeoxyglucose F 18 Injection doses in the studies ranged from 200 MBq to 740 MBq with a median and mean dose of 370 MBq.

In the studies, the diagnostic performance of Fludeoxyglucose F 18 Injection varied with the type of cancer, size of cancer, and other clinical conditions. False negative and false positive scans were observed. Negative Fludeoxyglucose F 18 Injection PET scans do not exclude the diagnosis of cancer. Positive Fludeoxyglucose F 18 Injection PET scans can not replace pathology to establish a diagnosis of cancer. Non-malignant conditions such as fungal infections, inflammatory processes and benign tumors have patterns of increased glucose metabolism that may give rise to false-positive scans. The efficacy of Fludeoxyglucose F 18 Injection PET imaging in cancer screening was not studied.

14.2 Cardiology

The efficacy of Fludeoxyglucose F 18 Injection for cardiac use was demonstrated in ten independent, prospective studies of patients with coronary artery disease and chronic left ventricular systolic dysfunction who were scheduled to undergo coronary revascularization. Before revascularization, patients underwent PET imaging with Fludeoxyglucose F 18 Injection (74 to 370 MBq, 2 to 10 mCi) and perfusion imaging with other diagnostic radiopharmaceuticals. Doses of Fludeoxyglucose F 18 Injection ranged from 74 to 370 MBq (2 to 10 mCi). Segmental, left ventricular, wall-motion assessments of asynergic areas made before revascularization were compared in a blinded manner to assessments made after successful revascularization to identify myocardial segments with functional recovery.

Left ventricular myocardial segments were predicted to have reversible loss of systolic function if they showed Fludeoxyglucose F 18 accumulation and reduced perfusion (i.e., flow-metabolism mismatch). Conversely, myocardial segments were predicted to have irreversible loss of systolic function if they showed reductions in both Fludeoxyglucose F 18 accumulation and perfusion (i.e., matched defects).

Findings of flow-metabolism mismatch in a myocardial segment may suggest that successful revascularization will restore myocardial function in that segment. However, false-positive tests occur regularly, and the decision to have a patient undergo revascularization should not be based on PET findings alone. Similarly, findings of a matched defect in a myocardial segment may suggest that myocardial function will not recover in that segment, even if it is successfully revascularized. However, false-negative tests occur regularly, and the decision to recommend against coronary revascularization, or to recommend a cardiac transplant, should not be based on PET findings alone. The reversibility of segmental dysfunction as predicted with Fludeoxyglucose F 18 PET imaging depends on successful coronary revascularization. Therefore, in patients with a low likelihood of successful revascularization, the diagnostic usefulness of PET imaging with Fludeoxyglucose F 18 Injection is more limited.

14.3 Neurology

In a prospective, open label trial, Fludeoxyglucose F 18 Injection was evaluated in 86 patients with epilepsy. Each patient received a dose of Fludeoxyglucose F 18 Injection in the range of 185 to 370 MBq (5 to 10 mCi). The mean age was 16.4 years (range: 4 months to 58 years; of these, 42 patients were less than 12 years and 16 patients were less than 2 years old). Patients had a known diagnosis of complex partial epilepsy and were under evaluation for surgical treatment of their seizure disorder. Seizure foci had been previously identified on ictal EEGs and sphenoidal EEGs. Fludeoxyglucose F 18 Injection PET imaging confirmed previous diagnostic findings in 16% (14/87) of the patients; in 34% (30/87) of the patients, Fludeoxyglucose F 18 Injection PET images provided new findings. In 32% (27/87), imaging with Fludeoxyglucose F 18 Injection was inconclusive. The impact of these imaging findings on clinical outcomes is not known.

Several other studies comparing imaging with Fludeoxyglucose F 18 Injection results to subsphenoidal EEG, MRI and/or surgical findings supported the concept that the degree of hypometabolism corresponds to areas of confirmed epileptogenic foci. The safety and effectiveness of Fludeoxyglucose F 18 Injection to distinguish idiopathic epileptogenic foci from tumors or other brain lesions that may cause seizures have not been established.

16 HOW SUPPLIED/STORAGE AND DRUG HANDLING

Fludeoxyglucose F 18 Injection is supplied in a multi-dose, capped 30 mL and 50 mL glass vial containing between 0.740 to 7.40 GBq/mL (20 to 200 mCi/mL), of no carrier added 2-deoxy-2-[^{18}F-fluoro-D-glucose, at end of synthesis, in approximately 15 to 50 mL. The contents of each vial are sterile, pyrogen-free and preservative-free.

NDC 40028-511-30; 40028-511-50

Receipt, transfer, handling, possession, or use of this product is subject to the radioactive material regulations and licensing requirements of the U.S. Nuclear Regulatory Commission, Agreement States or Licensing States as appropriate.

Store the Fludeoxyglucose F 18 Injection vial upright in a lead shielded container at 25°C (77°F); excursions permitted to 15-30°C (59-86°F).

Store and dispose of Fludeoxyglucose F 18 Injection in accordance with the regulations and a general license, or its equivalent, of an Agreement State or a Licensing State.

The expiration date and time are provided on the container label. Use Fludeoxyglucose F 18 Injection within 12 hours from the EOS time.

17 PATIENT COUNSELING INFORMATION

Instruct patients in procedures that increase renal clearance of radioactivity. Encourage patients to:

- drink water or other fluids (as tolerated) in the 4 hours before their PET study.
- void as soon as the imaging study is completed and as often as possible thereafter for at least one hour.

Pregnancy: Advise pregnant women of the risk of fetal exposure to radiation with Fludeoxyglucose F 18 Injection [see Use in Specific Populations (8.1)].

Lactation: Advise lactating women that exposure to Fludeoxyglucose F 18 Injection through breast milk can be minimized by pumping and discarding breast milk and avoiding close (breast) contact with the infant for 9 hours after Fludeoxyglucose F 18 Injection [see Use in Specific Populations (8.2)].

Manufactured and distributed by:
PETNET Solutions, Inc.
810 Innovation Drive
Knoxville, TN 37932

PETNET Solutions

Legal information: On account of certain regional limitations of sales rights and service availability, we cannot guarantee that all products included in this publication are available through the Siemens Healthineers sales organization worldwide. Availability and packaging may vary by country and is subject to change without prior notice. Some/all of the features and products described herein may not be available in the United States.

The information in this document contains general technical descriptions of specifications and options as well as standard and optional features, which do not always have to be present in individual cases.

Siemens Healthineers reserves the right to modify the design, packaging, specifications, and options described herein without prior notice.

Please contact your local Siemens Healthineers sales representative for the most current information.

Note: Any technical data contained in this document may vary within defined tolerances. Original images always lose a certain amount of detail when reproduced.

"Siemens Healthineers" is considered a brand name. Its use is not intended to represent the legal entity to which this product is registered. Please contact your local Siemens Healthineers organization for further details.

Siemens Healthineers Headquarters
Siemens Healthcare GmbH
Henkestr. 127
91052 Erlangen
Germany
Phone: +49 9131 84-0
siemens-healthineers.com

Published by
Siemens Medical Solutions USA, Inc.
2501 N. Barrington Road
Hoffman Estates, IL 60192-2061
USA
Phone: +1 847-304-7700
siemens-healthineers.com/mi

Order No. A91MI-10546-M1-7600 | Printed in USA | MI-6061.CJ.CP.SNMMI.10K

siemens-healthineers.com/NMNS